CRANFIELD UNIVERSITY

ORIOL LÁZARO CASTELL

THE IMPACT OF ADDITIVE MANUFACTURING ON MICRO-TURBINE PARTS

SCHOOL OF ENERGY AND POWER
MSc in Advanced Mechanical Engineering

MASTER OF SCIENCE
Academic Year: 2016 - 1017

Supervisors: Prof. John Oakey and Dr. Nigel Simms
September 2017

CRANFIELD UNIVERSITY

SCHOOL OF ENERGY AND POWER
MSc in Advanced Mechanical Engineering

MASTER OF SCIENCE

Academic Year 2016 - 2017

ORIOL LÁZARO CASTELL

THE IMPACT OF ADDITIVE MANUFACTURING ON MICRO-TURBINE PARTS

Supervisor: Prof. John Oakey and Dr. Nigel Simms
September 2017

ABSTRACT

In the coming years, Additive Manufacturing will play an increasingly role in micro-turbine production, therefore the importance to know the impact of this type of manufacturing are crucial for the optimum design and performance of the device and the right definition of the stress fatigue generated. Is for this reason that the aim of this project is to study the impact that Additive Manufacturing puts on the design and the performance of a micro-turbine wheel, regarding the stresses generated on it.

To study the final stresses properly, a model of the micro-turbine has been developed with ANSYS Workbench. It includes an initial CFD study with ANSYS CFX to find the temperatures and pressures under which the micro-turbine works. Then, these temperatures are imported to ANSYS Thermal to calculate the temperature distribution in the geometry and after, CFX and ANSYS Thermal results are imported to ANSYS Structural to carry out a stress analysis.

The results of the project are taken from the execution of this model with the properties of Inconel 625, manufactured by Selective Laser Melting and manufactured by Casting, and a deep study of the stress generated at the junction between the blade and the hub is carried out at the end.

Keywords:

Inconel 625, Micro-turbine, Selective Laser Melting, Casting.

ACKNOWLEDGEMENTS

I would like to thank the sponsor of this project, HIETA Technologies. Without its support and information provided, the work presented here would not be possible.

I am thoroughly grateful to my academic supervisor Prof. John Oakey for all his support, help and guidance and throughout this MSc thesis, I could not have done this without him. I would also like to thank Dr. Nigel Simms for his help as a second supervisor.

Finally, thank you my family who has supported me unconditionally not only during my MSc thesis, but also my university years, with understanding and patience.

TABLE OF CONTENTS

LIST OF FIGURES

LIST OF TABLES

LIST OF EQUATIONS

LIST OF ABBREVIATIONS

IT	Information Technology
SLM	Selected Laser Melting
EDM	Electrical Discharge Machining
TBC	Thermal Barrier Coating
AM	Additive Manufacturing
YSZ	Yttria Stabilized Zirconia
EBPVD	Electron Beam Physical Vapor Deposition
APS	Air plasma spray
HVOF	High velocity oxygen fuel
ESAVD	Electrostatic Spray-Assisted Vapour Deposition
DVD	Direct Vapor Deposition
HIP	Hot Isostatic Pressing
ECM	Electrochemical Machining
CIM	Ceramic Injection Moulding
E	Young Modulus
CNC	Computer Numerical Control
CFD	Computational Fluid Dynamics
FEA	Finite Element Analysis

1 INTRODUCTION

For most of the 70 years of history of the gas turbine, the economy pushed the gas turbine industry to manufacture large engines in order to produce huge amounts of electric power, around 500MW (General Electric, 2016). In the last decades, the interest of power production into small scale has experienced a growing interest, and gas turbines giving 30 - 500kW (Zogg et al., 2007) of electric power, called micro-turbines, have gained positions into the market (Jain et al., 2015). This technology promises to bring the economic, environmental and convenience benefits to the advancements in the automotive industry, as well as, the electricity generation and mechanical power required by the commercial sector (Goli, Kondi and Timmanpalli, 2015). Moreover, during the last years, even smaller size machines, around 1 - 10kW have appeared and several are commercially available (Epstein, 2004). This trend goes hand with hand with the development of additive manufacturing what is increasing its importance due to the decrease of material waste, the allowance to manufacture more complicated parts than the traditional processes of manufacturing, and the possibility to manufacture prototypes faster decreasing the price.

Therefore, micro-turbine technology is increasing its importance in the energy market, and the prediction in the near future is that this way to generate energy, will become more popular because the decrease of the acquisition price, not only for the industry sector, also for domestic applications (Traverso, Calzolari and Massardo, 2017). Consequently, as explained above, additive manufacturing will play a key role to achieve this decrease in price of small combustion turbines and it is for this reason that the aim of this project is to study in depth the impact that the current additive manufacturing processes put on micro-turbine wheels, which is one of the most important parts of the mechanism, requiring the right design in order to resist the hard performance due to the high temperatures and stresses generated on it.

The objective of this thesis is to study the temperatures and the stresses generated on a micro-turbine using ANSYS, in order to understand the impact that additive manufacturing puts on the performance and the design of the

turbine, and see how it differs from the turbines manufactured by a conventional process. To achieve these results secondary objectives are needed. Firstly, the two types of manufacturing need to be understood and knowing how they are applied on the manufacture of the micro gas turbines. Secondly, the understanding of how ANSYS Workbench works in order to get realistic results from the simulations and learn how to input all the parameters. Once the model is completed, a discussion of the results obtained and the stress comparison between both types of manufacturing (additive manufacturing and casting) will allow to realise about what is the impact that this new-fangled process of manufacturing has on the micro-turbine performance and design regarding the stress distribution.

2 LITERATURE REVIEW

2.1 Gas turbine

The gas turbine is a Brayton cycle mechanical device that extracts its power from the energy of hot gases, coming from the combustion system, by expanding it through its blades (Krishnakanth et al., 2013). High speed and pressure is required at the inlet; hence a centrifugal or axial compressor is installed. This compressor is driven by the turbine and both devices are coupled to the same shaft. Assuming that there are no losses in either component, to control the power supplied by the turbine it is only necessary to change the volume of working fluid at constant pressure through the turbine blades, or modifying the pressure maintaining constant the volume of working fluid (Kauthalkar, Shikarwar and Sharma, 2013).

2.2 Micro-turbine

Micro-turbines are small-sized turbines used to generate electricity and their typically power output is from 30 to 500kW. Compared to the typical gas turbine generators, they also have lower pressure ratios, about 4, radial-flow design and incorporate recuperators (Zogg et al., 2007). They are considered ready to conquer the energy market due to the flexibility, the low maintenance and the future cost decrease, which will make them extremely cost effective in the near future (Traverso, Calzolari and Massardo, 2017). It is a derivative of automotive turbocharger technology and fabricated in much the same way (cast, forged, machined and assembled) from the same materials as steel, titanium and nickel-base super alloys (Epstein, 2004).

The turbine is capable to rotate in a range from 30,000 to 120,000rpm, and the generator is a high frequency electric alternator and operates with a converter for AC/DC. Moreover, it is the engine starter. The reliability of these devices is relatively high and some micro-turbines have already reached 25,000 hours of operation including shutdown and maintenance (Rosa Do Nascimento et al., 2013).

Concerning the environmental impact, micro-turbines have a high noise levels and require a specific acoustic system. However, the air cooling bearings avoid lubricants contamination by combustion products and prolongs the equipment useful life. Moreover, micro-turbine manufacturers usually uses heat exchangers to take profit of the combustion gases exhaust and preheat the air intake of the combustion chamber, achieving a thermal efficiency of 30% (Rosa Do Nascimento et al., 2013).

The commercial customer requirements for micro-turbines are that they need to be very clean, with low NO_x, CO and unburned hydrocarbons, have high efficiency and low maintenance, very low forced outage rate and low installation cost to provide fast payback to the owners (Goli, Kondi and Timmanpalli, 2015).

2.2.1 Breakdown

This type of turbines below few hundreds of kilowatts in size usually uses centrifugal machinery (Epstein, 2004), and consists of a supersonic radial flow compressor and turbine, connected by the same shaft. Radial-flow turbomachinery, can handle the very small volumetric flows of air and combustion products, with higher component efficiency and with simpler construction than axial-flow components (Soares, 2007). The electrical generator is also mounted on the same shaft. Hence there are only one rotating part, avoiding the needed of a gearbox and the problems due to considerable number of moving parts. This simplicity, makes this part relatively easy to manufacture and maintain, and presents a great potential for inexpensive and large scale manufacturing (Rosa Do Nascimento et al., 2013). Although, the low mechanical inertia of the shaft, makes micro-turbines difficult to control. The main parts are showed in Figure 1 (Traverso, Calzolari and Massardo, 2017).

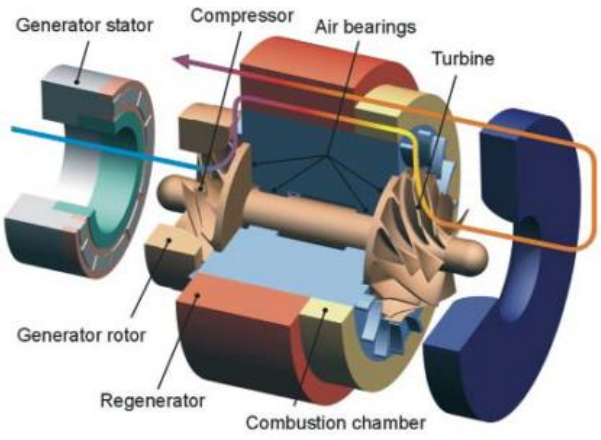

Figure 1: Sectional view of a micro gas turbine.

The inner bearing holding the shaft is hydrodynamic bearing, which contains grooves for lubrication, making the bearing smaller, cheaper and more efficient, and providing the bearing with low maintenance and high service life (Kingsbury, n.d.). The outer bearing utilizes a ceramic ball race. The heat exchanger has importance to increase the cycle efficiency of the micro turbine (Goli, Kondi and Timmanpalli, 2015).

2.2.2 Working cycle

The exhaust gases coming from the combustor with high velocity and temperature rotate the turbine wheel. The turbine wheel, the compressor and the generator are mounted on the same shaft, in consequence, the generator rotates with the same speed as the turbine and generates electricity. This electricity is conditioned through power electronics devices and supplied to the required areas. The fuel is injected to the combustor in the gaseous form and fresh and compressed air pass through the heat exchanger and is also introduced. The schematic process is showed in Figure 2.

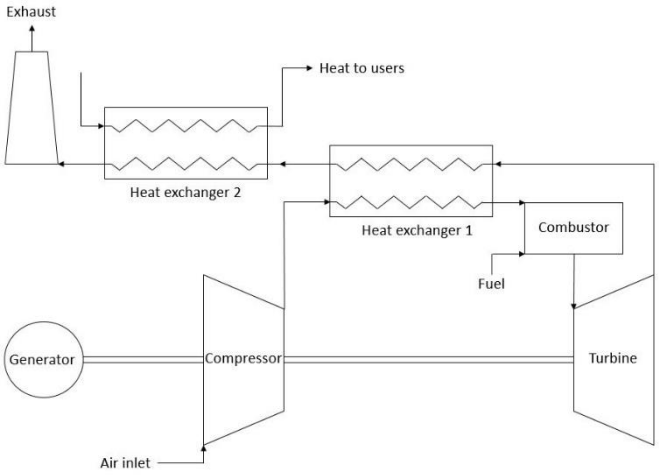

Figure 2: Micro-turbine working cycle.

The role of the heat exchanger is to take profit from the hot turbine exhaust gases, with a temperature about 500 - 600ºC, and increases the temperature of the air coming from the compressor (typically around 150ºC), increasing the overall efficiency of the micro gas turbine (U.S. Enviromend Protection Agency, 2015). This allows the cycle efficiency to take values as much as 30% while the average net efficiency of unrecovered micro-turbines is 17 % (Rosa Do Nascimento et al., 2013).

2.2.3 Turbine wheel working conditions

This thesis focuses only on the turbine wheel, then the operating conditions are explained only for this part. The following information is extracted from an experimental test of the operating conditions of a micro gas turbine device (Roberto Capata, 2015) which shows the working conditions of the turbine wheel from a Graupner/JetCat turbo-prop engine (this information can be extrapolated as an initial estimation to the performance of a micro gas turbine). As well as these values are contrasted with the experimentation of a Turbec T100 radial micro-turbine (Hohloch et al., 2017). The experiment shows that the inlet temperature range for the turbine is from 500 to 800ºC and for the outlet temperature is from 500 to 600ºC (Cadorin et al., 2012).

The turbine pressure ratio is the ratio of turbine pressure outlet to inlet pressure and decreases with higher turbine speed.

$$\beta_{turbine} = \frac{P_{output}}{P_{input}} \qquad \textbf{Equation 1}$$

The range for pressure ratio on a micro-turbine is from 0.5 for low turbine speed to 0.25 for high turbine speed, and the outlet pressure goes from 0.95 bar to 1 bar respectively, giving an inlet pressure range from 2 to 4bar approximately. The increase in pressure with higher turbine speed is due to the rising pressure losses caused by the subsequent components (Hohloch et al., 2017).

Concerning the inlet turbine flow, the value varies from 0.15 kg/s at low turbine speeds to 0.8 kg/s at high speeds. The inlet turbine flow is the result of air inlet plus inlet fuel mass flow (Cadorin et al., 2012).

$$m_{turbine,inlet} = m_{air,inlet} + m_{fuel,inlet} \qquad \textbf{Equation 2}$$

The fuel inlet flow goes from 0.001 kg/s to 0.010 kg/s demonstrating that most of the inlet turbine flow is composed by air.

Another interesting parameter is the rotational speed of the turbine wheel, which delimit the speed of the compressor and the generator (except some manufacturers who include a gearbox between the turbine-compressor shaft and

the generator shaft to reduce the speed on the generator). The rotational speed goes from 30,000 to 120,000rpm (Rosa Do Nascimento et al., 2013).

2.2.4 Performance

Commercial micro turbines from 25 to 500kW used for power generation produce both heat and electricity on a relatively small scale. Un-recuperated micro-turbines have an electrical efficiency around 15%. If they have recuperators, the electrical efficiency will be around 20 - 30%, and if it has heat recovery, the efficiency will arise up to 85% (Goli, Kondi and Timmanpalli, 2015).

The performance of micro gas turbines is strongly affected by temperature conditions. The decline observed at higher temperatures is explained by the lower air density and consequently lower mass flow rate through the power unit (Caresana et al., 2010).

The electrical efficiency of the current micro-turbines in the market are shown in Figure 3 (Gillette, 2010).

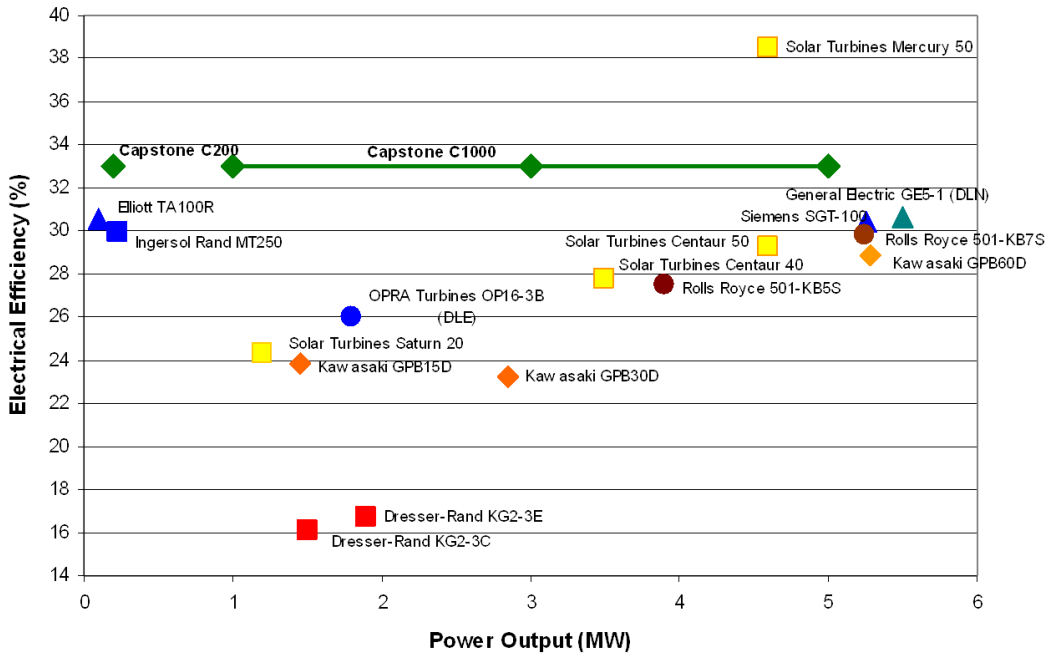

Figure 3: The electrical efficiency of the competitive offerings in the micro-turbine size range.

2.2.5 Turbine wheel materials

Current micro-turbine turbine wheels are manufactured with nickel-based alloys, providing them with lightweight and good resistance. However, as the turbine wheel is exposed to high inlet temperatures, normal light weighted materials cannot be used. These turbines are subjected to a long-term exposure to high temperature up to 800ºC, so heat resistance is an essential prerequisite. Therefore, light common materials like aluminium or titan-based alloys cannot be used.

Thermal creep, which is a time-dependent deformation under high levels of stress below the Yield Strength of the material, is also a problem when choosing the material of the turbine. This phenomenon is consequence of the high temperature of the turbine, and to avoid it, materials with high melting temperature must be used, as well as creep test data needs to be consulted during the material selection.

Some innovative solutions for the temperature problems of the turbine have appeared during the last years and are still being tested on micro-turbines. One of them are the Thermal Barrier Coatings (TBC) with a ceramic material. This type of coating should be selected so that is refractory enough to resist the high temperatures at the surface and has a low bulk thermal conductivity to minimize heat transfer to the metallic zone. Moreover, the thermal expansion of the selected coating should closely match the metallic one to minimize potential stresses. Nowadays, the most widely used ceramic coating material in turbines industry is Yttria stabilized zirconia (YSZ). Another consideration is that this coating must have a grain and pore structure to minimize thermal conduction to the metal-ceramic interface. The coating should have enough porosity, so it reduces the thermal conductivity while simultaneously adhering to the metal turbine bond-coat layer (Estrada, 2007). The current techniques used to TBC are Electron beam physical vapor deposition (EBPVD), Air plasma spray (APS), High velocity oxygen fuel (HVOF), Electrostatic spray-assisted vapour deposition (ESAVD) and Direct vapor deposition (DVD).

The last years SLM techniques are increasing sharply in the turbine manufacturing. Materials like Inconel or Hastelloy X are examples of high temperature and corrosion resistant nickel-based alloys which can be manufactured with this method. In most cases, these alloys contain chrome, iron, niobium and molybdenum and other alloy components, and they are often known as super alloys. Nickel-based alloys withstand higher temperatures than steels and they are also highly weldable. Their resistance to temperature is achieved through a mixture of dispersion hardening, precipitation hardening and solid solution strengthening. Nickel-based alloys exhibit good mechanical characteristic values such as high tensile strength and good endurance strength. Inconel can be used at temperatures of up to 700°C. Hastelloy X can even be used at temperatures of up to 1200°C. This makes these alloys ideally suited for aerospace technologies and for turbine production. Moreover, through post processing, such as hardening, heat treatment or hot isostatic pressing (HIP), the components' properties can be adapted to meet specific requirements (SLM Solutions, 2017).

Continued improvements in powder synthesis, processing, and densification have resulted in the development of a current generation of silicon nitride ceramics having controlled microstructures consisting of elongated grains. These so-called self-reinforced or in-situ toughened materials exhibit superior performance as reflected by increased strength, higher fracture toughness, and enhanced resistance to creep rupture (Soares, 2007). A silicon nitride rotor for a radial-flow micro gas turbine with a capacity of $30KW_{el}$ was developed by Fraunhofer. The ceramic rotor exhibits long-term stability up to 1200ºC at maximum operating loads and can be mass-produced. Depending on chemical composition, sintering and post processing, specific properties can be improved. The post processing led to high strength as well as high oxidation resistance and fatigue strength up to 1200ºC. The final data can be seen in Table 1 (Stockmann et al., n.d.).

Table 1: Silicon nitride data.

Operating temperature (ºC)	1200
Fracture toughness (MPa·$m^{1/2}$)	6.8
Yield Strength (MPa)	1000
Fatigue strength at 1200ºC (MPa)	500

2.2.6 Turbine wheel manufacture

The turbine is the part of the micro-turbine machine which gives the motion to the shaft, therefore it is the most important part of the device and needs a sophisticated method of manufacture, in order to accomplish the hard specifications required due to the strong conditions of stress and temperature.

During the last years, advanced manufacture plays a key role in manufacture, and it influences positively to the fabrication of micro-turbines.

2.2.6.1 Conventional manufacture of micro-turbines: Investment casting

Producing a turbine wheel with such specific demands of performance, is a technique developed over many years, since the micro-turbines appeared. The turbine wheel is usually manufacture with nickel-based superalloys, a high strength investment casting. These types of alloys are designed to withstand high temperatures and it is a trade-off in machinability. Therefore, an investment casting process has been developed during many years to achieve the best results, and minimize the machining on it (Ramamurthy and Thennavarajan, 2008).

The conventional process of investment casting has the following steps, showed in Figure 4 (James, 2015):

Figure 4: Investment casting steps.

The first step for the investment casting is to manufacture the wax pattern for the process from a 3D model. The wax is used for the ease of melt out and the possibility to reuse it. Several wax patterns are assembled on a tree and typically the pattern is destroyed during the process, so a new one is required for each casting. Once the tree and the patterns are assembled, metal casting pattern is then dipped in a refractory slurry whose composition includes extremely fine-grained silica, water and binders. A ceramic coating is built over the wax surface. The pattern is then repeatedly dipped into the slurry to increase the thickness of the ceramic coat. Once the ceramic coat has the toughness required, it is dried in air to harden it. Then the wax is melted at 90 – 175°C and it flows out the shell (The library of Manufacturing, n.d.).

The ceramic shell is then heated to 550 - 1100°C to strengthen further the mould and eliminate any rest of wax, water or contaminants. The metal casting is poured while the mould is still hot allowing the liquid metal to flow easily through the mould cavity and shrinking together as they cool, which gives a better dimensional accuracy. After the casting is solidified, the ceramic shell is broken from the piece and all the parts are cut away from the tree (The library of Manufacturing, n.d.).

When the casting process finish, grinding, milling and electrical discharge machining (EDM) processes are required (Figure 5).

Figure 5: Conventional manufacture post-processing.

To finish the micro-turbine manufacture, a final coating is carried on, increasing the material properties.

2.2.6.2 Advanced Manufacturing of micro-turbines

The most widely additive manufacturing technique used for micro-turbine manufacturing is Selective Laser Melting (SLM). This type of manufacturing, as a difference of conventional casting, allows an initial fast testing and validation process before to start the final integrated development.

2.2.6.2.1 Selective Laser Melting

Concerning the advanced manufacturing techniques on micro-turbines manufacture, testing and validation with SLM process can be seen in Figure 6 (James, 2015). This process is completely different from conventional manufacturing, allowing efficiency and precision to the process. Moreover, this type of additive manufacturing allows the fabrication of nickel-based alloy micro-turbines wheels. The first stage starts with the design of the model and its simulation to approve the model before to start the real process with Selected Laser Melting (SLM). SLM is a rapid prototyping, 3D printing or additive manufacturing practise which uses a high-power density laser to melt and fuse metallic powder together. This process has a limiting factor, the high surface roughness ($R_a \geq 5\mu m$). Is for this reason that a post-processing method to meet the requirements of surface roughness ($R_a \geq 0.8\mu m$) is needed. Therefore, to achieve this small roughness, micro machining process is required (Such and Meiners, 2015).

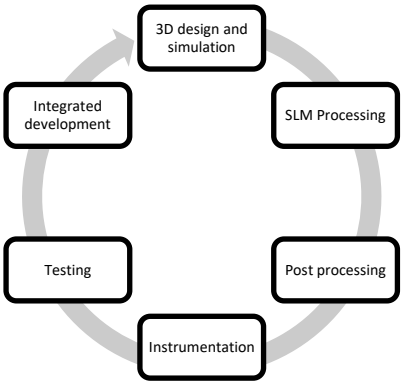

Figure 6: Additive manufacturing testing cycle.

After the post-processing, during instrumentation stage, all the measurements and critical dimensions are required to be checked to see if the turbine meets the initial requirements. To finish the cycle, a test is carried out showing the quality of the product through an objective way. When the testing and validation cycle is completed, advanced manufacturing allows integrated development with iterative and fast cycles.

The process above has many advantages, it allows parallel and integrated development process, radical development approaches, ambitious and short development goals, and short iterative cycles (James, 2015).

Once the testing and verifying cycle and the real performance of the micro-turbine prototype is accepted, the process chain for SLM production starts (Figure 7). The raw material for this process are the powder (with diameter lower than 50μm),

then the machine is conditioned and the process designed. The control parameters for the machining are implemented on the SLM machine and the turbine processing starts (James, 2015).

Figure 7: SLM process.

The post-processing starts when the micro-turbine is ready after the SLM process, then a quality control detects if defects appeared during the additive manufacture process. If the SLM process pass the quality control, the micro-turbine receive a heat treatment, to improve the strength of the turbine material, but this process can however result in undesirable residual stresses, which may lead to cracking and distortion of the component treated (Fry, n.d.). Another quality control is carried out to check if the heat treatment is right and the turbine goes to the machining part to finish the turbine (Figure 8).

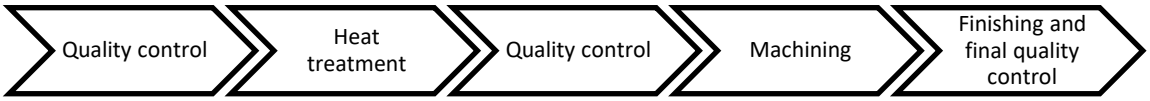

Figure 8: Post-processing.

At the final part of the micro-turbine machining the piece is submitted to a final quality control.

Advanced manufacturing process reduces costs and improves the response time for customers during the micro-turbine design process or for small production quantities, as well as, provides a good opportunity for improved efficiency within the repair and refurbishment business. However, the underlying characteristics and properties of many metal powders (especially high-temperature super-alloys) are not yet well-understood and tested to the industry's exacting standards (Aller, 2016).

It is expected that properties of laser built parts will be different from traditional manufacturing. One of the problems of this technique is the large residual stress found on the fabricated pieces because the rapid temperature cycles and steep temperature gradients occur in the scanned layers. This residual stresses in

general appears at the top and bottom of the part, and the most important parameters determining the magnitude and shape of the residual stress profiles are the material properties, the sample and substrate height, the laser scanning strategy and the heating conditions (Fry, n.d.).

SLM Additive manufacture (AM) metal parts often have much finer grains than moulded or cast structures, consequence of very fast solidification of laser heated material. This happens due to the rapid conduction of heat from the molten zone into the surrounding metal. These high speeds of cooling can lead to the formation of unbalanced crystal phases. When the part is being created layer-by-layer the individual lines of material are gradually melted and recrystallized. Therefore, it would be expected that the resulting structure of AM in all cases will be fine-grained. However, for AM methods the dendrite crystals are usually oriented vertically to the applied layer and the crystals have at least the height of the thickness of one layer or even higher. This phenomenon is explained by the fact that the laser energy sometimes is so large that it once again remoulded the bottom layer of the manufactured unit, which eliminated visible borders and enabled crystal growth through several layers due to repeated re-crystallization. Therefore, the structure and properties of the material depend on the selected parameters of the production and attributes of the melted powder (Hanzl et al., 2015).

Moreover, the mechanical properties of the SLM parts have an anisotropic behaviour. These anisotropy is explained by the orientation of the elongated structural grains. This grain orientation depends on the conditions during the solidification phase. Generally, these grains grow in a direction from the cooler side to the warmer side (the upper surface is exposed to the laser beam while the bottom surface rests on a solidified metal substrate). The elongated grains are oriented in the direction of the thermal gradient (Hanzl et al., 2015).

Therefore, the laser power settings and scanning speeds affect directly to mechanical properties of a part built with SLM, and different combination of these two variables will affect the mechanical behaviour of the output parts. Also, the

building directions affects to the anisotropy in tensile properties, and as much number of layers the isotropy increases and the tensile properties increases.

Inconel 625 properties with SLM fabrication can be seen in Figure 9 (Wang et al., 2016).

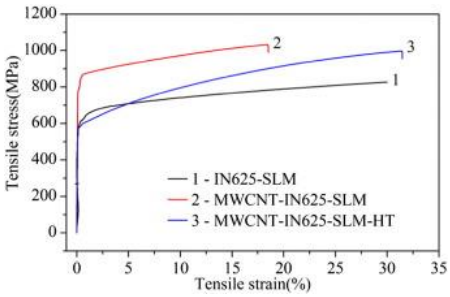

Samples	Tensile properties			
	Ultimate tensile strength/MPa	Yield strength at 0.2% offset/MPa	Elongation/%	Young's modulus/GPa
Wrought [42]	827	414	30	207.5
Smurov et al. [43]	1030 ± 50	800 ± 20	~ 8–10	–
IN625-SLM	878.5 ± 1.5	641.5 ± 23.5	30 ± 2	196 ± 12
MWCNT-IN625-SLM	998 ± 34	788 ± 29	19.1 ± 0.1	378 ± 12
MWCNT-IN625-SLM-HT	1000 ± 3	585 ± 10	31.5 ± 0.5	293 ± 5

Figure 9: The stress-strain curves of SLM produced IN625 (1), MWCNT-IN625 (2) and heat-treated MWCNT-IN625 (3) (left) and their mechanical properties (right).

An example of a final cooled turbine manufactured with SLM using the material CM247LC can be seen in Figure 10 (HIETA Technologies., n.d.).

Figure 10: HIETA Technologies Wheel turbine.

2.2.6.2.2 Electron Beam Melting

Electron Beam Melting is an additive manufacturing process that is quite similar to SLM, and is capable to produce very dense models. The difference is that EBM

uses an electron beam instead than a laser to melt the metal powder. But until some months that technique was only applicable to a limited number of metals (Element®, 2016).

The recent development of this technique by pioneer Arcam EBM® systems, utilise a high-power electron beam that generates the energy needed for high melting capacity and high productivity, enabling fast and accurate beam control. This allows melting at multiple points simultaneously, without compromising the surface finish, precision or built speed. During the process, partial pressure of He is introduced at $4x10^{-6}$bar to control the environment, which is necessary to maintain the chemical specification of the built material (Arcam, 2016).

For each layer in the build, the electron beam heats the entire powder bed to an optimal process temperature, specific to the material used. As a result, the components produced with the EBM® process are free from residual stresses and have a microstructure free from martensitic structures. With this process, the material properties are better than cast and comparable to wrought material (Arcam, 2016).

The process of this advanced manufacturing method is the same as SLM, the only difference is the machine used to manufacture the piece (Figure 11).

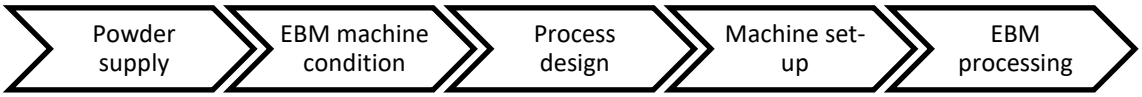

Figure 11: EBM process.

Arcam offers a total solution for a selection of standard materials. For these materials Arcam provides metal powder, process settings and support of materials like Titanium Ti6Al4V, Titanium Ti6Al4V ELI, Titanium Grade 2, Cobalt-Chrome, ASTM F75 or Inconel 718 (Arcam, 2016).

After the EBM process, un-melted powder is removed from the built components. The rapid removal rate afforded by electrochemical machining (ECM) process in high temperature superalloys (Figure 12), makes feasible high-quality and dimensionally accurate turbine geometries. Material tensile test data for EBM

produced superalloys tensile specimens, enable comparison to handbook cast properties of these materials (Turbines, 2012).

Figure 12: EBM post-processing.

2.2.6.2.3 Ceramic Injection Moulding

Ceramic Injection Moulding (CIM) concerns the manufacturing of a ceramic turbine wheels. It is a new and innovative process that provides cost effective solutions for complex, repeatable and ultra-high precision ceramic components (Morgan Advanced Materials, 2017).

For the fabrication of a ceramic turbine, the near-net-shape CIM process is used. This method is implementable for large production quantities, providing low loss of material. In this process, a heated thermoplastic compound composed of ceramic powders and an organic binder (feedstock) is pressed into a mould cavity under high pressure to form a near-net-shaped part. The volume of the rotor imposes numerous demands on the mould cavity and the feedstock, with the greatest challenge proving to be the unbinding process. This problem is solved by an innovative combination of chemical and thermal treatment of the part to enable sintering of defect-free rotors. Capstone® C30 gas turbine located at Fraunhofer IFF install this type of ceramic rotor (Stockmann et al., n.d.).

2.2.7 Microstructure characteristics of Inconel 625

In this section, a comparison between the conventional manufacturing of Inconel 625 microstructure and SLM technique is carried out.

2.2.7.1 Additive manufacturing

The microstructure of the 625 alloy changes depending on the conditions used during the casting process. However, if the temperatures used for sintering are at or slightly above the solidus for as-cast and wrought Alloy 625 (1288 and 1290°C respectively), the densities will usually be above 99% of that of wrought material (8.44 g/cm^3). Thus, using these high temperatures, long holding times

are not required to achieve high densities. As well as, the thermal gradients have a pronounced effect on the microstructure (Valencia et al., 1994).

In Figure 13 (Valencia et al., 1994) can be seen microstructures obtained with shorter holding times resulted in a uniform grain size. Figure 13 (right) shows the microstructure obtained after a total holding time of 24 minutes at 1288°C presenting a grain size of 20pm in longitudinal and 19pm in the transverse. Figure 13 (left) shows the microstructures for 30 minutes holding time. Shorter total holding times during incremental travel produce a uniform and smaller grain size which translates into a relatively higher Yield strength than the specimens sintered for longer periods of time (Valencia et al., 1994).

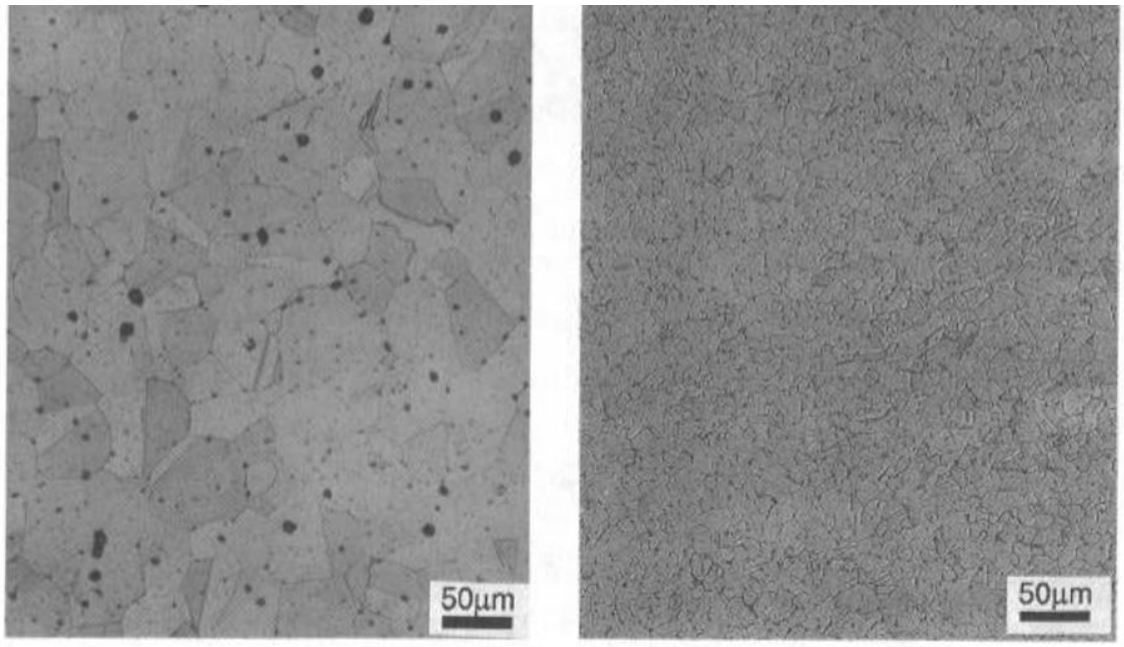

Figure 13: Casting at 1289°C/30 (left) minutes and at 1288°C /24 minutes (right).

2.2.7.2 Selective laser melting

Inconel 625 powder has a good forming performance to manufacture SLM parts. The formation of this morphology can be attributed to the laser heat source induced by the moving laser. The powder is continuously melted in the front of the pool and the melted liquid metal rapidly solidifies as soon as the laser moves away (the SLM cooling rates are about 10^6K/s). Then, the uneven temperature distribution generates a difference between the density and the surface tension.

As a result, the molten pool keeps stirring and generally, forms convection throughout the entire process, leading to the formation of “V” shape morphology, as can be seen in Figure 15(left) (Li et al., 2015). The angle of the V shape depends on the laser speed, the faster the laser scans, the smaller the V angle becomes (Li et al., 2015).

The morphology of the YZ section - Figure 14 (Li et al., 2015) - presents a “scales” shape as illustrated in Figure 15(right) (Li et al., 2015). In this experiment, the layer thickness was 0.02mm and most of the previous layer was re-melted by the following process. The scales shape matched the Gaussian distribution of laser energy. Due to most of the laser energy being focused on the laser beam centre, a depression appears at the bottom of the molten pool as indicated by the arrows. If the density of laser energy increases, a key hole is likely to form which will potentially improve the joint between adjacent layers (Li et al., 2015).

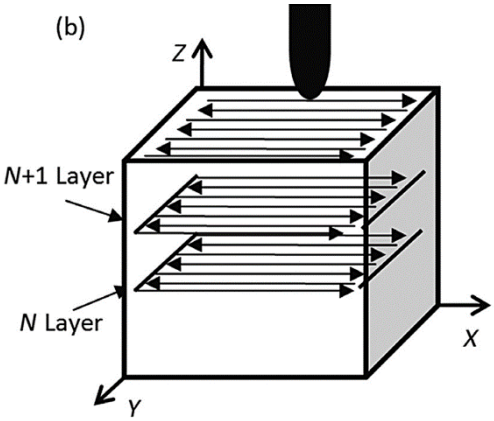

Figure 14: Bidirectional scan mode of the laser for SLM process.

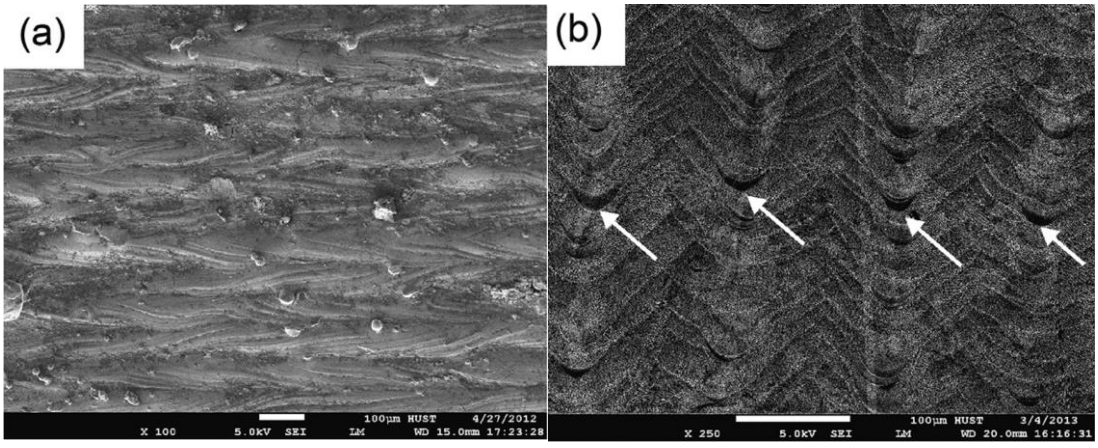

Figure 15: Microstructure of the top surface of an Inconel 625 sample manufactured with SLM (left) and “scales” shape of YZ direction for an Inconel 625 sample manufactured with SLM (right).

3 METHODOLOGY

The methodology used for the calculation of the stresses consists with three main parts. At the beginning, a simulation of the flow on the turbine with CFX was done to know the temperature and pressure generated on the micro-turbine surface. Once these values were known it was possible to import them to a Thermal-steady analysis and know how the temperature was distributed in the turbine geometry. At the end, the pressure from CFX and the temperature from Thermal-steady were imported to a Structural-steady analysis in order to get the stress generated in the micro-turbine.

The study was carried out with the material properties of Inconel 625 manufactured by casting and with Inconel 625 manufactured by SLM.

All the procedure can be seen in Figure 16, which shows the Workbench interface of the project, and all the parts created to calculate the final stress distribution of the micro-turbine.

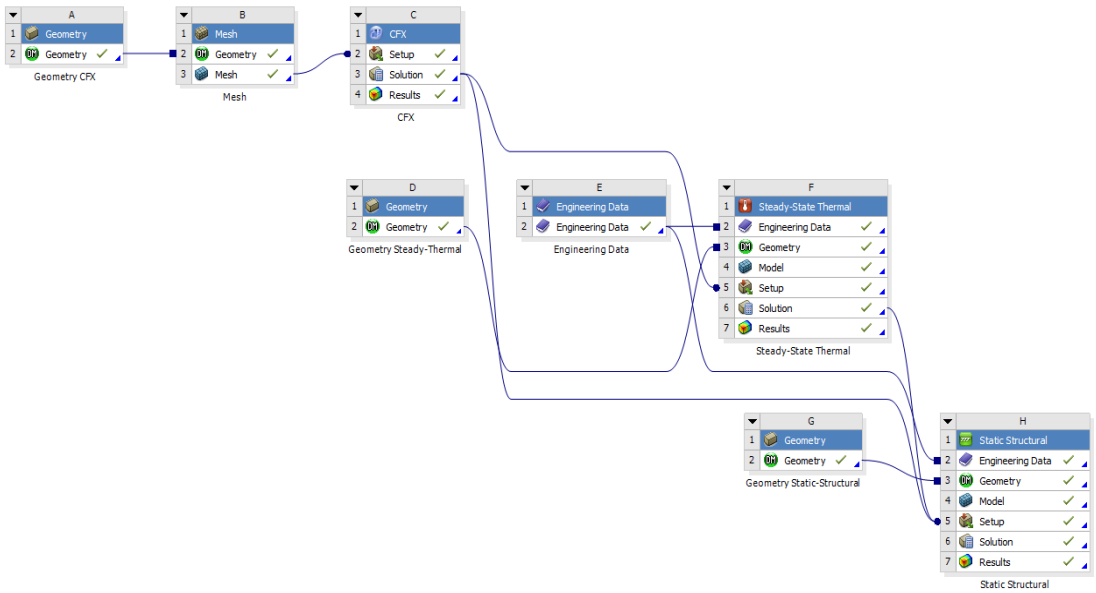

Figure 16: ANSYS project interface.

3.1 Geometry

The geometry analysed was a radial turbine provided by the company HIETA Technologies, an additive manufacturing company. This geometry has a

diameter of 6.2cm and 11 blades. The geometry can be seen in Figure 17, which is composed by the turbine wheel and the subjection shaft.

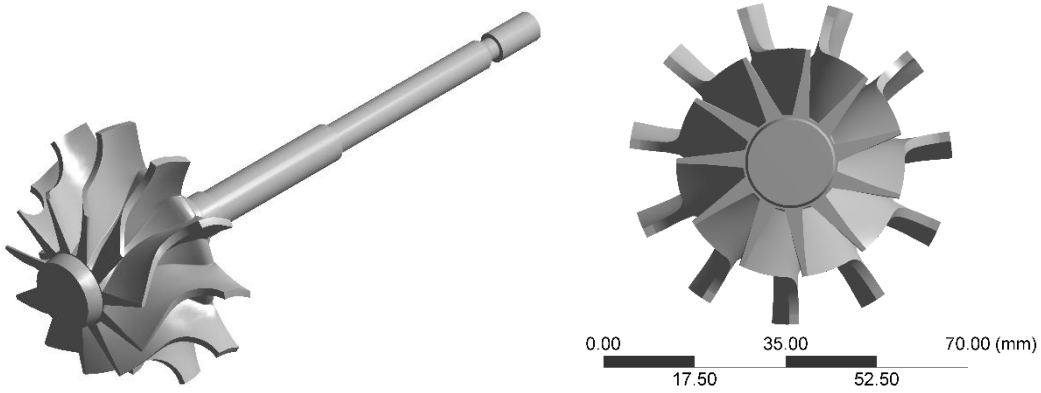

Figure 17: Isometric (left) and frontal (right) view of the radial turbine analysed.

This geometry allowed to carry out a study with a real geometry, which gives more realistic results and the possibility to see the difference between the stresses generated, depending on the two types of manufacturing.

3.2 Material properties

The material used for the comparison between the two types of manufacturing was as stated above Inconel 625. The properties depending on the temperature, to make even more realistic the results could not be obtained during this brief period of the thesis, and this could be one of the next steps of the project. Therefore, to carry out the study, the curves of the Young Modulus depending on the temperature were approximated for both materials. This approximation allowed to achieve the results of this thesis, but they should be compared with the real values, and it requires experimentation.

3.2.1 Conventional manufacturing: Casting

The mechanical properties used for Inconel 625 manufactured by casting were obtained from the web page MatWeb (Appendix B) and are shown in Table 2.

Table 2: Main properties of Inconel 625 manufactured by casting.

Mechanical properties at 20°C	
Tensile Strength [MPa]	836.3
Yield Strength [MPa]	390
Modulus Elasticity [GPa]	208
Poisson Ratio	0.28
Shear Modulus [GPa]	81.4

The Young Modulus used was 208GPa at 20°C, corresponding to Inconel 625 (Annealed 1180°C + Aged 760°C). This value was extrapolated to make it dependant on the temperature, following the same slope as the natural Inconel 625 properties (Appendix C).

The final curve used for the Young Modulus (E) versus the temperature is shown in Figure 18.

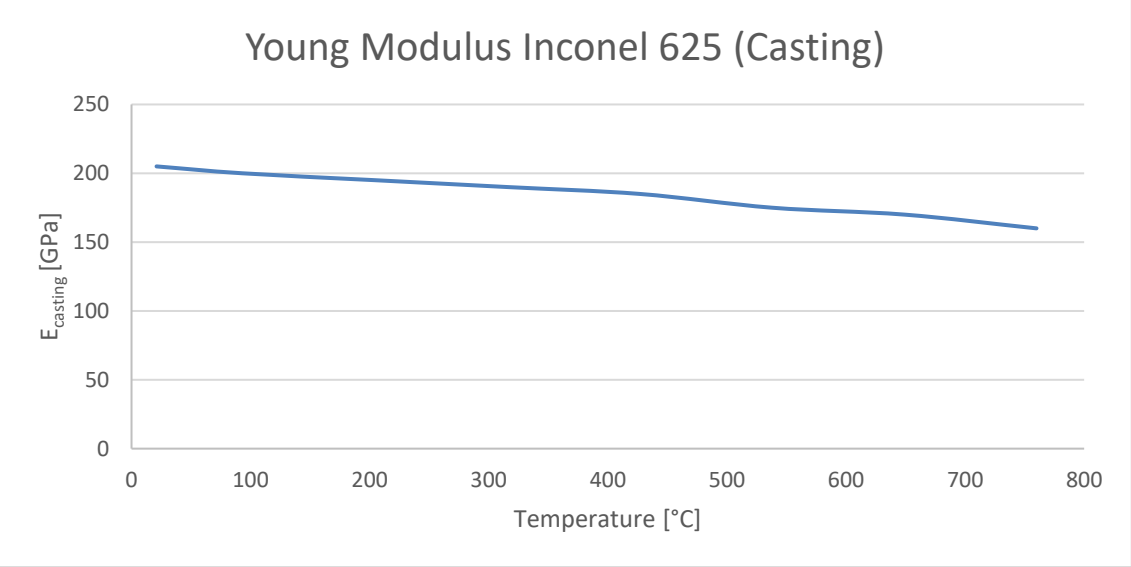

Figure 18: Approximated curve of the Young Modulus of Inconel 625 manufactured by casting versus the Temperature.

As can be seen in the plot above, the Young Modulus decreases about 50GPa with an increment of the temperature of 800°C.

For the thermal study, the thermal conductivity was required to perform the analysis. Knowing that the thermal conductivity is approximately the same for the Inconel 625 manufactured by casting and by SLM, the following thermal conductivity, showed in Figure 19, was taken for both type of materials and was extracted from the properties of Inconel 625 showed in Appendix C.

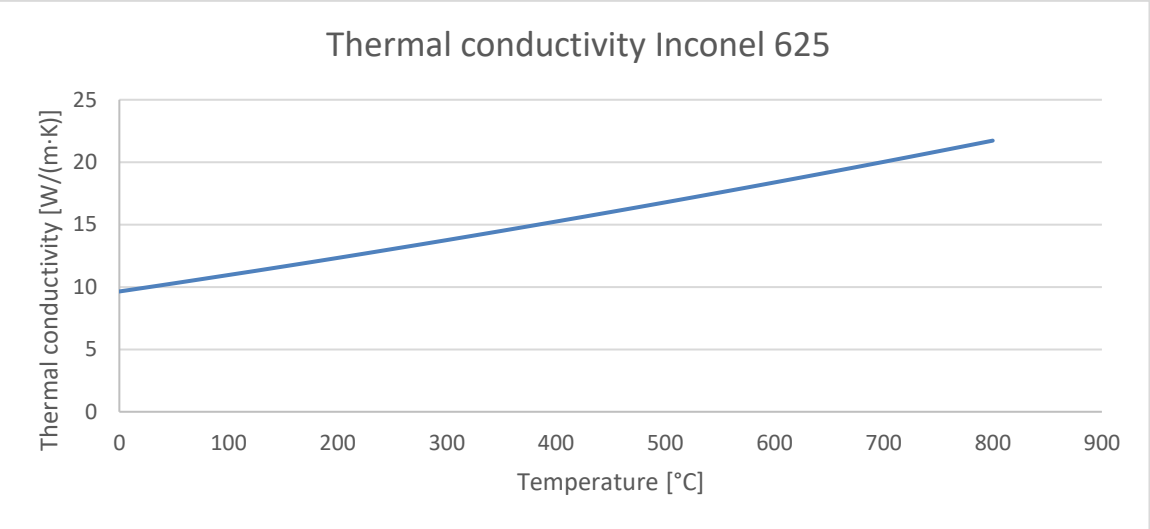

Figure 19: Thermal conductivity of Inconel 625 versus the Temperature.

3.2.2 Additive manufacturing: Selective Laser Melting

The mechanical properties used for this material were taken from the CRP Meccanica web page, a CNC machining company. The data sheet can be seen in Appendix A and the main properties are stated in Table 3.

Table 3: Main properties of Inconel 625 manufactured by SLM.

Mechanical properties at 20°C	
Tensile Strength in horizontal direction XY [MPa]	827
Tensile Strength in vertical direction Z [MPa]	827
Yield Strength in horizontal direction XY [MPa]	414

Yield Strength in vertical direction Z [MPa]	414
Modulus Elasticity in horizontal direction XY [GPa]	170
Modulus Elasticity in horizontal direction Z [GPa]	160
Maximum operating temperature under load [°C]	650

The Young Modulus was also approximated with the same criteria as the casting manufacture and following the slope of the Young Modulus in Appendix C, due to the impossibility to find specific and accurate data, for example the σ-ε curve depending on the temperature. Following the section 2.2.7.2, the difference for this type of manufacturing is that the Inconel 625 manufactured with SLM (stress relieved) introduce anisotropy to the piece and the properties change depending on the direction as can be seen in Table 3 and in Figure 20.

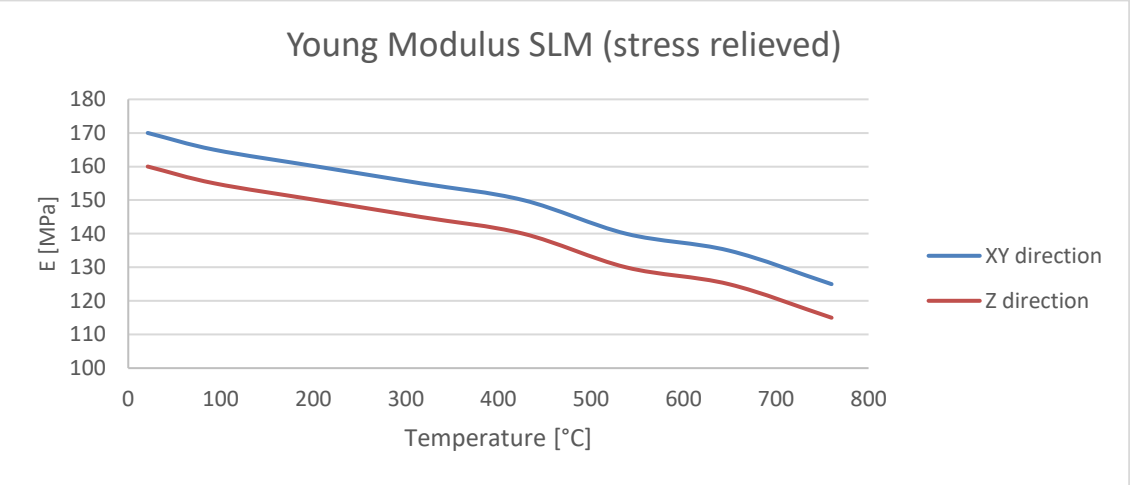

Figure 20 Young Modulus of Inconel 625 manufactured by SLM versus the Temperature.

3.3 CFX

This Computational Fluid Dynamics (CFD) software tool delivers reliable and accurate solutions for turbomachinery applications. And it is recognized for its outstanding accuracy, robustness and speed with rotating machinery (ANSYS, 2017). The CFX analysis is the first part of the model, and gives the conditions of pressure and temperature under the turbine works.

The main problem of this analysis was that the real conditions of this geometry were not known. Therefore, it was necessary to carry out an accurate analysis in order to realise which were the approximate operating conditions for this turbine, and making the simulation more reliable.

3.3.1 Fluid domain

The first step was to construct the fluid domain. This domain was designed with Solidworks, and after imported to ANSYS. In ANSYS was used the operation *Boolean* to subtract the turbine geometry from the fluid domain, and the result is shown in Figure 21.

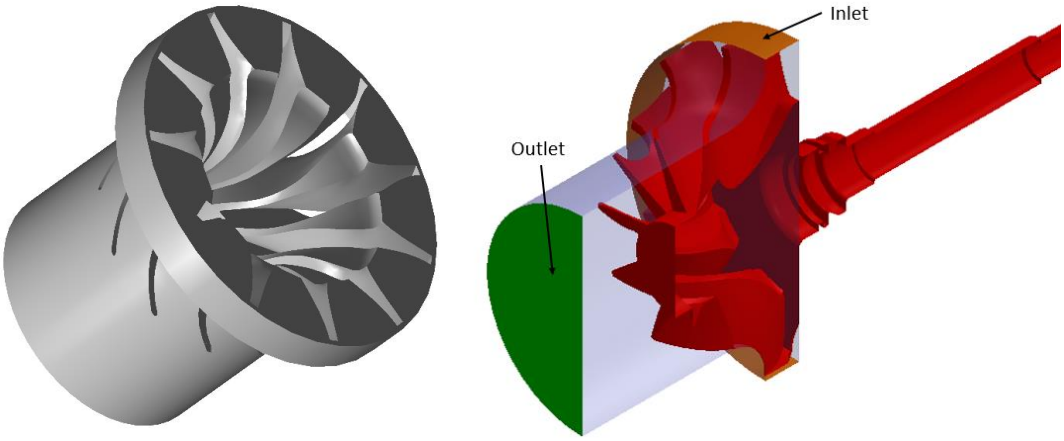

Figure 21: CFX fluid domain for the turbine wheel geometry (left) and sectional view of the turbine and the fluid domain (right).

The inlet height of the fluid domain is 7.8mm and the total length of the geometry 50mm.

3.3.2 CFX Mesh

This was the most important part of the CFX analysis to get reliable and accurate results and it required a special attention. The final model was analysed without any simplification, because the appearance of many difficulties to apply circular symmetry and after import the results to ANSYS Thermal and ANSYS Structural due to the geometry given.

To catch the wall effects was necessary to calculate the first boundary layer for the mesh over the blades. The first step was to calculate the velocity at the inlet:

$$v_{inlet} = \frac{Flow}{Area} = 155.57 \frac{m}{s} \quad \textbf{Equation 3}$$

The dynamic viscosity of the fluid at 4bar and 800ºC is 4.579x10^{-5} Pa·s^{-1}, then:

$$Re = \frac{\rho \cdot v_{inlet} \cdot D_h}{\mu} = 261{,}191.5 \quad \textbf{Equation 4}$$

Where ρ is the density of the air, v_{inlet} the velocity at the inlet, D_h the hydraulic diameter and μ the dynamic viscosity.

To calculate the skin friction coefficient, the Blasius equation was used:

$$Cf = 0.079 \cdot Re^{-0.25} = 3.495x10^{-3} \quad \textbf{Equation 5}$$

Then, it was possible to calculate the wall shear stress and shear velocity (also called friction velocity):

$$\tau_w = 0.5 \cdot Cf \cdot \rho \cdot {v_{inlet}}^2 = 52.44\ Pa \quad \textbf{Equation 6}$$

$$u_T = \left(\frac{\tau_w}{\rho}\right)^{0.5} = 6.503 \frac{m}{s} \quad \textbf{Equation 7}$$

Therefore, taking a y^{+} = 30, the first layer thickness had to be:

$$\delta_y = \frac{y^+ \cdot \mu}{\rho \cdot u_T} = \frac{30 \cdot 4.579x10^{-5}\ {Pa}/{s}}{1.24\ {kg}/{m^3} \cdot 6.503\ {m}/{s}} = 1.7x10^4\ m \quad \textbf{Equation 8}$$

The final input parameters for the mesh generation were a Size function of Proximity and Curvature, Fine Relevance Centre, Medium Smoothing, Slow Transition and Fine Span angle centre. The minimum face and edge size was 0.015mm and the maximum 3mm. The growth rate was the common value of 1.2.

To generate the right boundary layer - Figure 22 -, the inflation mode was activated on the hub and blades surfaces, with an inflation option of *First boundary layer* equal to 0.017mm as calculated above.

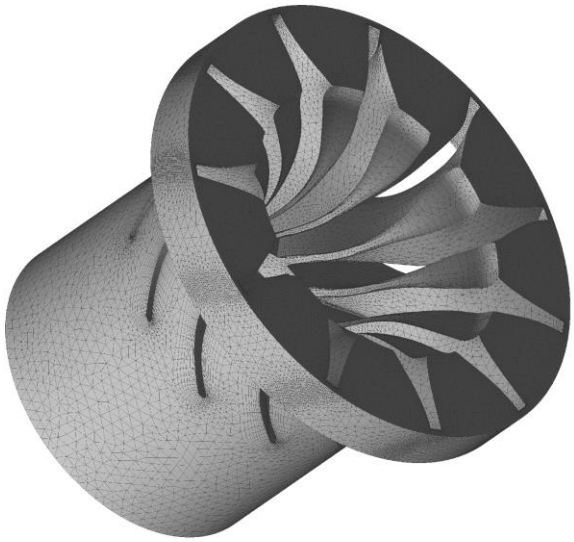

Figure 22: CFX fluid domain mesh for the turbine wheel geometry.

The final mesh had 764,048 elements and 1,582,908 nodes. The mesh sensitivity explained below was carried out to generate the optimum mesh and check the robustness of the model.

3.3.2.1 Mesh sensitivity

A total of four meshes were analysed to get the optimum number of elements. The parameter analysed for the mesh sensitivity was the isentropic efficiency with an operating conditions close to the final expected values. The difference between the biggest mesh with 1,480,211 elements got a difference between the mesh three with 764,048 elements, of 0.34%. This value was lower than 1%, so was assumed that the isentropic efficiency converged. Figure 23 shows the isentropic efficiency against the number of elements, and can be seen that after 764,048 elements, the curve became almost constant.

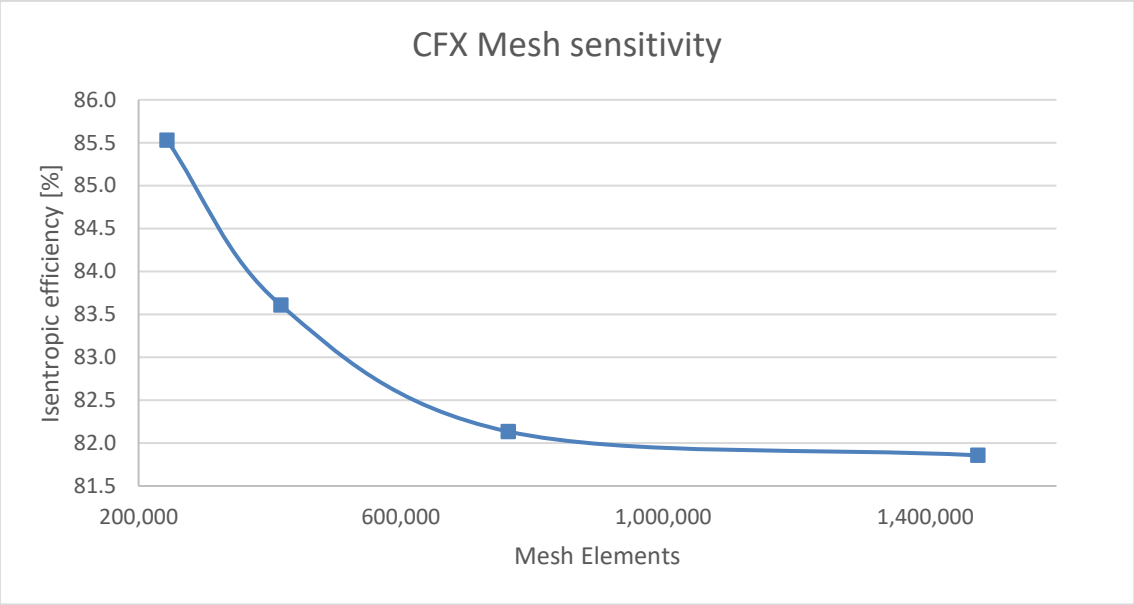

Figure 23: Mesh sensitivity for the CFX model.

3.3.3 Boundary conditions

The fluid domain mesh was imported to CFX in order to study the operating conditions and knowing the temperature and pressure distributions on the turbine wheel. The analysis was with a steady state.

The basic boundary conditions defined were at the inlet and the outlet of the turbine. As can be seen in Figure 24 the inlet domain was marked with inflow arrows and the outlet domain as outflow arrows.

Once the inlet and outlet were defined, the angular velocity was introduced, as well as the direction of rotation. The value of the rotation speed as explained in section 2.2.3, varies from 80,000 to 120,000rpm for the micro-turbines, so a rotation speed sensitivity was done in section 3.3.4, between the velocities 90,000 and 110,000rpm. The Figure 24 also shows the direction of rotation for the radial turbine.

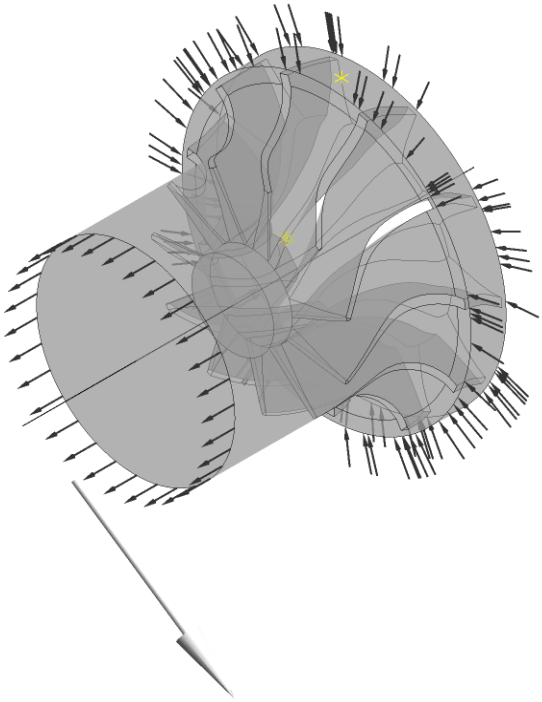

Figure 24: Inlet and Outlet domain and the direction of rotation of the turbine.

The fluid assigned was Air Ideal Gas, as the effect of the fuel was considered negligible, because as explained in section 2.2.3, is less than 1% of the total flow. The reference pressure was set at 1bar, the heat transfer was defined as Total energy and the turbulence model assigned was the Shear stress transport, the common model used for this type of turbines.

The inflow/outflow boundary conditions were studied and, as the rotation speed, it was seen how the variation of this parameters changed the final operating conditions. Therefore, following the section 2.2.3, the value for the pressure at the inlet were studied between 2 and 4bar, and the temperature between 550 and 650ºC. The outlet pressure was set constant at 1 bar.

For the inflow direction condition, a value of 70 degrees respect the radial direction was assigned, as seen in Figure 25.

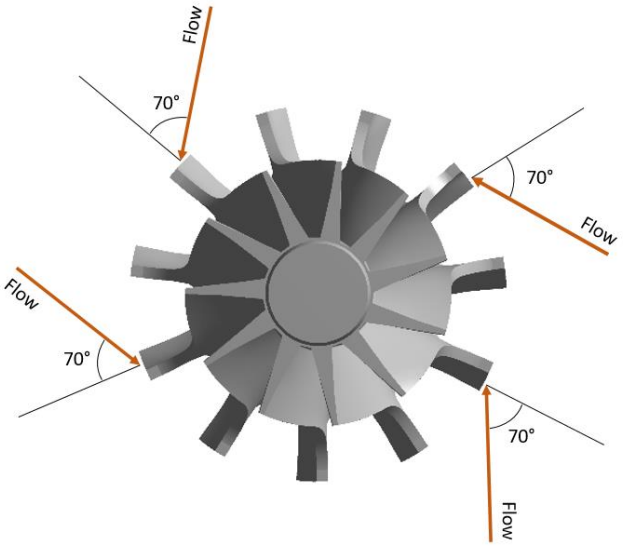

Figure 25: Inflow of the turbine.

In order to introduce this value in CFX, cylindrical coordinates were required, therefore, the inflow direction was set as:

$$(a, r, t) = (0, -1, \tan(70°))$$

The 0 implies no axial flow at the rotor inlet, the -1 implies downward inflow and tan(70º) implies the value of 70 degrees respect the radial direction.

After that, the solver parameters were set: the maximum iterations were fixed at 600, the convergence criteria at RMS and the residual target at 10^{-6}.

The values for the results were obtained from the following expressions, defined in CFX.

The real efficiency was calculated as:

$$Efficiency = \frac{Power}{volFlow \cdot dPtot} \qquad \textbf{Equation 9}$$

The power in Watts:

$$Power = Torque \cdot Rotation\ speed \qquad \textbf{Equation 10}$$

The torque was obtained from:

$$Torque = torque\_z()@REGION{:}TurbineSurface \qquad \textbf{Equation 11}$$

dPtot was defined as:

$$dPtot = massFlowAve(Total\ Pressure\ in\ STn\ Frame)@REGION:Inlet - massFlowAve(Total\ Pressure\ in\ STn\ Frame)@REGION:Outlet$$ **Equation 12**

volFlow was:

$$volFlow = (massFlow()@REGION:Inlet) / (areaAve(Density)@REGION:Inlet)$$ **Equation 13**

3.4 Thermal analysis

A thermal analysis is used to calculate the temperature distribution and related thermal quantities in a system or component. The most important thermal quantities of interest are the temperature distributions, the amount of heat lost or gained, the thermal gradients and thermal fluxes.

Thermal simulations play an important role in the design of micro-turbines, and usually are followed with a stress analysis to calculate the thermal stresses due to thermal expansions and contractions. This thermal analysis can be carried on with Ansys Thermal in order to calculate the temperature distribution on the turbine blades, and after importing them to Ansys structural to analyse the stresses due to the temperature.

3.4.1 ANSYS Thermal mesh

The mesh for this analysis can be seen in Figure 26 (left). The Size function was Proximity and Curvature with a fine Relevance centre, low Smoothing, fast Transition and medium Span angle centre. The final minimum element size was 0.5mm and the maximum was 5mm.

There are three sizing refinements to improve the mesh in the required zones. The first sizing was on the edge where the blades are connected with the hub, this sizing was set to 0.5mm with hard behaviour to ensure that the size was constant. These zones can be seen in Figure 26 (right).

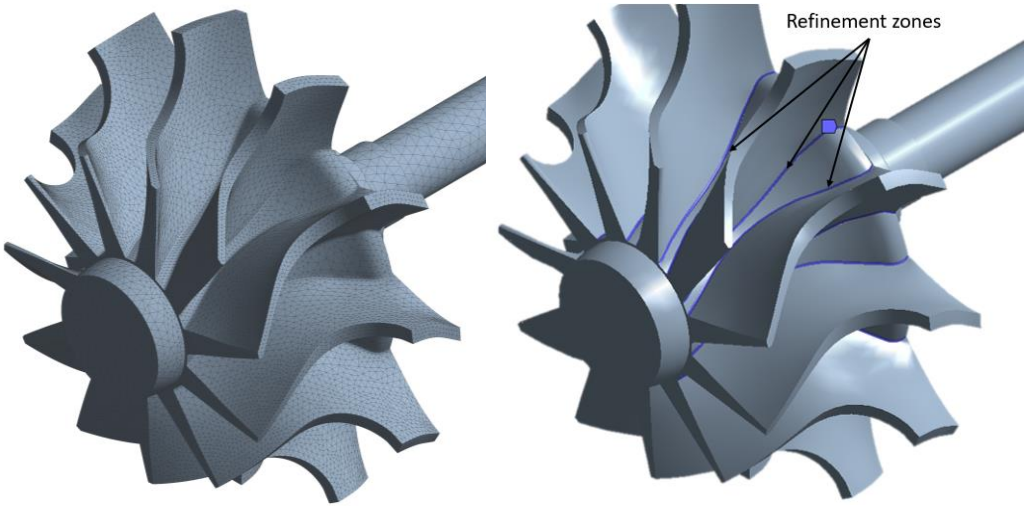

Figure 26: Thermal analysis mesh for the turbine geometry (left) and refinement zone (right).

The other refined zone was the shaft, this zone ended up with a constant temperature through all the shaft, so a big elements were enough to know the temperature distribution. Therfore a sizing of 1.5mm with hard behaviour were enough for this zone. It can be seen in Fiugre 27 (left).

And the last zone to fix the size was the top part of the turbine, the temperature on this zone was almost constant so the size for this area was enough with a sizing of 1mm with hard behaviour to ensure the constant size of the elements. The zone is showed in Figure 27 (right).

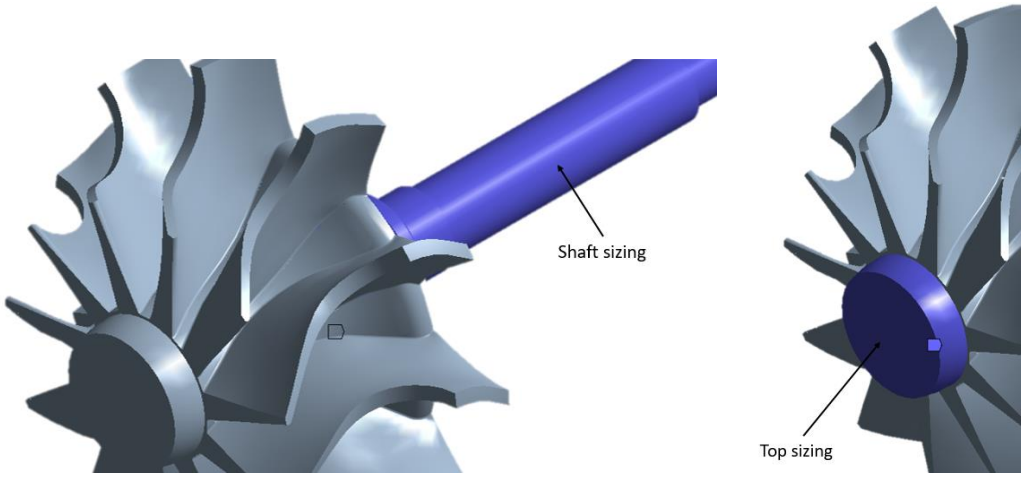

Figure 27: Thermal analysis controlled mesh for the shaft zone (left) and for the top zone (right).

The total and optimum number of elements for this mesh was 317,929. This was corrobored with the mesh sensitivity carried out below.

3.4.1.1 Mesh sensitivity

The mesh sensitivity for the Thermal analysis was carried out for different points of the body, and the temperature maximum and minimum were controlled. The points are shown in Figure 28.

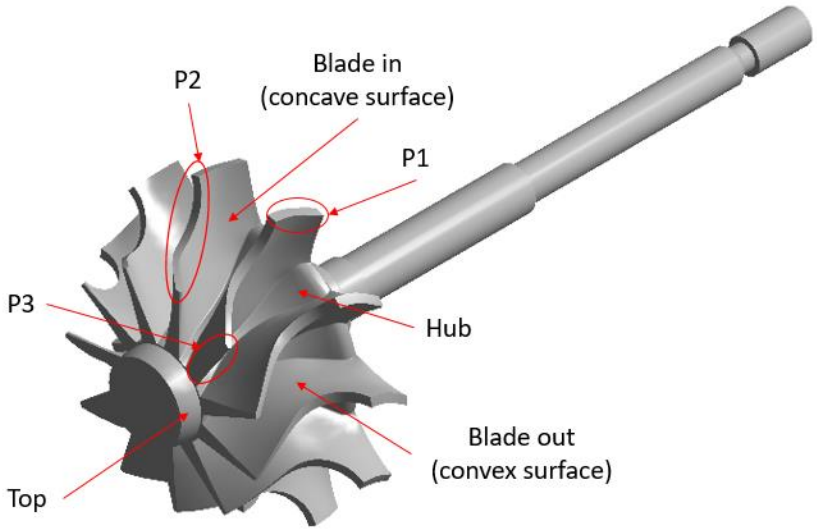

Figure 28: Control points for the mesh sensitivity.

The results of the analysis can be seen in the Figure 29 and the Figure 30. The plots show that after 317,929 elements, the temperatures of the control points became constant with a difference between the last mesh studied (1,564,419 elements) and the mesh chosen (317,929 elements) less than 1%, so the mesh was converged and this value was taken as the optimum elements number. The values for the minimum temperature were the values which fluctuates more at the beginning, and after these results all of them had a low variation.

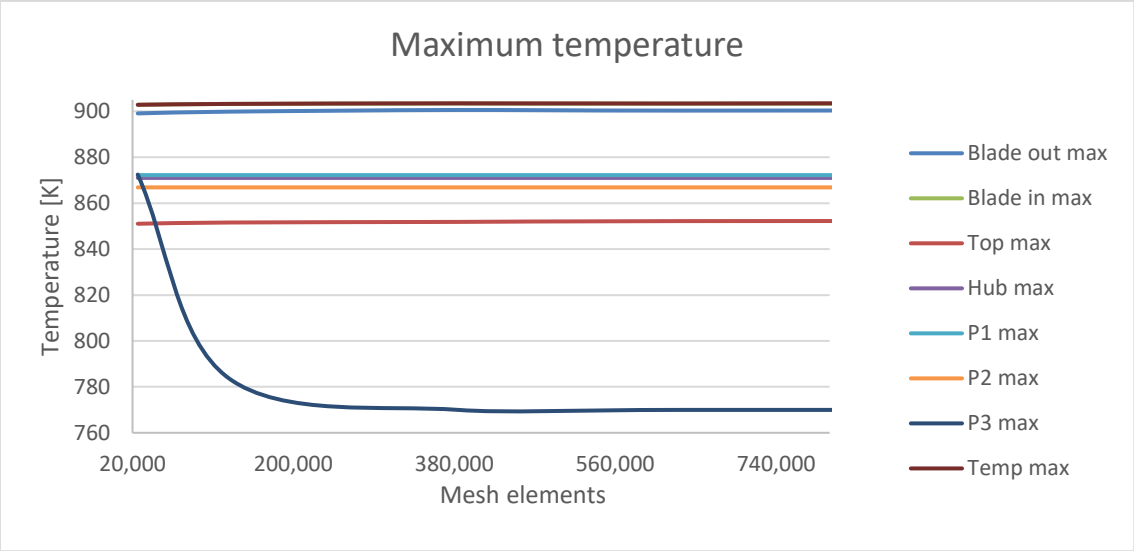

Figure 29: Maximum temperature of the control points of the mesh sensitivity.

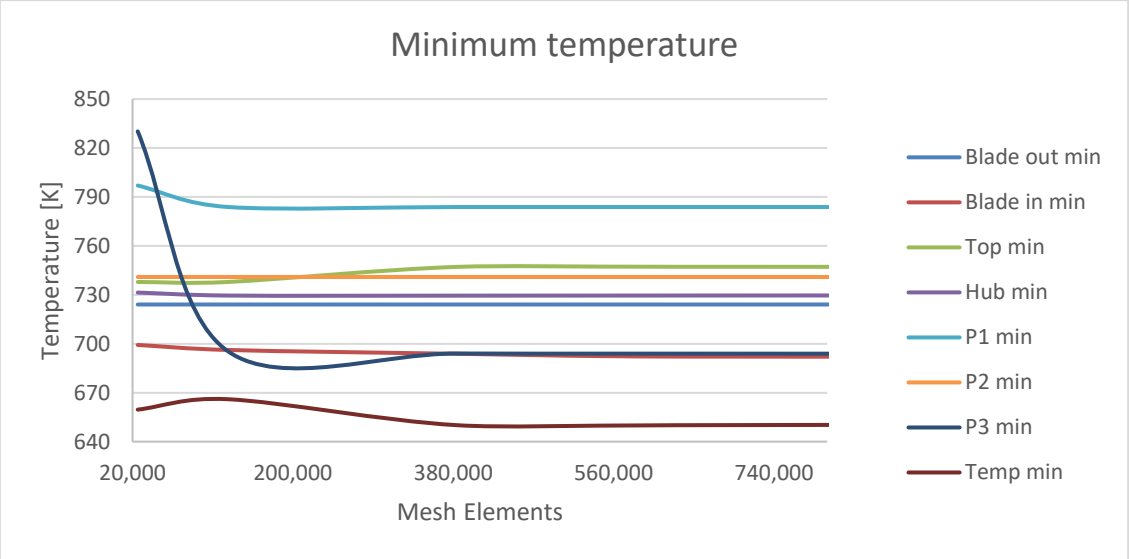

Figure 30: Minimum temperature of the control points of the mesh sensitivity.

3.4.2 Boundary Conditions

The boundary conditions were the surface temperature imported from the CFX analysis. It required to import the temperature on two different zones, the first zone was the hub, which incurred the zones showed in figure 31 (left), and the second zone was the blades surface showed in red in Figure 31 (right). The import of this surface temperature from CFX allowed the possibility to know the temperature distribution on the body turbine after executing ANSYS Thermal.

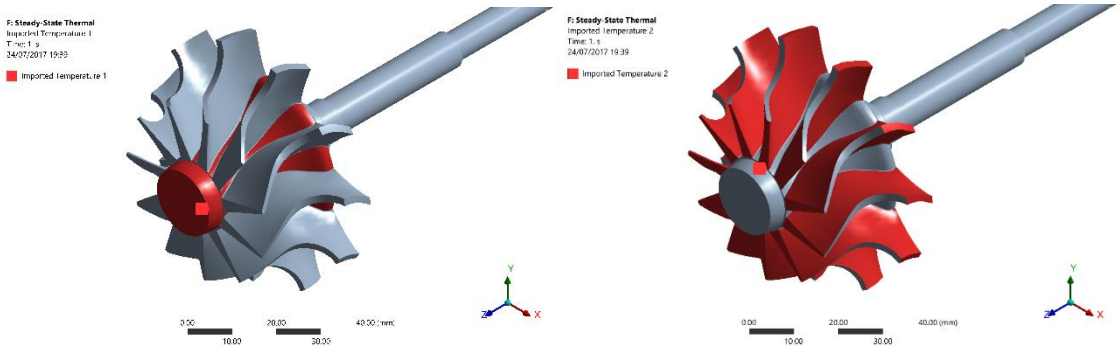

Figure 31: Hub zone (left) and blades zone (right).

Figure 32 shows the imported temperature plot, this temperature distribution on the surface was used to calculate the internal body temperature.

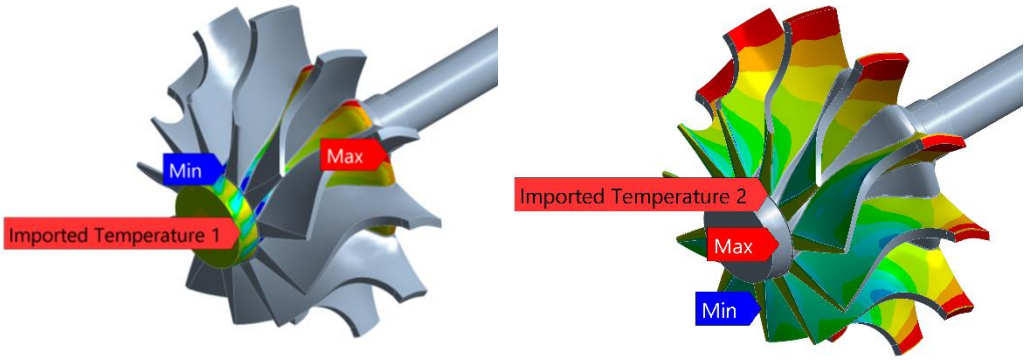

Figure 32: Imported temperature of the Hub zone (left) and the Blades zone (right).

3.5 Structural analysis

The stress generated on a micro gas turbine, apart from coming from the temperatures distribution, is also consequence of the pressure that the combusted gases exert on the turbine blades during the expansion process, combined with the rotation of the turbine blades. This pressure can be calculated with ANSYS CFX and after importing them to ANSYS Structural to calculate the stresses generated on the micro gas turbine.

3.5.1 ANSYS Structural mesh

The micro-turbine mesh designed for the structural analysis - Figure 33 - differs from the thermal analysis mesh. It required more accuracy at zones where the stress was higher to catch all the effects. The most important refinement zone was the joint between the blades and the hub. This is the zone with higher stresses on the turbine (excluding the shaft because this thesis focuses only on the turbine geometry without the shaft). Therefore, an element size of 0.8mm was specified at this zone.

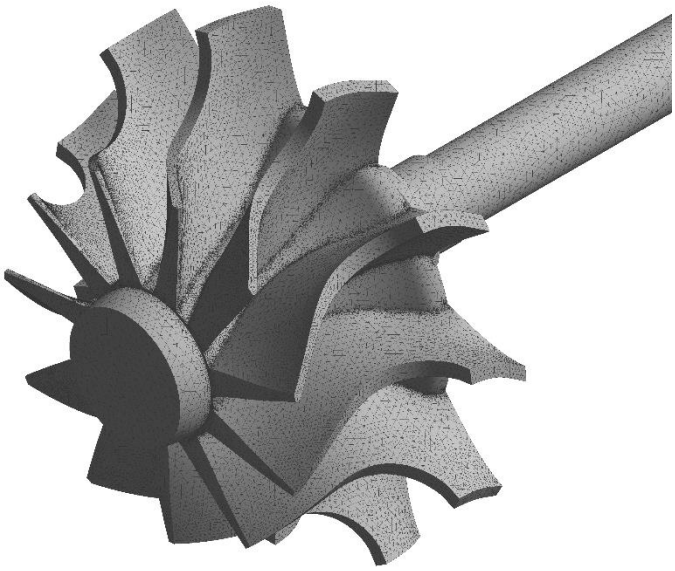

Figure 33: Micro-turbine mesh for the Structural analysis.

On all the corners between the junction of the blade-hub and the bottom part of the turbine, a sphere of 0.5mm of radius and a sizing of 0.08mm was applied, and some changes were observed before and after it.

Moreover, a sizing of 1mm and hard behaviour on the shaft was applied to avoid small elements.

The Size Function used was Proximity and Curvature, a Medium Relevance Centre, a Medium Smoothing, a Medium Span Angle Centre and Fast transition. The minimum size for the faces and edges was 0.08mm and the maximum 1mm.

The total elements for the optimised mesh was 960,582 as can be seen in the mesh sensitivity below.

3.5.1.1 Mesh sensitivity

Since the zone of interest is the joint between the blades and the hub, the maximum stress generated on the joint at both parts of the blade was plotted. Figure 34 shows the mesh sensitivity carried out at this zone.

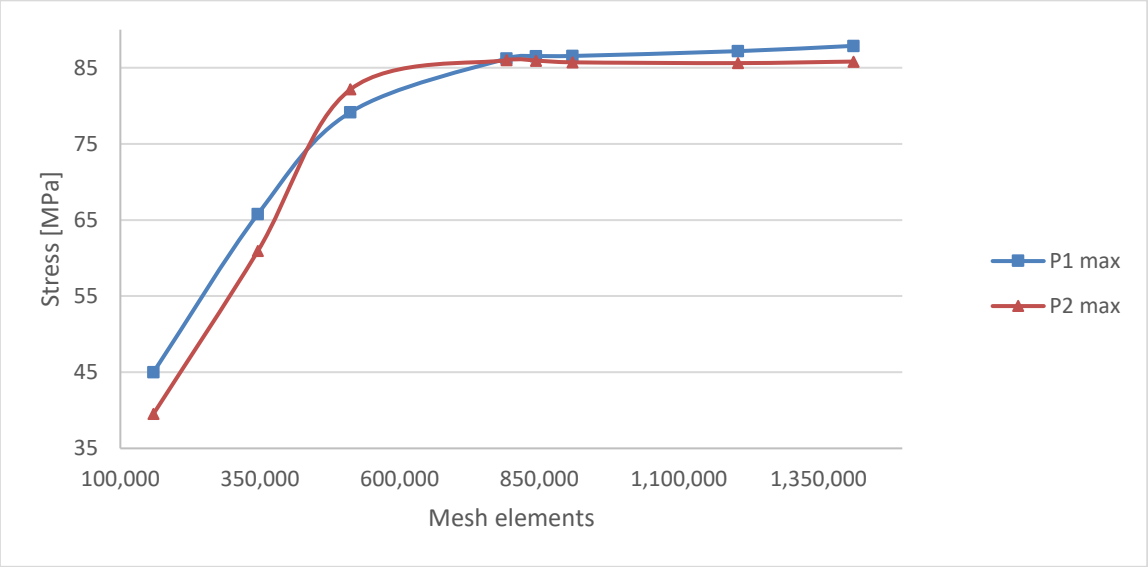

Figure 34: Mesh sensitivity of the Structural analysis.

The mesh sensitivity showed that the key point for the mesh elements was 960,582. The stress value at this point of elements differed from the last value less than 1%, then it was considered that the mesh converged.

3.5.2 Boundary Conditions

The boundary conditions applied for the Structural analysis were the pressures imported from CFX, the temperatures imported from the Thermal analysis, and the subjection of the turbine.

The pressure imported is shown in Figure 35, which was divided by the hub zone and the blades zone.

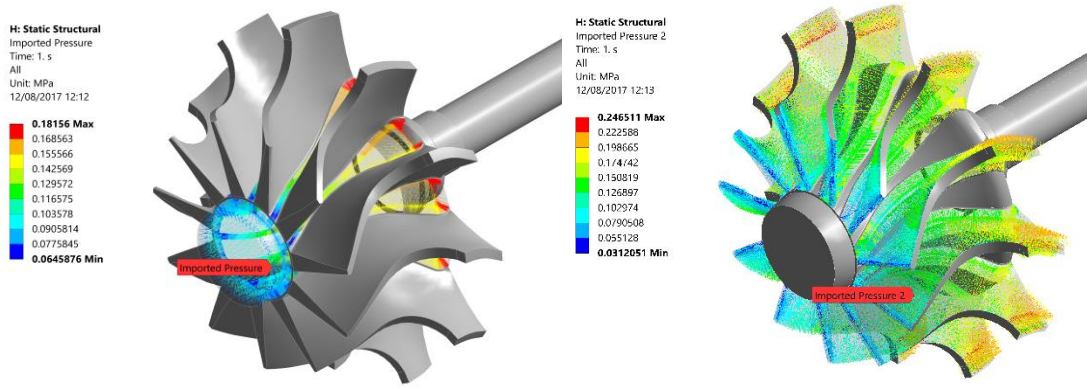

Figure 35: Imported pressure of the hub (left) and the blades (right).

The temperature imported is shown in Figure 36. It shows the body temperature of the turbine, which influences the stresses generated depending on the temperature of the point.

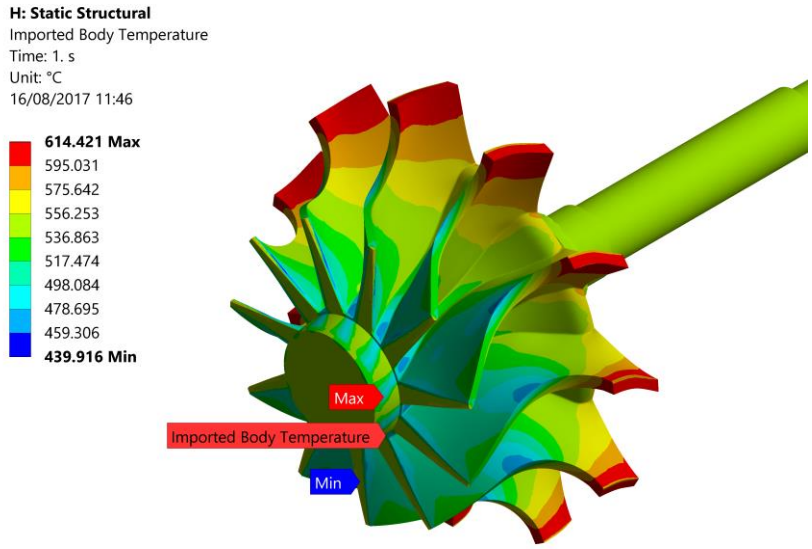

Figure 36: Imported temperature from Thermal analysis.

And the last input needed to specify was the subjection point of the turbine. It is shown in Figure 37. The exact subjection does not influence the stresses on the blade studied, since the stresses on the shaft were not studied.

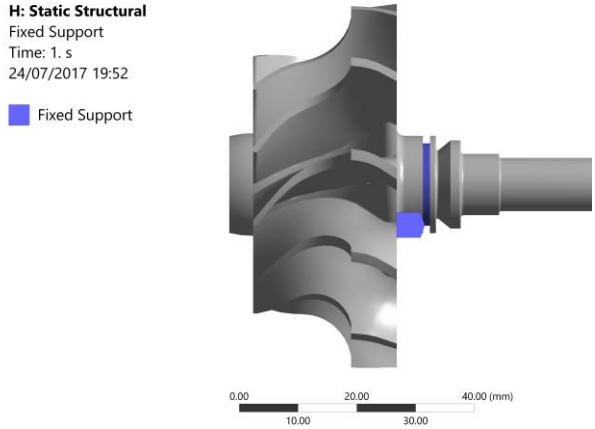

Figure 37: Subjection point of the turbine.

4 RESULTS AND ANALYSIS

4.1 CFX

The operating conditions for this geometry were not known. Therefore, to observe how the operating conditions influence the final stress generated on the geometry, a sensitivity analysis was done for the inlet pressure, the inlet temperature and the rotation speed.

The inlet pressure was studied between 2 and 4bar and the temperature at the inlet between 550 and 650°C (the maximum working temperature of Inconel 625 is approximately 650°C). Moreover, each of these ranges were simulated for the rotation speeds between 90,000 and 110,000rpm.

The outlet pressure was fixed during all the analysis at 1bar and the inflow angle at 70° with respect to the radial direction.

The results obtained for the Efficiency and Power with a rotation speed of 90,000rpm are shown in Figure 38 and Figure 39.

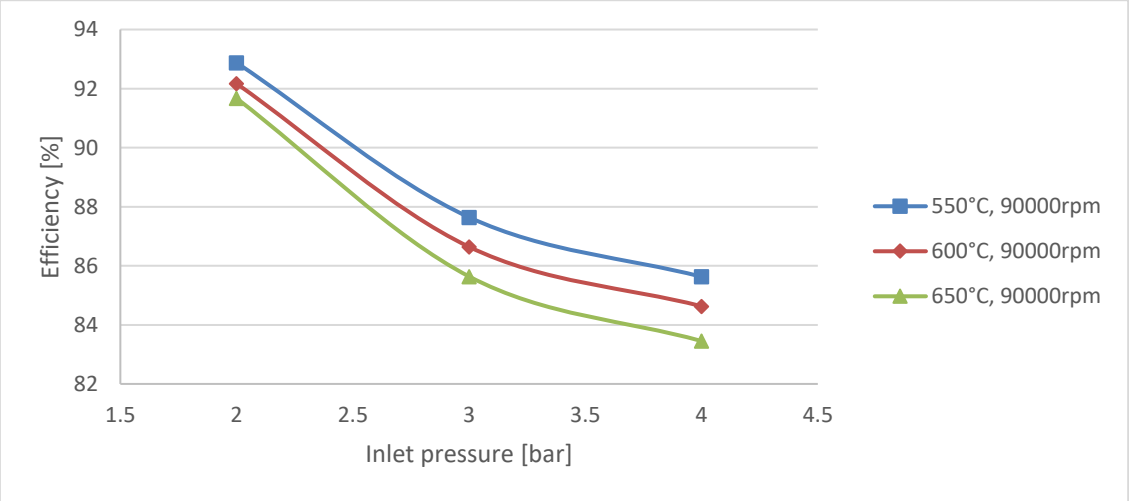

Figure 38: Efficiency versus Inlet pressure for a rotation speed of 90,000 rpm.

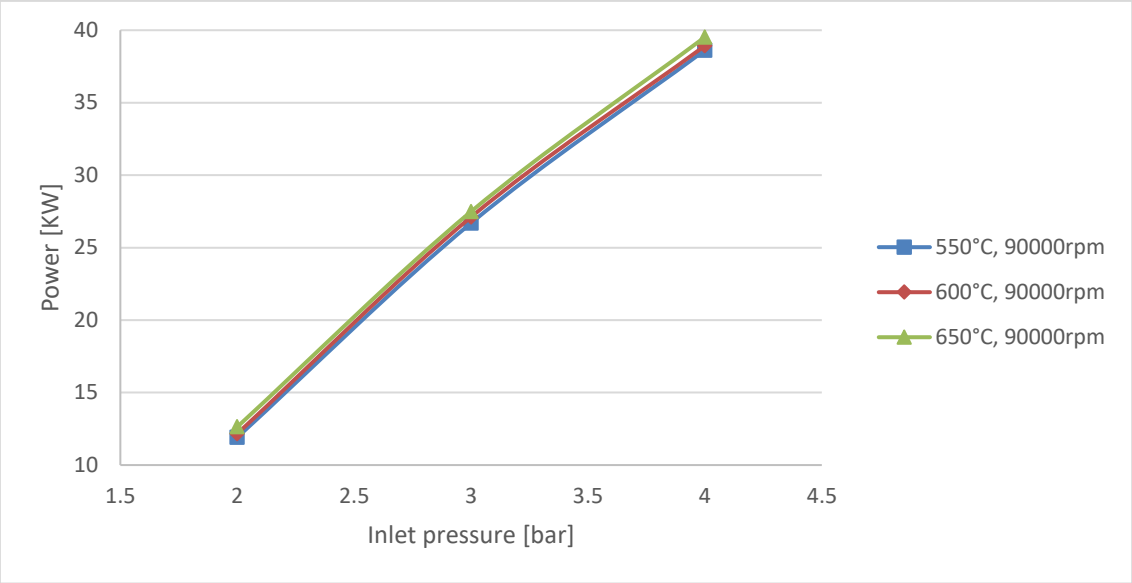

Figure 39: Power versus Inlet pressure for a rotation speed of 90,000rpm.

It is clear that when the pressure is 2bar, the efficiency does not change so much with the temperature variation, and the values are between 91.5 - 92.5%. However, when the pressure increases, the value for the efficiency starts to differ depending on the temperature, between 83 - 86%.

The power plot shows that the temperature does not have a considerable influence on the output power. However, the output power increases considerably when the inlet pressure arises (between 12 - 40kW). Moreover, with an increase of the temperature the output power slightly increases, but the efficiency decreases.

The same behaviour is shown in Figure 40 and 41, where the rotation speed was fixed to 100,000 rpm. However, the efficiency and power is slightly higher for this rotation speed than the efficiency and power for 90,000rpm.

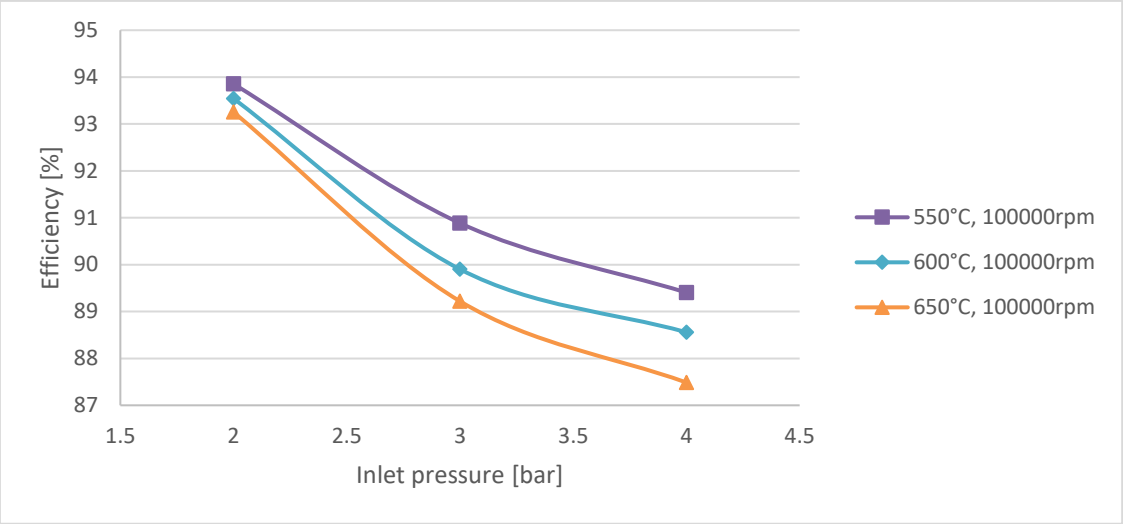

Figure 40: Efficiency versus Inlet pressure for a rotation speed of 100,000 rpm.

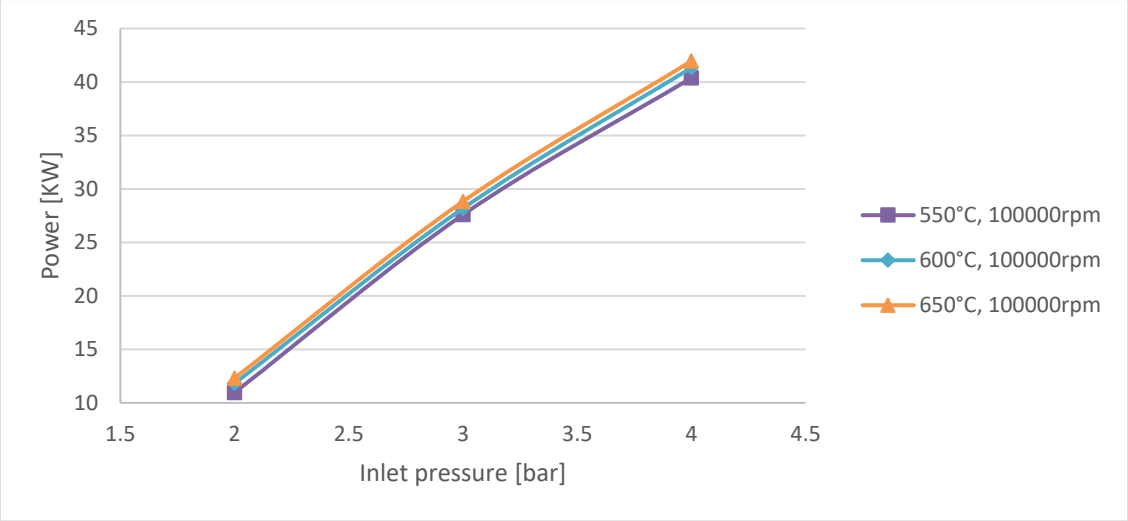

Figure 41: Power versus Inlet pressure for a rotation speed of 100,000rpm.

For a rotation speed of 110,000rpm, the behaviour obtained is quite different, especially when the inlet pressure is 2bar.

The plots are shown in Figure 42 and Figure 43.

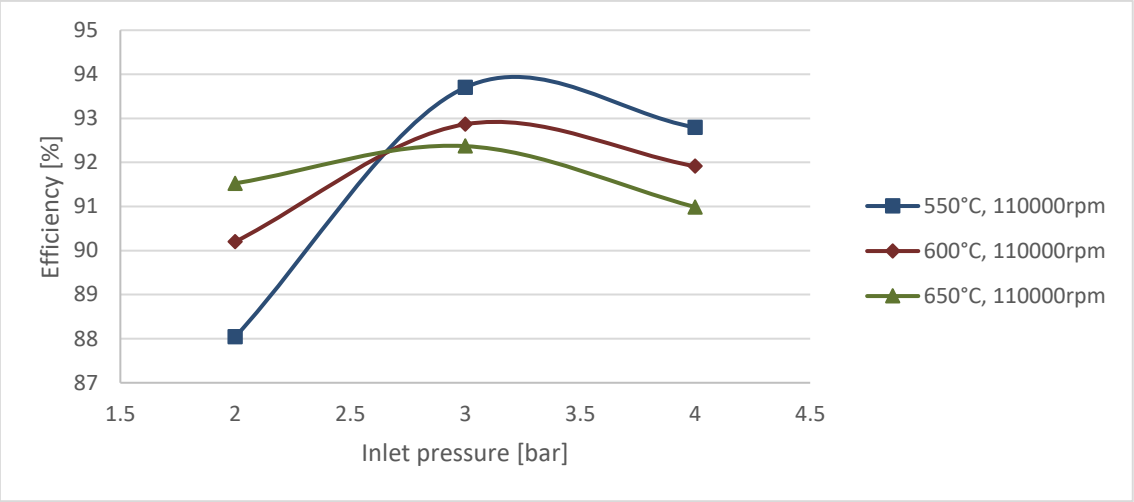

Figure 42: Efficiency versus Inlet pressure for a rotation speed of 110,000rpm.

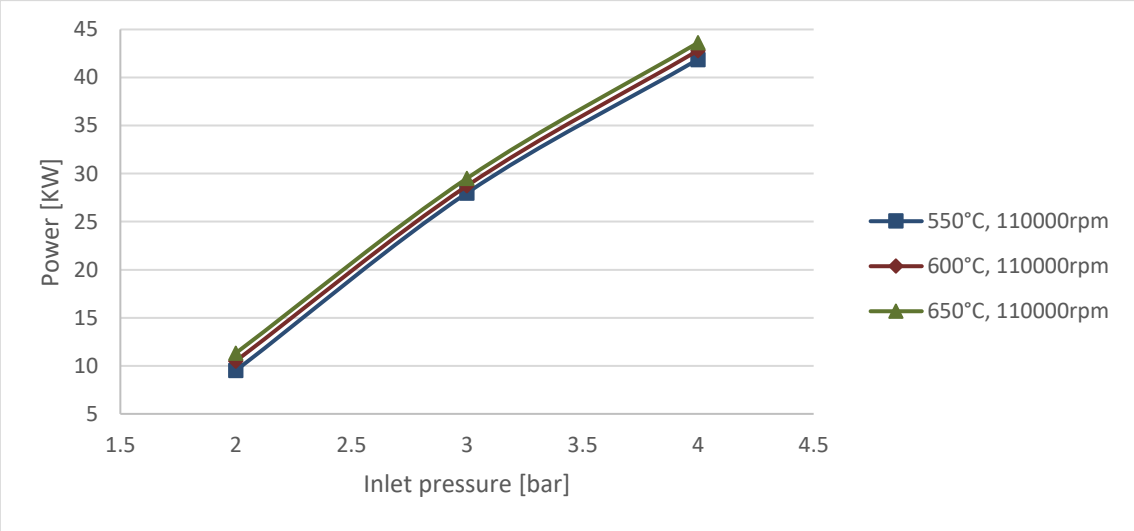

Figure 43: Power versus Inlet pressure for a rotation speed of 110,000rpm.

Figure 42 and Figure 43 show that the efficiency and output power when the inlet pressure is 2bar and the rotation speed 110,000rpm is lower than the efficiency and power obtained for 90,000 and 100,000rpm at the same pressure. This behaviour is due to the inflow angle which is not the right one. Compared with the flow when the inflow angle is the right one (Figure 44), this situation generates a vortex (Figure 45), thereby a decrease of the turbine efficiency.

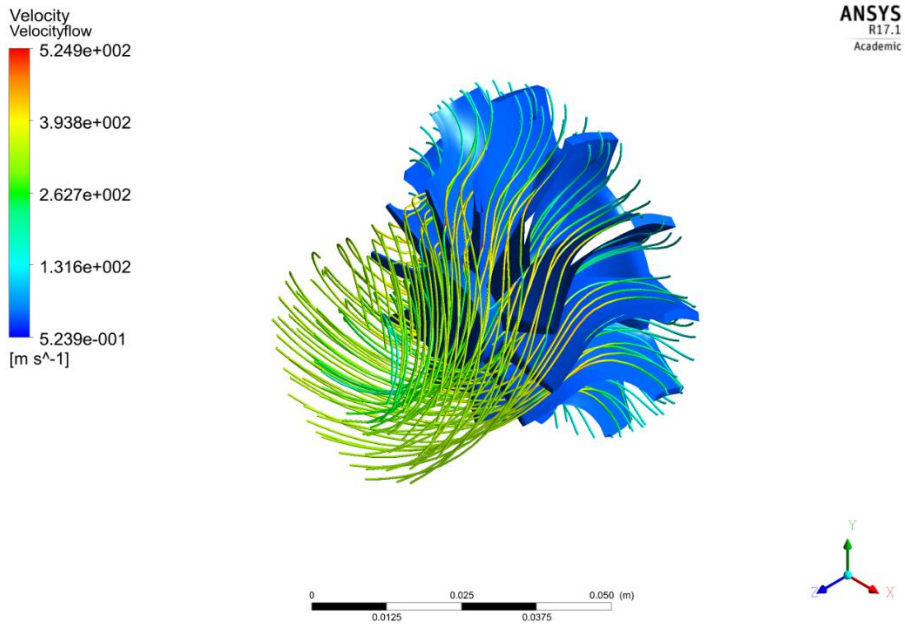

Figure 44: Velocity flow without vortex generation under operating conditions of P_{in} = 3bar, T_{in} = 650°C and rotation speed 110,000rpm.

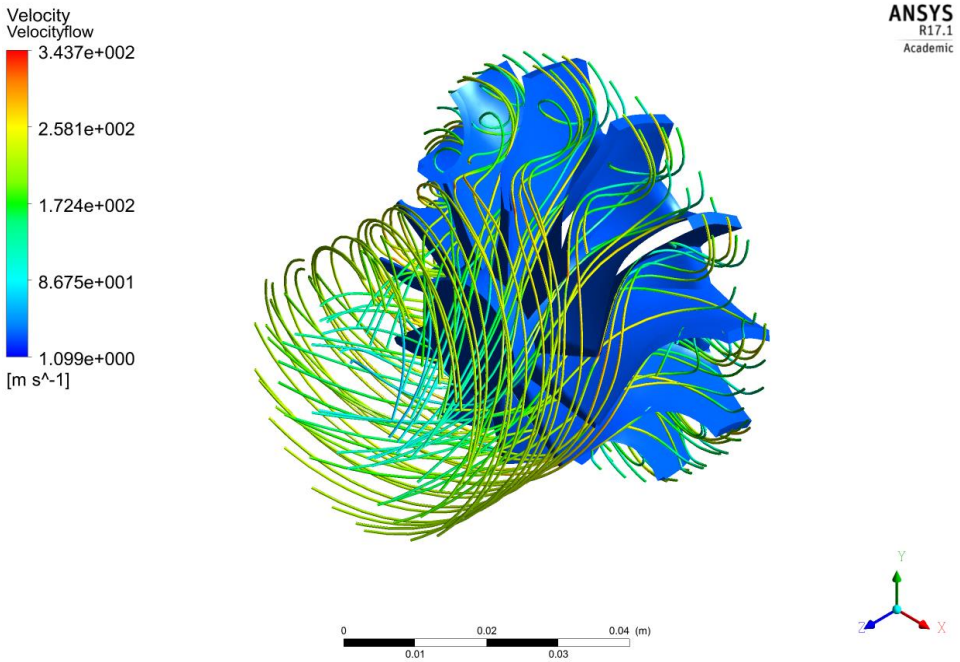

Figure 45: Velocity flow with vortex generation under operating conditions of P_{in} = 2bar, T_{in} = 550°C and rotation speed 110,000rpm.

4.2 Thermal analysis

Since this step is not relevant for the study and is only a transition between the input parameters at the initial part of the model and the final stresses calculated at the output, in this section is explained only the temperature distribution for a turbine under the operating conditions of P_{in} = 3bar, T_{in} = 650°C and a rotation speed of 110,000rpm, which generates an output power of 29.5kW and an efficiency of 92.4%. The behaviour against the temperature can be extrapolated to the other operating conditions studied in this thesis.

The results show that the maximum temperature is located at the inlet point of the turbine, where the hot inlet flow insides. The temperature decreases through the blade from the inlet to the outlet. For this case, the flow temperature at the inlet part of the turbine has approximately 620°C as can be seen in the Figure 46, and this flow generates a temperature on the turbine geometry of 614°C at the inlet part (Figure 47). Following the same criteria, the flow temperature at the outlet is 470°C, thereby a temperature of 440°C at the outlet part of the turbine.

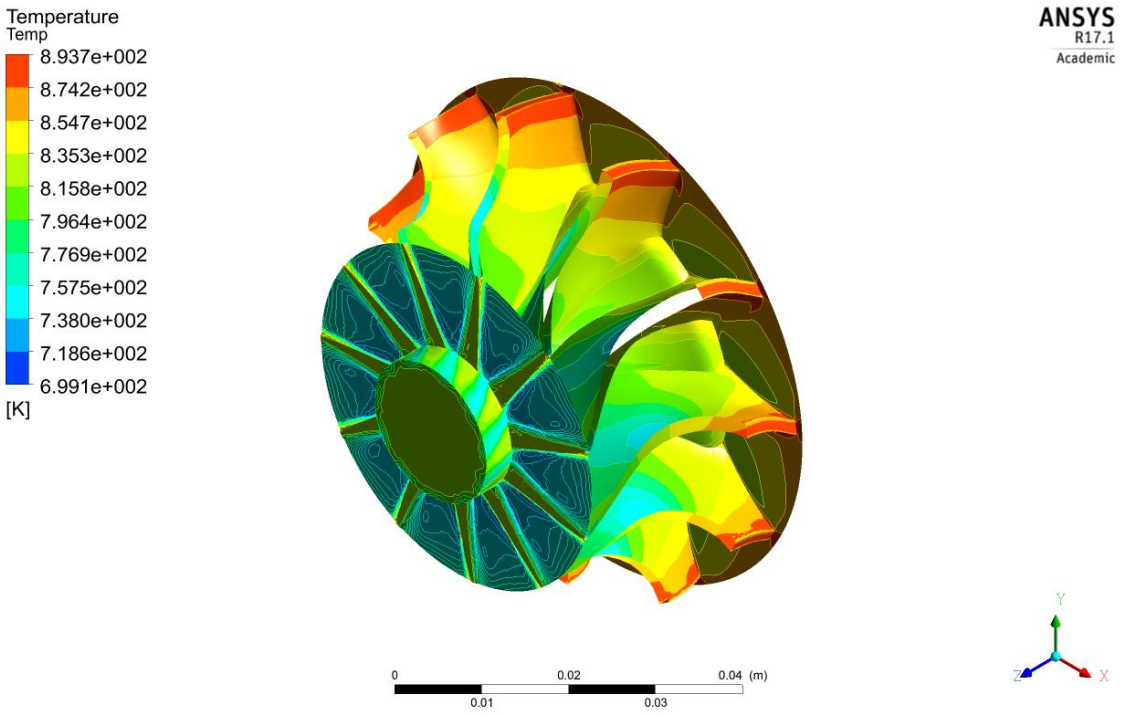

Figure 46: Flow temperature distribution on the turbine surface under operating conditions of P_{in} = 3bar, T_{in} = 650°C and rotation speed 110,000rpm.

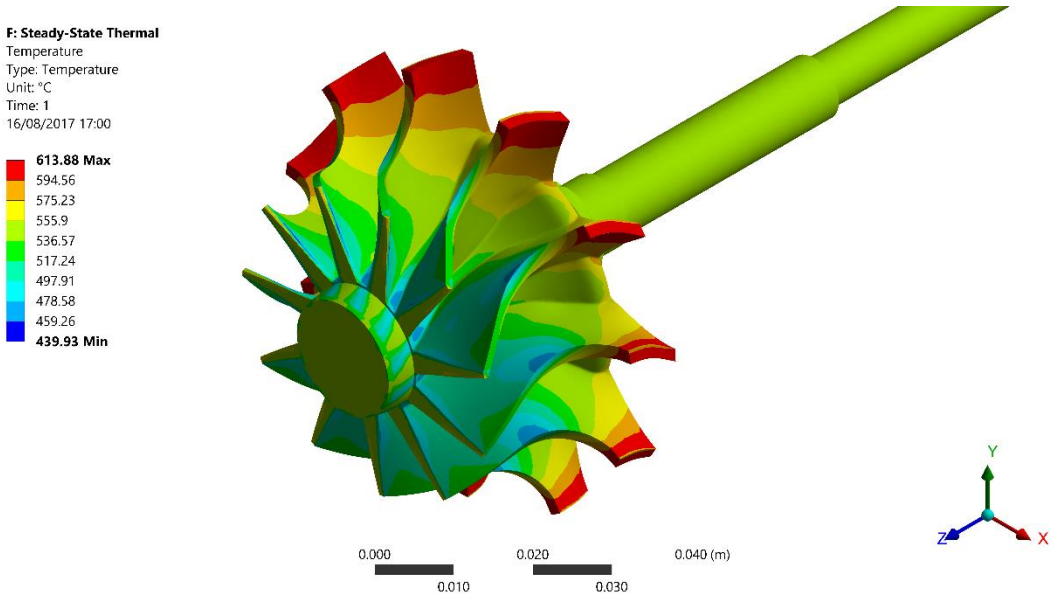

Figure 47: Turbine body distribution under the operating conditions of P_{in} = 3bar, T_{in} = 650°C and rotation speed 110,000rpm.

4.3 Structural analysis

This is the key analysis for this project because it allows obtaining the stress generated on the turbine depending on the operating conditions.

The stresses distribution differs slightly between all the operating conditions analysis. They have different stress values, but the maximum stresses are located approximately at the same place. Due to this, as an overview of the stress distribution on the turbine, the results explained in Figures 48 and 49 are obtained when the geometry works under the operating conditions of P_{in} = 3bar, T_{in} = 650°C and a rotation speed 110,000rpm.

Figure 48 shows the stress distribution when the micro-turbine is manufactured with the SLM. The results compared with the turbine manufactured with casting in Figure 49 are slightly different, but not a big difference is observed because the exact values are not appreciated. However, on the edge between the blades and the hub it is possible to appreciate that the stress at the middle of the edge is higher for the SLM manufactured turbine. This behaviour is studied more in depth in sections 4.3.1, 4.3.2, 4.3.3.

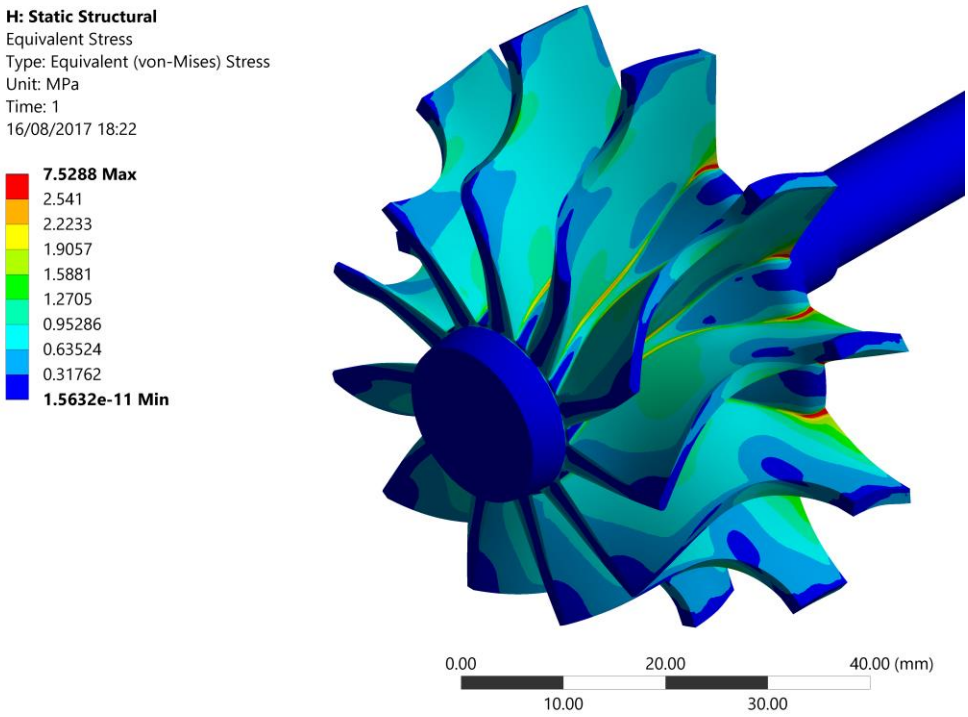

Figure 48: Stress distribution on a turbine manufactured with SLM and under the operating conditions of P_{in} = 3bar, T_{in} = 650°C and rotation speed 110,000rpm.

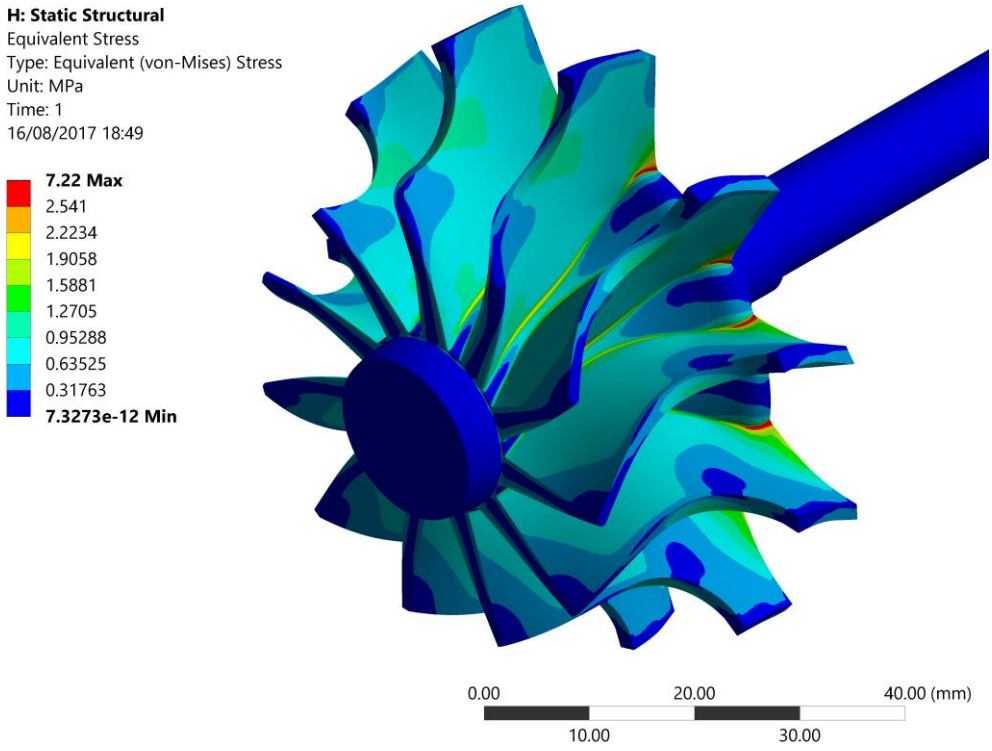

Figure 49: Stress distribution on a turbine manufactured with Casting and under the operating conditions of P_{in} = 3bar, T_{in} = 650°C and rotation speed 110,000rpm.

The stress comparison between the different operating conditions and the both types of manufacturing is focused on the joint edge between the blades and the hub because it is the edge which concentrates the highest stresses. The path and the direction can be seen in Figure 50.

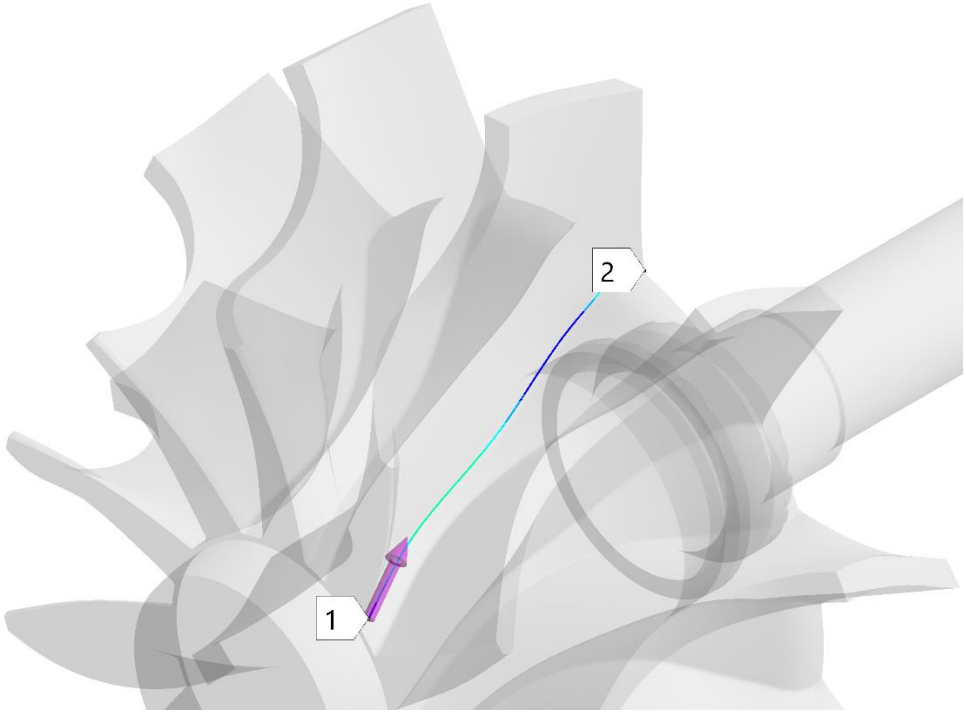

Figure 50: Path to calculate the stresses generated.

4.3.1 Structural analysis results for a rotation speed of 90,000rpm

In this section, the results for the lower rotation speed studied are explained. The rotation speed is 90,000rpm and the stress results on the path can be seen in Figure 51 for the Inconel manufactured with casting, and in Figure 52 for the Inconel manufactured with SLM.

After plotting the stress results from ANSYS Structural, the results give the differences between one type of manufacturing and the other, and how they are related to the operating conditions. For both types of manufacturing, the maximum stress is generated at the end of the path, where the inflow insides the turbine geometry. The highest stress is achieved for the harshest operating conditions studied of T_{in} = 650°C and P_{in} = 4bar. Both plots show that when the temperature at the inlet increases, the stress visibly increases where the higher

stress is located, and moderately where the stress is lower. Moreover, the stress increases notably when the inlet pressure arises. Moreover, the maximum stress changes more from 2 to 3bar than from 3 to 4bar. Therefore, the behaviour against the operating conditions is approximately the same for both types of manufacture.

However, the stress distribution changes from one type of manufacturing and the other, the plots show how the stress fluctuation is relatively higher for the SLM, and this fluctuation increases with the increment of the inlet pressure, which can induce a higher fatigue, and consequently a decrease of the useful life of the turbine, if the geometry works under hard operating conditions.

All the following stress values are taken from the curves with 650ºC. The stress when X = 9.5mm achieves one of the maximums (0.74MPa) at the middle zone of the blade for casting manufacture, when P_{in} = 2bar. The maximum stress point in that zone when the manufacture is SLM is at X = 10.1mm (0.83MPa). When P_{in} = 3bar this point is X = 8.2mm (Casting 1.84MPa) and X = 9.8mm (SLM 2MPa). For P_{in} = 4bar, the maximum stress point at the middle of the blade zone is X = 8.2mm (Casting 3.15MPa, SLM 3.4MPa) for both types of manufacture.

When P_{in} = 2bar, the stress at the minimum stress zone fluctuates due to the generation of small vortex on the blade. For the casting, the minimum stress point is at X = 22.8mm (0.47MPa), and for SLM the point is at X = 19.3mm (0.32MPa). Following the same criteria, for P_{in} = 3bar, the minimum stress appears for both types of manufacture at X = 20.7mm (Casting 1.14MPa, SLM 0.94MPa). Looking at the curves when the inlet pressure is 4bar, the minimum stress is generated at X = 21.2mm (Casting 1.67MPa, SLM 1.39MPa).

The maximum stress for the casting is generated at the end of the studied path, and the maximum values for each pressure is when T_{in} is 650°C. The values for 2bar, 3bar and 4bar and 650°C for the casting are 2.26MPa, 5.04MPa and 6.92MPa respectively, and 2.14MPa, 4.87MPa and 6.71MPa for the SLM.

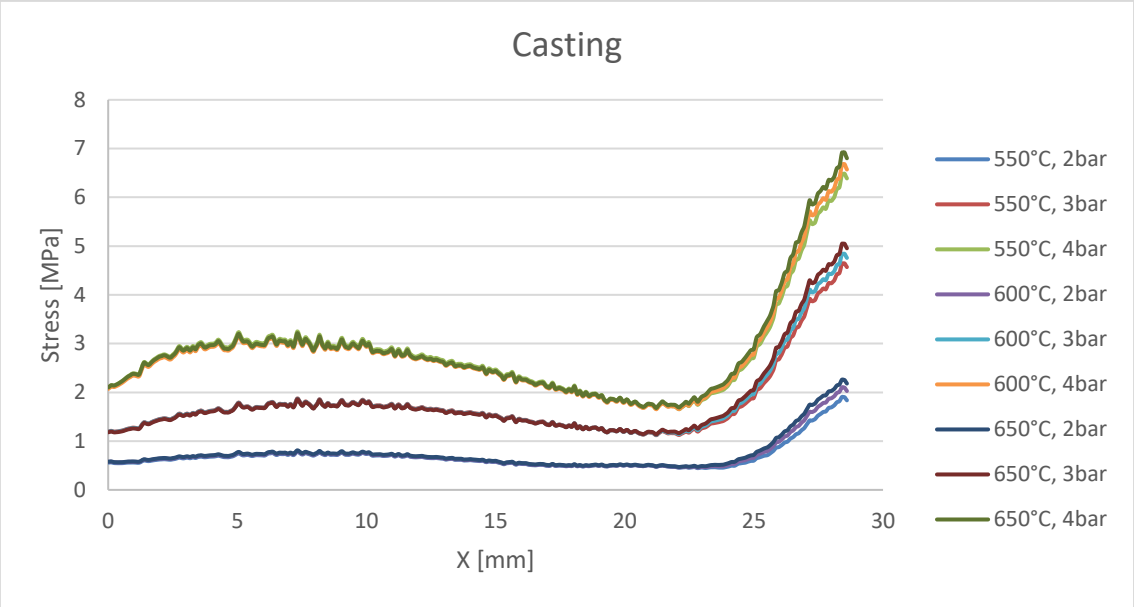

Figure 51: Stress vs X under different operating conditions, 90,000rpm and Inconel 625 (Casting).

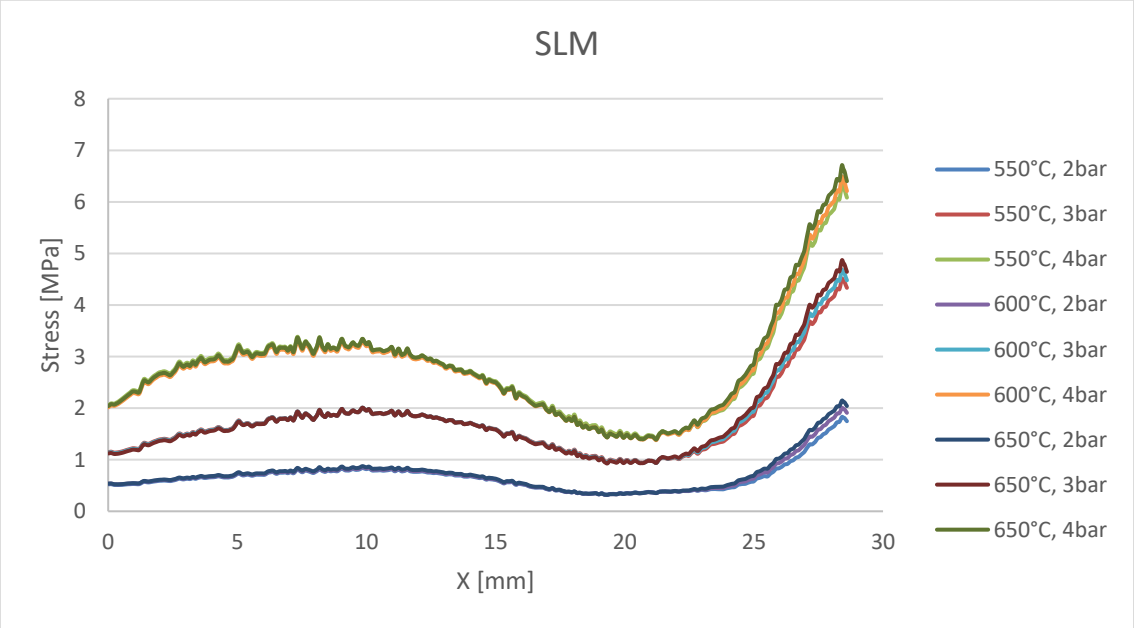

Figure 52: Stress vs X under different operating conditions, 90,000rpm and Inconel 625 (SLM).

Figure 53 shows the percentage of difference between the stress values explained above for each type of manufacture. The plot shows that the difference is influenced by the pressure and the stress value. When the inlet pressure

increases, the difference decreases, and when the stress value increases the difference value also decreases.

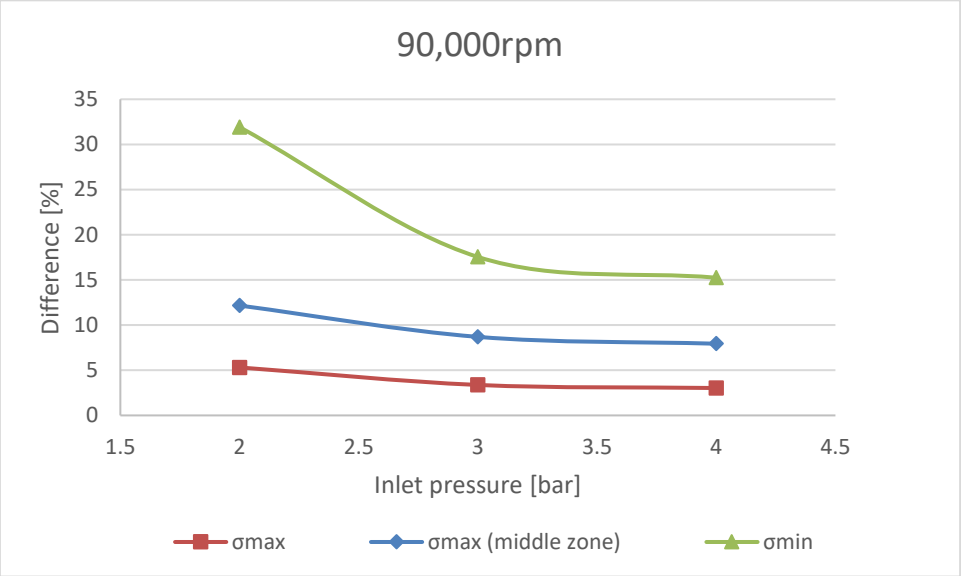

Figure 53: Difference between the values for Casting and SLM versus the inlet pressure for 90,000rpm.

4.3.2 Structural analysis results for a rotation speed of 100,000rpm

In the same way, for 100,000rpm, the plots in Figures 54 and 55 show the same behaviour against the increment of pressure and temperature explained above.

Concerning the points with maximum stress at the middle zone of the edge when the inlet temperature is 650°C, the values for P_{in} = 2bar are X = 8.2mm (Casting 0.74MPa) and X = 9.85mm (SLM 0.81MPa). For P_{in} = 3bar, the values are X = 7.33mm (Casting 1.84MPa) and X=9.04mm (SLM 1.97MPa) and for P_{in} = 4bar, X = 5.05mm (Casting 3.23MPa) and X = 8.2mm (SLM 3.4MPa).

The minimum stress when T_{in} = 650°C and for P_{in} = 2bar is located at X = 23.8mm (Casting 0.42MPa) and X = 19.2mm (SLM 0.31MPa). When P_{in} = 3bar, the values are X = 22.1mm (Casting 1.10MPa) and X = 21.2mm (SLM 0.92MPa) and for P_{in} = 4bar are X = 22.1mm (Casting 1.63MPa) and X = 20.7mm (SLM 1.4MPa).

The maximum stress values appear also at the end of the path. For P_{in} = 2bar, the maximum stress value is 1.66MPa for casting and the lower value of 1.58MPa for SLM. When P_{in} = 3bar, the value is 4.33MPa for casting and 4.19MPa for SLM,

and for P_{in} = 4bar the casting value of 5.97MPa is also higher than the SLM value of 5.82MPa.

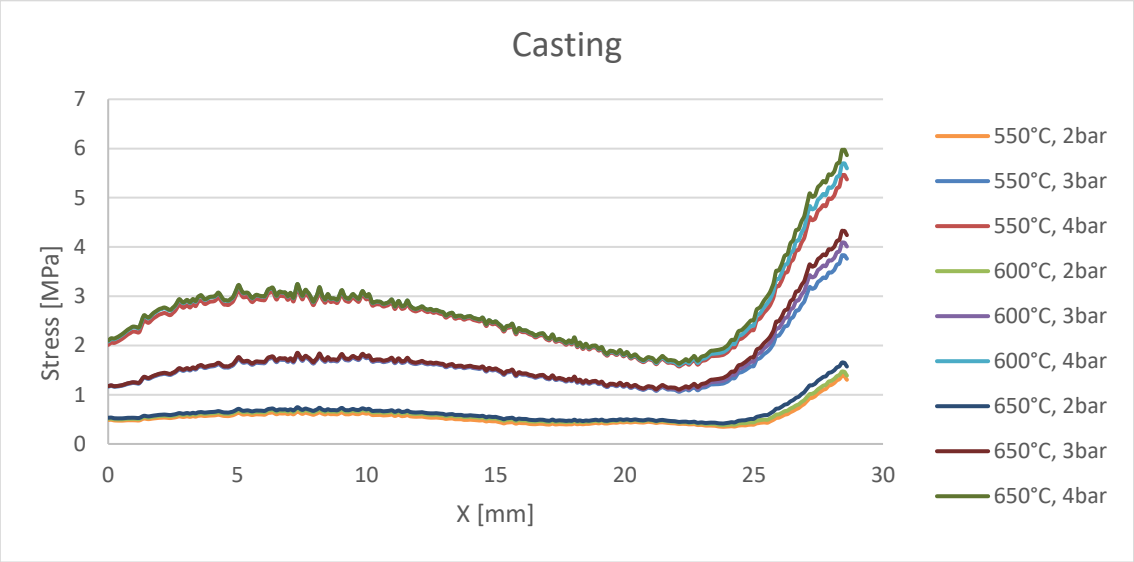

Figure 54: Stress vs X under different operating conditions, 100,000rpm and Inconel 625 (Casting).

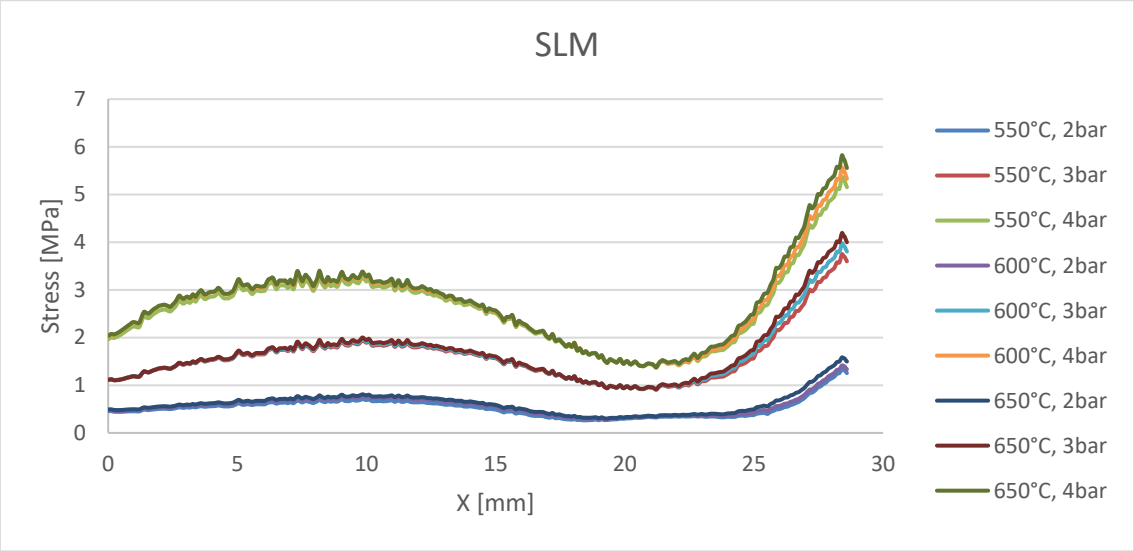

Figure 55: Stress vs X under different operating conditions, 100,000rpm and Inconel 625 (SLM).

As it is done at the previous section 4.3.1, Figure 56 shows how the difference between the values of stress between the casting manufacture and the SLM manufacture decrease with the increment of the pressure and the stress value.

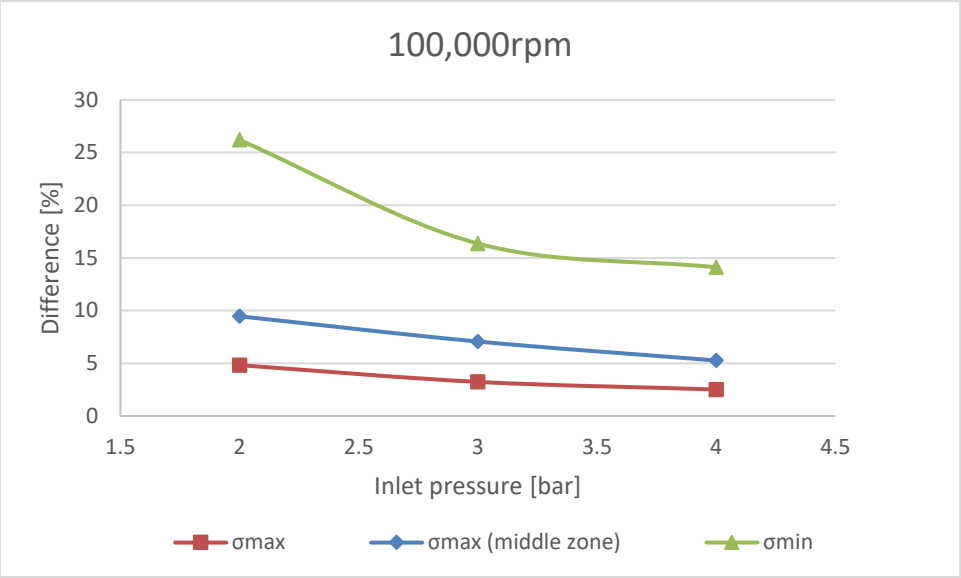

Figure 56: Difference between the values for Casting and SLM versus the pressure with 100,000rpm.

4.3.3 Structural analysis results for a rotation speed of 110,000rpm

The same explanation than sections 4.3.1 and 4.3.2 can be used for a rotation speed of 110,000rpm, the plots in Figures 57 and 58 shows the same behaviour against the increment of pressure and temperature. However, for this rotation speed, the pressure when the inlet pressure is 2bar and the inlet temperature 550°C has a different behaviour than the other rotation speeds. This is because of the higher pressure on the blade at the inlet induced by the vortex generated.

The points with maximum stress at the middle zone of the edge for this rotation speed are X = 7.32mm (Casting 0.66MPa) and X = 9.85mm (SLM 0.72MPa) for P_{in} = 2bar. For P_{in} = 3bar, the values are X = 7.33mm (Casting 1.78MPa) and X= 9.85mm (SLM 1.93MPa), and for P_{in} = 4bar are X = 7.33mm (Casting 3.18MPa) and X = 9.9mm (SLM 3.32MPa).

The minimum stress for P_{in} = 2bar is located at X = 24.3mm (Casting 0.35MPa) and X = 18.5mm (SLM 0.26MPa). When P_{in} = 3bar, the minimum stress points are X = 22.1mm (Casting 1.05MPa) and X = 21.2mm (SLM 0.89MPa) and for P_{in} = 4bar the values are X = 22.1mm (Casting 1.56MPa) and X = 21.1mm (SLM 1.38MPa).

The maximum stress when T_{in} = 650°C appears also at the end of the path, for P_{in} = 2bar the casting value is 1.06MPa and the value for SLM is 1.04MPa. For P_{in} = 3bar is 3.41MPa for casting and 3.34MPa for SLM, and for P_{in} = 4bar, 4.92MPa is the maximum stress value for casting and 4.85MPa for SLM.

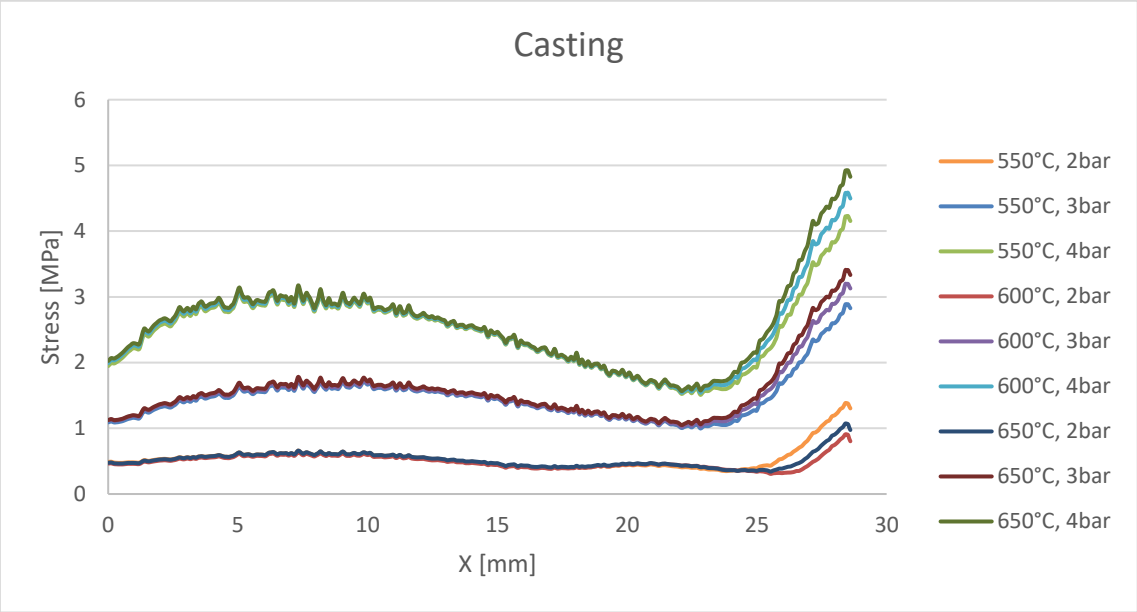

Figure 57: Stress vs X under different operating conditions, 110,000rpm and Inconel 625 (Casting).

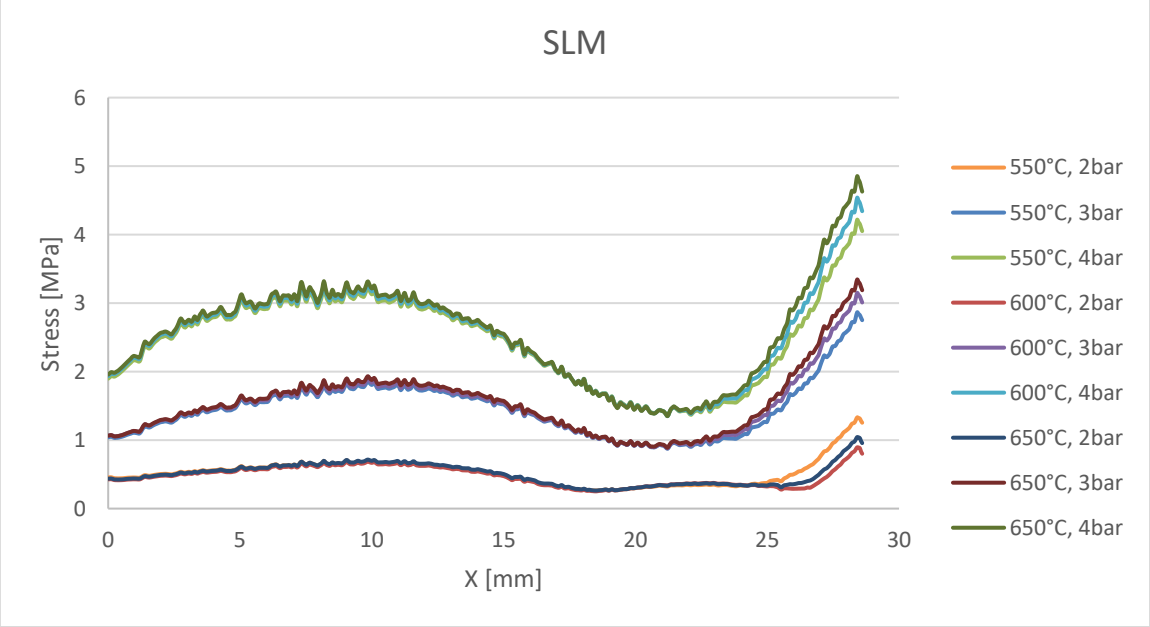

Figure 58: Stress vs X under different operating conditions, 110,000rpm and Inconel 625 (SLM).

In Figure 59 can be seen the differences between the values studied for casting and SLM follow the same trend than the values studied in sections 4.3.1 and 4.3.2, but for 110,000rpm, the difference for the stress values at higher pressure are lower than the values obtained at 90,000rpm and 100,000rpm.

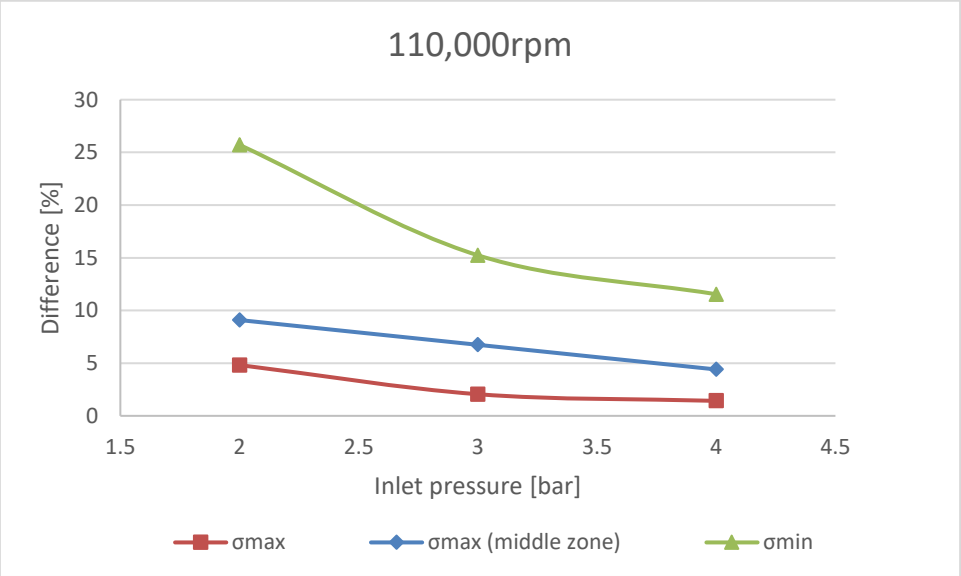

Figure 59: Difference between the values for Casting and SLM versus the pressure with 100,000rpm.

4.3.4 Comparison

The studied path points for the σ_{max} at the middle zone in Figure 60 shows how the SLM manufactured turbine has always higher stress at these points, and it increases with the pressure. The trend for the stress at this point is to decrease with the increment of rotation speed.

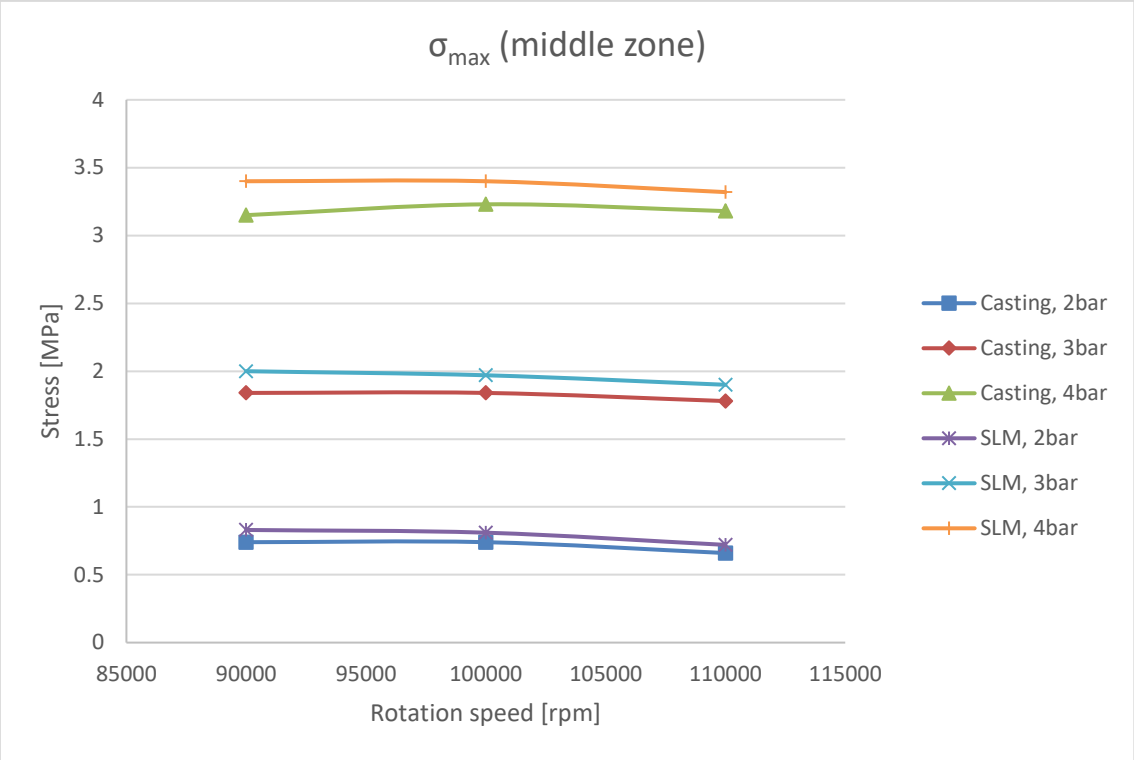

Figure 60: Stress versus rotation speed for σ_{max} (middle zone).

Figure 61 with σ_{min} shows approximately the same behaviour, but with a significant difference, the SLM manufactured turbine has always the lower minimum stress. The same behaviour can be seen in Figure 62, where the maximum stress is plotted for the different pressures and rotation speeds. It also shows how the stress for the casting is higher than the SLM manufactured turbine. This behaviour is due to the proximity to the free surface and the anisotropy of the material. Moreover, another important thing to explain is that the stress becomes also equal for both types of manufactures when the pressure and the rotation speed increase.

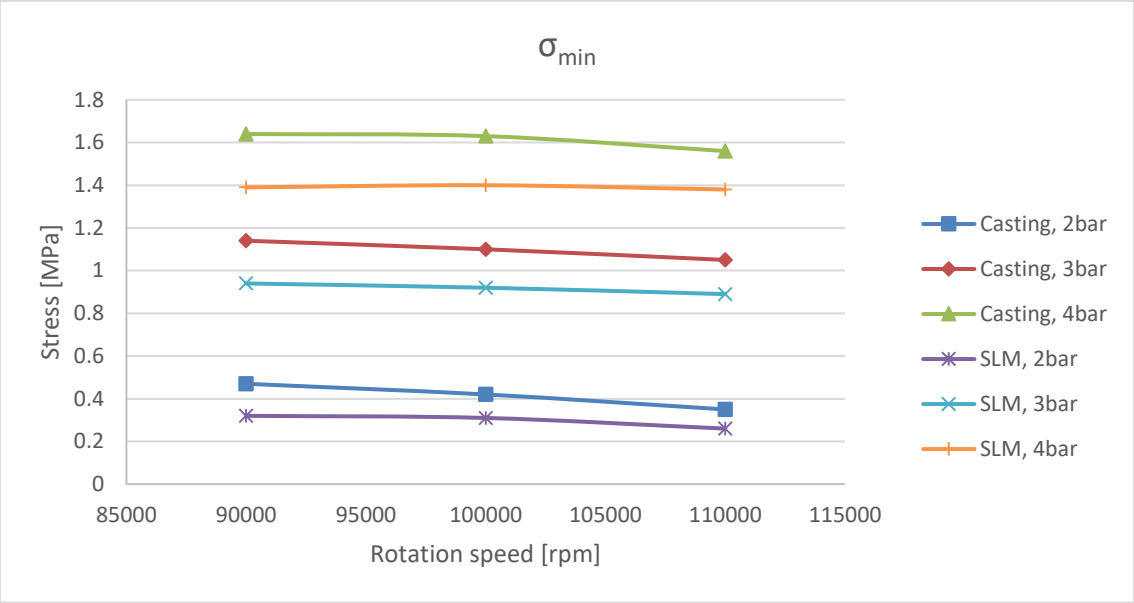

Figure 61: Stress versus rotation speed for σ_{min}.

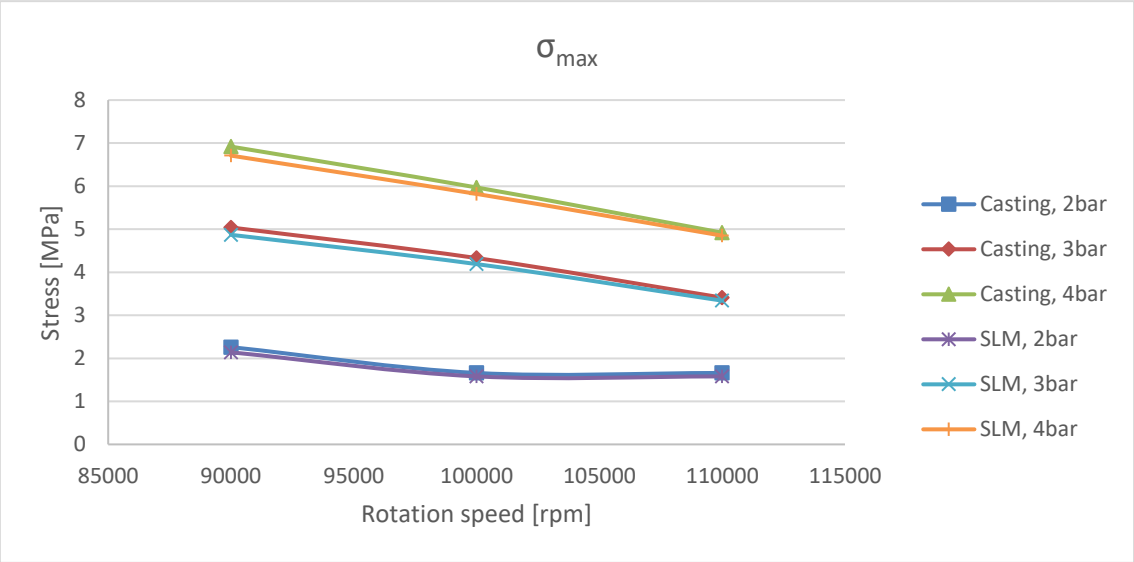

Figure 62: Stress versus rotation speed for σ_{max}.

To conclude the structural analysis, section 4.3, Figure 63 shows how the difference between the SLM manufacture and the casting manufacture decreases when the stress increases. Furthermore, when the rotation speed arises, the difference decreases together with the pressure.

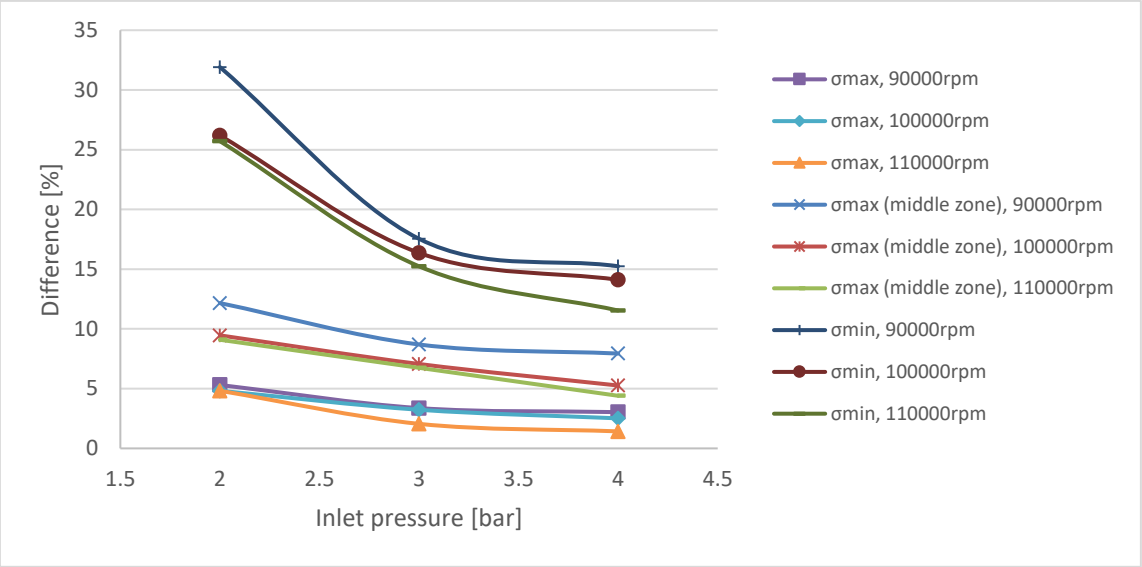

Figure 63: Difference between casting and SLM results versus Inlet pressure comparison.

5 DISCUSSION

Several points can be extracted from the results and analysis section. Firstly, concerning the overall performance of the turbine. When the inlet pressure is low the overall efficiency is less influenced by the temperature, an increment of the inlet pressure generates an increase of output power, if the temperature rises the output power is higher but the overall efficiency decreases. Moreover, when the rotation speed increases, the inflow angle may change to avoid the vortex generation, because the presence of a vortex decreases the efficiency and the output power.

Secondly, with reference to the operating conditions influencing the stress distribution, the stress on the blade base increases when the inlet pressure of the turbine increases, however, it increases more from 2 to 3bar than from 3 to 4bar. The inlet temperature generates an increase of the stress, but it is only noticeable at the inlet part of the turbine, where the temperatures and stresses are higher. Furthermore, if a vortex appears on the turbine blade, the stress at the inlet zone becomes higher.

Thirdly, regarding the study of the impact introduced on a micro-turbine due to SLM manufacture. It includes the impact of the SLM manufacture compared with the investment casting, the traditional manufacturing and widely used for micro-turbines manufacturing. The difference between both types of manufacturing declines with the increase of the inlet pressure and with the increase of the rotation speed as it was seen in Figure 63. The higher stress difference between both types of manufacturing is reached by σ_{min}, followed by the point with maximum stress at the central zone of the path studied and σ_{max} respectively. Furthermore, the stress at the point with maximum stress at the central path zone is higher for the SLM manufacture in contradistinction to the σ_{min} and σ_{max} points. This behaviour is due to the proximity of σ_{max} to the free surface and the anisotropy of the material. The decrease of the σ_{max} for SLM manufacture influences the σ_{min} point, generating also a lower stress for this point than the casting manufacturing. Therefore, the SLM manufacture generates lower stress at the inlet part of the turbine, and higher stress at the outlet.

Therefore, several conclusions are extracted from the study. The joint between the blade and the hub is the critical area of the turbine for the two types of manufacturing and the turbine manufactured by SLM has lower stress at the inlet part than the turbine manufactured by casting. However, the stress generated at the middle of the critical area is higher for the turbine manufactured by casting. This shows the necessity to consider the type of manufacturing before to start the production, in order to strengthen the areas affected by the anisotropy (specially the middle of the critical area, where the stress fluctuation is higher). Moreover, the increase of the stress in this area and the necessity to reinforce it, can create design problems. As well as, the reliability of materials manufactured by selective laser melting is lower than casting and the final results depend a lot on the right study of the optimum conditions (velocity, laser power, working atmosphere, etc.) of the manufacturing process. If these conditions are not the optimum, the variability of the mechanical properties introduced, generates more variability at the middle of the critical area, giving the possibility to appear higher stresses where it was not expected and in consequence higher fatigue.

6 CONCLUSIONS AND FUTURE RESEARCH

The overall aim of this thesis was to determine the impact that additive manufacture have on a micro-turbine wheel. This was assessed through a Workbench 17.1 model, including a CFX analysis, a Thermal analysis and a Structural analysis to calculate the stress generated on the turbine.

To conclude, the results obtained from the Workbench model are:

- The critical area is the joint between the blade and the hub for both types of manufacturing.
- If the type of manufacturing is SLM, it needs to be determined before the micro-turbine design to avoid problems at the middle of the critical area and reinforce it.
- The stress fluctuation at the critical zone is higher for SLM and can increase the stress fatigue.
- The reliability of materials manufactured by SLM is lower allowing the possibility to future problems.

However, the results of this thesis are obtained with a CFD and FEA model and using an approximation of the material properties for both manufacturing processes due to the inaccessibility to the real data. Therefore, a further study should be carried out, studying through an experimental method the real properties and stresses generated, in order to compare them with the results of the model designed in this thesis. Moreover, this thesis can be complemented by the study of varied materials and several types of additive manufacturing, and finding what is the best for the micro-turbines manufacturing. Another improvement can be the study of the rugosity introduced on the microturbine surface due to the additive manufacturing processes, what can influence the aerodynamics of the turbine.

REFERENCES

Aller, M. (2016) *Advanced Materials and Processes for the Next Generation of Gas Turbine Design*., *Power Engineering* Available at: http://www.power-eng.com/articles/print/volume-120/issue-9/features/advanced-materials-and-processes-for-the-next-generation-of-gas-turbine-design.html (Accessed: 23 May 2017).

ANSYS (2017) *ANSYS CFX*. Available at: www.ansys.com/products/fluids/ansys-cfx (Accessed: 20 July 2017).

Arcam (2016) '*JUST ADD: Arcam – the innovative leader in additive manufacturing solutions for the production of orthopedic implants and aerospace components.*', p. 19.

Cadorin, M. et al. (2012) 'Analysis of a Micro Gas Turbine Fed by Natural Gas and Synthesis Gas: MGT Test Bench and Combustor CFD Analysis', *Journal of Engineering for Gas Turbines and Power*, 134(7), p. 71401.

Caresana, F. et al. (2010) 'Micro Gas Turbines', *Journal of Gas Turbines.*

Element® (2016) *DMLS vs SLM 3D Printing for Metal Manufacturing*. Available at: https://www.element.com/nucleus/2016/06/29/dmls-vs-slm-3d-printing-for-metal-manufacturing (Accessed: 2 June 2017).

Epstein, A.H. (2004) 'Millimeter-Scale, Micro-Electro-Mechanical Systems Gas Turbine Engines', *Journal of Engineering for Gas Turbines and Power*, 126(2), p. 205.

Estrada, C. a (2007) 'New Technology Used in Gas Turbine Blade Materials .', *Scienctia et Technica Año XIII*, (36), pp. 297–301.

Fry, T. (n.d.) '*Residual Stresses in Materials at High Temperature: The Link to Hardness and Scale Exfoliation*', (March 2009)

General Electric (2016) *POWERing the World: Gas power systems catalog.*

Gillette, S. (2010) *Microturbine Technology Matures*., *Journal of Energy and*

Power Engineering.

Goli, K.C. et al. (2015) ‘Principles and Working of Microturbine’, *Ijiert*, pp. 1–7.

Hanzl, P. et al. (2015) ‘The influence of processing parameters on the mechanical properties of SLM parts’, *Procedia Engineering*, pp. 1405–1413.

HIETA Technologies. (n.d.) *SLM Process*. Available at: https://www.hieta.biz/our-products/cooled-turbine-wheel (Accessed: 15 June 2017).

Hohloch, M. et al. (2017) ‘*EXPERIMENTAL CHARACTERIZATION OF A MICRO GAS TURBINE TEST RIG*’, pp. 1–11.

Jain, S. et al. (2015) ‘*Study on the Parameters Influencing Efficiency of Micro-gas Turbines*’, pp. 1–9.

James, A. (2015) ‘Advanced Manufacturing for Large Industrial Gas Turbines’, *UTSR Workshop*. Atlanta.

Kauthalkar, S.P. et al. (2013) ‘*Analysis of Thermal Stresses Distribution Pattern on Gas Turbine Blade using Ansys*’, 1(2), pp. 1–10.

Kingsbury, I. (n.d.) ‘*Hydrodynamic bearings*’

Krishnakanth, P.V. et al. (2013) ‘Structural & Thermal Analysis of Gas Turbine Blade by Using F.E.M’, *International Journal of Scientific Research Engineering & Technology*, 2(May), pp. 60–65.

Li, S. et al. (2015) ‘Microstructure Characteristics of Inconel 625 Superalloy Manufactured by Selective Laser Melting’, *Journal of Materials Science and Technology*, 31(9), pp. 946–952.

Morgan Advanced Materials (2017) *Ceramic Injection Moulded Components*. Available at: http://www.morgantechnicalceramics.com/en-gb/products/ceramic-injection-moulded-components/ (Accessed: 2 June 2017).

Ramamurthy, S. and Thennavarajan, S. (2008) ‘*Cost Effective Method for Manufacturing Micro Gas Turbine Components*’.

Roberto Capata (2015) ‘Experimental Tests of the Operating Conditions of a

Micro Gas Turbine Device', *Journal of Energy and Power Engineering*, 9(4).

Rosa Do Nascimento, M.A. et al. (2013) '*Micro Gas Turbine Engine: A Review*'.

SLM Solutions (2017) *SLM METAL POWDER*. Available at: https://slm-solutions.com/products/accessories-and-consumables/slm-metal-powder (Accessed: 31 May 2017).

Soares, C. (2007) *Microturbines: Applications for distributed energy systems*. Burlington: ELSEIVER.

Stockmann, I.J. et al. (n.d.) '*HIGH-PERFORMANCE CERAMICS FOR GAS TURBINES – FROM MATERIALS TO COMPONENTS*', pp. 2–3.

Such, A. and Meiners, W. (2015) *POST-PROCESSING OF SLM-MANUFACTURED*.

The library of Manufacturing (n.d.) *Investment Casting*. Available at: http://thelibraryofmanufacturing.com/investment_casting.html (Accessed: 22 May 2017).

Traverso, A. et al. (2017) '*Transient Analysis of and Control System for Advanced Cycles Based on Micro Gas Turbine*', 127(April 2005), pp. 340–347.

Turbines, H. (2012) '*Hydrogen Turbines Turbine Component Rapid Manufacturing Via Electron Beam Melting / Electrochemical Machining*'.

U.S. Enviromend Protection Agency (2015) 'Catalogof de CHP Technologies Section 5.Characterization - Microturbines', *Epa*, (March).

Valencia, J.J. et al. (1994) 'Microstructure and Mechanical Properties of Inconel 625 and 718 Alloys Processed by Powder Injection Molding', *The Minerals, Metals & Materials Society*, pp. 935–945.

Wang, P. et al. (2016) 'Microstructural characteristics and mechanical properties of carbon nanotube reinforced Inconel 625 parts fabricated by selective laser melting', *Materials & Design*, 112 Elsevier Ltd, pp. 290–299.

Zogg, R. et al. (2007) 'Using Microturbines', *ASHRAE Journal*, 49(April).

APPENDICES

Appendix A : Data sheet of Inconel 625 manufactured by SLM from CRP Meccanica

SLM/DMLS INCONEL 625

INCONEL 625 is a heat and corrosion resistant nickel alloy. Parts built in INCONEL 625 have chemical composition corresponding to UNS N06625, AMS 5666F, AMS 5599G, W.Nr 2.4856, DIN NiCr22Mo9Nb.
This type of alloy is characterized by having high tensile, creep and rupture strength. Conventionally cast or wrought components in this type of nickel alloy have typically excellent fatigue and thermal-fatigue properties combined with good oxidation resistance. INCONEL 625 is expected to have good corrosion resistance in various corrosive environments. Especially sea-water applications require high pitting and crevice corrosion resistance, stress-corrosion resistance against chloride-ions, high tensile and corrosion fatigue strength.
Parts built from INCONEL 625 can be heat treated and material properties can be varied within specified range. Parts can be machined, spark-eroded, welded, micro shot-peened, polished and coated in both as-built and in heat treated conditions.

Technical Data	Test Method	
Typical achievable part accuracy, small parts	---------	approx. ± 40 – 60 µm
Typical achievable part accuracy, large parts	---------	± 0.2 %
Min. wall thickness [1]	---------	approx. 0.3 - 0.4 mm
Surface roughness [2] after shot-peening	---------	R_a 4 – 6.5 µm, R_z 20 - 50 µm
Surface roughness [2] after polishing	---------	R_z up to < 0.5 µm

Physical and Chemical properties of parts	Test Method	
Material composition	---------	Ni (balance ≥ 58.00 wt-%) Cr (20.00 - 23.00 wt-%) Mo (8.00 - 10.00 wt-%) Nb (3.15 - 4.15 wt-%) Fe (≤ 5.00 wt-%) Ti (≤ 0.40 wt-%) Al (≤ 0.40 wt-%) Co (≤ 1.0 wt-%) C (≤ 0.10 wt-%) Ta (≤ 0.05 wt-%) Si, Mn (each ≤ 0.50 wt-%) P, S (each ≤ 0.015 wt-%)
Relative density	---------	approx. 100 %
Density	---------	min. 8.4 g/cm^3

Mechanical properties of parts at 20°C (68°F)	Test Method	As Built	Stress Relieved [4]
Tensile strength [3] in horizontal direction (XY)	ISO 6892-1:2009(B) Annex D	typ. 990 ± 50 MPa typ. 144 ± 7 ksi	min. 827 MPa (120 ksi) typ.1040 ± 100 MPa (151 ±15 ksi)
Tensile strength [3] in vertical direction (Z)	ISO 6892-1:2009(B) Annex D	typ. 900 ± 50 MPa typ. 131 ± 7 ksi	min. 827 MPa (120 ksi) typ. 930 ± 100 MPa (135 ±15 ksi)
Yield strength (Rp 0.2 %) [3] in horizontal direction (XY)	ISO 6892-1:2009(B) Annex D	typ. 725 ± 50 MPa typ. 105 ± 7 ksi	min. 414 MPa (60 ksi) typ. 720 ± 100 MPa (104 ±15 ksi)
Yield strength (Rp 0.2 %) [3] in vertical direction (Z)	ISO 6892-1:2009(B) Annex D	typ. 615 ± 50 MPa typ. 89 ± 7 ksi	min. 414 MPa (60 ksi) typ. 650 ± 100 MPa (94 ±15 ksi)
Modulus of elasticity [3] in horizontal direction (XY)	ISO 6892-1:2009(B) Annex D	typ. 170 ± 20 GPa typ. 25 ± 3 Msi	typ. 170 ± 20 GPa typ. 25 ± 3 Msi
Modulus of elasticity [3] in vertical direction (Z)	ISO 6892-1:2009(B) Annex D	typ.140 ± 20 GPa typ. 20 ± 3 Msi	typ. 160 ± 20 GPa typ. 23 ± 3 Msi
Elongation at break [3] in horizontal direction (XY)	ISO 6892-1:2009(B) Annex D	typ. (35 ± 5) %	min. 30 %, typ. (35 ± 5) %
Elongation at break [3] in vertical direction (Z)	ISO 6892-1:2009(B) Annex D	(42 ± 5) %	min. 30 %, typ. (44 ± 5) %
Hardness [5]	EN ISO 6508-1	---------	approx. 30 HRC (287 HB)

Thermal properties of parts	Test Method	
Maximum operating temperature for parts under load	---------	approx. 650 °C approx. 1200 °F
Oxidation resistance to	---------	980 °C 1800 °F

Other	Available Colors
	Light Gray

Appendix B : Properties of Inconel 625 manufactured by casting from MatWeb

Special Metals INCONEL® 625LCF® Nickel Superalloy (UNS N06626) Annealed 2150°F (1180°C) + Aged 1400°F (760°C)

Categories: Metal; Nonferrous Metal; Nickel Alloy; Superalloy

Material Notes: Tensile strength (ultimate and yield), elongation, and hardness values are for samples annealed 2150°F (1180°C)/5 minutes/AC + Aged 1400°F (760°C)/100h/AC. This produces ASTM grain size 5.0. Other property values are typical of this alloy.

Data provided by the manufacturer, Special Metals.

Vendors: Click here to view all available suppliers for this material.

Please click here if you are a supplier and would like information on how to add your listing to this material.

Physical Properties	Metric	English	Comments
Density	8.44 g/cc	0.305 lb/in³	

Mechanical Properties	Metric	English	Comments
Hardness, Rockwell B	95	95	
Tensile Strength, Ultimate	836.3 MPa	121300 psi	
Tensile Strength, Yield	390 MPa @Strain 0.200 %	56500 psi @Strain 0.200 %	
Elongation at Break	50 %	50 %	
Modulus of Elasticity	208 GPa	30200 ksi	
Poissons Ratio	0.28	0.28	
Shear Modulus	81.4 GPa	11800 ksi	

Electrical Properties	Metric	English	Comments
Electrical Resistivity	0.000132 ohm-cm	0.000132 ohm-cm	
Magnetic Permeability	1.0006	1.0006	at 200 Oersted (15.9 kA/m)

Thermal Properties	Metric	English	Comments
CTE, linear	12.8 µm/m-°C @Temperature 21.0 - 100 °C	7.11 µin/in-°F @Temperature 69.8 - 212 °F	Mean
	13.3 µm/m-°C @Temperature 21.0 - 300 °C	7.39 µin/in-°F @Temperature 69.8 - 572 °F	Mean
	13.9 µm/m-°C @Temperature 21.0 - 500 °C	7.72 µin/in-°F @Temperature 69.8 - 932 °F	Mean
	14.9 µm/m-°C @Temperature 21.0 - 700 °C	8.28 µin/in-°F @Temperature 69.8 - 1290 °F	Mean
Specific Heat Capacity	0.410 J/g-°C	0.0980 BTU/lb-°F	
Thermal Conductivity	9.70 W/m-K	67.3 BTU-in/hr-ft²-°F	
Melting Point	1290 - 1350 °C	2350 - 2460 °F	
Solidus	1290 °C	2350 °F	
Liquidus	1350 °C	2460 °F	
Maximum Service Temperature, Air	650 °C	1200 °F	resistance to low cycle and thermal fatigue

Component Elements Properties	Metric	English	Comments
Aluminum, Al	<= 0.40 %	<= 0.40 %	
Carbon, C	<= 0.030 %	<= 0.030 %	
Chromium, Cr	20 - 23 %	20 - 23 %	
Cobalt, Co	<= 1.0 %	<= 1.0 %	
Iron, Fe	<= 5.0 %	<= 5.0 %	
Manganese, Mn	<= 0.50 %	<= 0.50 %	
Molybdenum, Mo	8.0 - 10 %	8.0 - 10 %	
Nickel, Ni	>= 58 %	>= 58 %	
Niobium, Nb (Columbium, Cb)	3.15 - 4.15 %	3.15 - 4.15 %	Includes Ta
Nitrogen, N	<= 0.020 %	<= 0.020 %	
Phosphorous, P	<= 0.015 %	<= 0.015 %	
Silicon, Si	<= 0.020 %	<= 0.020 %	
Sulfur, S	<= 0.015 %	<= 0.015 %	
Titanium, Ti	<= 0.40 %	<= 0.40 %	

Appendix C : Inconel 625 properties

C.1 Mechanical properties

Temperature (K)	Yield strength (Pa)	Tensile strength (Pa)	Elastic modulus (Pa)	Poisson ratio
273	3.75E+08	1.44E+09	1.97E+11	3.00E-01
323	3.49E+08	1.41E+09	1.94E+11	3.05E-01
373	3.26E+08	1.38E+09	1.91E+11	3.10E-01
423	3.06E+08	1.35E+09	1.86E+11	3.12E-01
473	2.90E+08	1.32E+09	1.82E+11	3.13E-01
523	2.77E+08	1.30E+09	1.78E+11	3.13E-01
573	2.67E+08	1.28E+09	1.75E+11	3.13E-01
623	2.60E+08	1.27E+09	1.73E+11	3.13E-01
673	2.56E+08	1.26E+09	1.72E+11	3.15E-01
723	2.54E+08	1.25E+09	1.71E+11	3.19E-01
773	2.54E+08	1.25E+09	1.70E+11	3.21E-01
823	2.53E+08	1.25E+09	1.70E+11	3.24E-01
873	2.51E+08	1.26E+09	1.69E+11	3.25E-01
923	2.47E+08	1.27E+09	1.66E+11	3.28E-01
973	2.39E+08	1.28E+09	1.60E+11	3.29E-01
1023	2.25E+08	1.30E+09	1.51E+11	3.29E-01
1073	2.05E+08	1.32E+09	1.36E+11	3.30E-01
1123	1.74E+08	1.34E+09	1.16E+11	3.30E-01
1173	1.32E+08	1.37E+09	8.73E+10	3.30E-01
1273	9.50E+07	1.30E+08	8.70E+10	3.30E-01
1473	3.50E+07	3.60E+07	5.30E+10	3.30E-01

C.2 Thermal properties

Temperature (K)	Conductivity (W/m K)	Density (kg/m3)	Specific heat (J/kg K)	Enthalpy (J/m3)
273	9.64	8446	405.5	9.35E+08
293	9.8991	8440	410.36	1.00E+09
323	10.292	8430.7	417.65	1.11E+09
373	10.958	8414.6	429.8	1.29E+09
423	11.637	8398.3	441.95	1.47E+09
473	12.33	8381.8	454.1	1.66E+09
523	13.038	8365.3	466.25	1.85E+09
573	13.758	8348.7	478.4	2.05E+09
623	14.493	8331.9	490.55	2.25E+09
673	15.242	8314.6	502.7	2.46E+09
723	16.004	8296.9	514.85	2.67E+09
773	16.78	8278.6	527	2.88E+09
823	17.57	8259.9	539.15	3.10E+09
873	18.374	8211.3	551.3	3.33E+09
923	19.191	8162.7	563.45	3.56E+09
973	20.022	8111.9	575.6	3.79E+09
1023	20.868	8083.8	587.75	4.03E+09
1073	21.726		599.9	4.27E+09
1123	22.599		612.05	4.52E+09
1173	23.486		624.2	4.77E+09
1223	24.386		636.35	5.02E+09
1273	25.3		648.5	5.28E+09
1323	26.228		660.65	5.55E+09
1373	27.17		672.8	5.82E+09
1423	28.125		684.95	6.09E+09
1473	29.094		697.1	6.37E+09
1523	30.078		709.25	6.65E+09

Appendix D Mesh sensitivity results

D.1 CFX

Mesh sensitivity CFX	
Mesh Elements	Efficiency [%]
243,393.00	86.53
417,081.00	83.61
764,068.00	82.13
1,480,211.00	81.86

D.2 Thermal

Mesh sensitivity Thermal								
Elements	Blade out max	Blade out min	Blade in max	Blade in min	Top max	Top min	Hub max	Hub min
25,860.00	899.09	724.08	902.85	699.28	851.04	737.90	871.00	731.41
127,419.00	899.85	724.08	903.22	696.20	851.57	737.90	871.00	729.55
384,422.00	900.58	724.08	903.41	693.87	851.84	747.14	871.00	729.49
632,706.00	900.32	724.08	903.34	692.14	852.18	747.18	871.00	729.57
1,564,419.00	900.58	724.08	903.41	692.14	852.32	747.05	871.00	729.75

Mesh sensitivity Thermal							
P1 max	P1 min	P2 max	P2 min	P3 max	P3 min	Temp min	Temp max
872.21	797.02	866.87	740.93	872.45	830.20	659.63	902.84
872.21	783.83	866.87	740.93	783.83	695.30	666.01	903.22
872.21	783.83	866.87	740.93	769.96	694.04	650.08	903.47
872.21	783.83	866.87	740.93	769.96	693.96	650.08	903.40
872.21	783.83	866.87	740.93	769.96	693.81	651.08	903.80

D.3 Structural

Mesh sensitivity Structural		
Mesh Elements	P1 max [MPa]	P2 max [MPa]
159,335.00	45.01	39.54
346,291.00	65.78	60.93
512,184.00	79.17	82.17
791,653.00	86.22	86.00
844,541.00	86.52	85.93
909,653.00	86.55	85.71
1,205,922.00	87.18	85.61
1,413,014.00	87.88	85.81

Appendix E : CFX results

Efficiency	Power (kW)	Tin (*C)	Pin (bar)	RPM
92.8751	11.912	550	2	90000
87.643	26.6965	550	3	90000
85.629	38.6244	550	4	90000
92.168	12.1614	600	2	90000
86.642	27.1122	600	3	90000
84.63	38.9274	600	4	90000
91.669	12.6341	650	2	90000
85.638	27.4891	650	3	90000
83.451	39.5249	650	4	90000

Efficiency	Power (kW)	Tin (*C)	Pin (bar)	RPM
93.854	10.9692	550	2	100000
90.885	27.5856	550	3	100000
89.405	40.3753	550	4	100000
93.542	11.8193	600	2	100000
89.902	28.1813	600	3	100000
88.558	41.3332	600	4	100000
93.252	12.3148	650	2	100000
89.219	28.8265	650	3	100000
87.486	41.9529	650	4	100000

Efficiency	Power (kW)	Tin (*C)	Pin (bar)	RPM
88.044	9.51217	550	2	110000
93.701	27.9879	550	3	110000
92.795	41.886	550	4	110000
90.201	10.507	600	2	110000
92.866	28.7297	600	3	110000
91.912	42.8121	600	4	110000
91.526	11.3292	650	2	110000
92.37	29.5097	650	3	110000
90.987	43.6277	650	4	110000

Appendix F : Structural data results for 90,000rpm from ANSYS Structural (example)

The table below has the values for the stress on the path at the concave part of the blade (front), what was studied at the results section, and the convex part of the blade (Back).

Casting				SLM			
650°C, 2bar	Front	650°C, 2bar	Back	650°C, 2bar	Front	650°C, 2bar	Back
x (mm)	Stress (MPa)	x (mm)	Stress (MPa)	x (mm)	Stress (MPa)	x (mm)	Stress (MPa)
0	0.57759	0	2.1762	0	0.53682	0	2.3665
5.65E-02	0.57993	4.99E-02	2.2503	5.65E-02	0.5379	4.99E-02	2.4104
0.11238	0.58234	9.98E-02	2.3317	0.11238	0.53904	9.98E-02	2.46
0.17546	0.57533	0.14969	2.3728	0.17546	0.53176	0.14969	2.4904
0.23854	0.5686	0.19963	2.4174	0.23854	0.52475	0.19963	2.5247
0.30964	0.56728	0.24946	2.4607	0.30964	0.52389	0.24946	2.5802
0.38073	0.5662	0.29943	2.5055	0.38073	0.52327	0.29943	2.6377
0.46749	0.56709	0.34929	2.5001	0.46749	0.52537	0.34929	2.6564
0.55423	0.56838	0.39921	2.4992	0.55423	0.52793	0.39921	2.6796
0.65768	0.5742	0.44917	2.497	0.65768	0.53363	0.44917	2.69
0.76111	0.58009	0.499	2.4993	0.76111	0.53941	0.499	2.7046
0.85932	0.58099	0.54916	2.4665	0.85932	0.54225	0.54916	2.6804
0.95751	0.58243	0.59922	2.443	0.95751	0.54565	0.59922	2.6653
1.0762	0.57958	0.64997	2.4022	1.0762	0.54382	0.64997	2.6237
1.195	0.57688	0.70091	2.3693	1.195	0.5421	0.70091	2.5901
1.2887	0.60176	0.75207	2.3506	1.2887	0.5653	0.75207	2.5681
1.3825	0.62674	0.80371	2.3338	1.3825	0.58866	0.80371	2.5482
1.4725	0.61984	0.85777	2.3051	1.4725	0.58338	0.85777	2.521
1.5625	0.61297	0.91204	2.2778	1.5625	0.57814	0.91204	2.4955
1.6594	0.62168	0.96545	2.2884	1.6594	0.58641	0.96545	2.5092
1.7563	0.6311	1.0186	2.2992	1.7563	0.59529	1.0186	2.5231
1.8647	0.63918	1.0722	2.2317	1.8647	0.603	1.0722	2.4499
1.9731	0.64728	1.1257	2.1647	1.9731	0.61072	1.1257	2.3772
2.0758	0.65072	1.1833	2.1638	2.0758	0.61326	1.1833	2.3821
2.1785	0.65427	1.2409	2.163	2.1785	0.61587	1.2409	2.3872
2.2909	0.64843	1.3025	2.1417	2.2909	0.6108	1.3025	2.3704
2.4033	0.64277	1.3642	2.1205	2.4033	0.60586	1.3642	2.354
2.4947	0.65138	1.4199	2.068	2.4947	0.61562	1.4199	2.2909
2.5861	0.66006	1.4756	2.0155	2.5861	0.62544	1.4756	2.228
2.6676	0.67356	1.5279	2.0036	2.6676	0.63997	1.5279	2.2217
2.749	0.68726	1.5802	1.9921	2.749	0.65465	1.5802	2.2161
2.8281	0.67969	1.6322	1.977	2.8281	0.64695	1.6322	2.1961
2.9071	0.67225	1.6842	1.9621	2.9071	0.63935	1.6842	2.1764
2.9801	0.67998	1.737	1.9408	2.9801	0.64634	1.737	2.1526
3.053	0.68775	1.7897	1.9196	3.053	0.65336	1.7897	2.1291
3.1107	0.68151	1.8403	1.8681	3.1107	0.65	1.8403	2.0707
3.1684	0.67561	1.891	1.8172	3.1684	0.6469	1.891	2.0131
3.2248	0.6838	1.943	1.7901	3.2248	0.6566	1.943	1.985
3.2812	0.69204	1.9951	1.7632	3.2812	0.66634	1.9951	1.9571
3.3334	0.68658	2.0482	1.7176	3.3334	0.65922	2.0482	1.8993
3.3856	0.68138	2.1014	1.6722	3.3856	0.65231	2.1014	1.8418
3.4366	0.69203	2.1604	1.6782	3.4366	0.66181	2.1604	1.8488
3.4877	0.70273	2.2195	1.6844	3.4877	0.67136	2.2195	1.8562
3.5426	0.70583	2.277	1.6221	3.5426	0.67813	2.277	1.7818
3.5976	0.7095	2.3347	1.5606	3.5976	0.6853	2.3347	1.7082
3.6682	0.70226	2.3876	1.5313	3.6682	0.67671	2.3876	1.6722
3.7388	0.69625	2.4404	1.5024	3.7388	0.66912	2.4404	1.6366
3.8327	0.70092	2.4939	1.4755	3.8327	0.67435	2.4939	1.6027
3.9266	0.70708	2.5473	1.4487	3.9266	0.68061	2.5473	1.5688
4.0204	0.70993	2.5984	1.427	4.0204	0.68344	2.5984	1.54
4.1142	0.71314	2.6494	1.4054	4.1142	0.68651	2.6494	1.5114
4.1931	0.72103	2.7034	1.389	4.1931	0.69472	2.7034	1.4915

4.272	0.72966	2.7572	1.3727	4.272	0.70349	2.7572	1.4717
4.3739	0.71454	2.8125	1.3551	4.3739	0.69174	2.8125	1.4521
4.4758	0.69945	2.8677	1.3381	4.4758	0.68001	2.8677	1.4332
4.5669	0.69759	2.9349	1.3228	4.5669	0.67982	2.9349	1.4131
4.658	0.69576	3.0022	1.3079	4.658	0.67967	3.0022	1.3934
4.7452	0.70642	3.0837	1.267	4.7452	0.68788	3.0837	1.3448
4.8323	0.7173	3.1652	1.2264	4.8323	0.69634	3.1652	1.2967
4.9396	0.74816	3.2283	1.1955	4.9396	0.72747	3.2283	1.2619
5.0469	0.77952	3.2914	1.1649	5.0469	0.75916	3.2914	1.2274
5.1322	0.75654	3.3505	1.1763	5.1322	0.73955	3.3505	1.2394
5.2175	0.73487	3.4097	1.1877	5.2175	0.721	3.4097	1.2515
5.3107	0.73917	3.4624	1.1716	5.3107	0.7289	3.4624	1.2326
5.404	0.74408	3.515	1.1557	5.404	0.7374	3.515	1.2138
5.4874	0.73227	3.566	1.1388	5.4874	0.72602	3.566	1.1951
5.5709	0.72069	3.617	1.1221	5.5709	0.71486	3.617	1.1764
5.6509	0.72956	3.6697	1.1054	5.6509	0.72482	3.6697	1.1573
5.731	0.73905	3.7223	1.0888	5.731	0.73524	3.7223	1.1383
5.823	0.73716	3.7867	1.0892	5.823	0.73484	3.7867	1.1384
5.9149	0.73604	3.851	1.0896	5.9149	0.73515	3.851	1.1386
5.987	0.73282	3.914	1.0817	5.987	0.73438	3.914	1.1308
6.0591	0.73098	3.9771	1.074	6.0591	0.73496	3.9771	1.123
6.1283	0.75143	4.0485	1.0595	6.1283	0.75548	4.0485	1.1051
6.1975	0.77198	4.1199	1.0452	6.1975	0.77608	4.1199	1.0873
6.2828	0.77803	4.1812	1.0205	6.2828	0.78377	4.1812	1.0611
6.3681	0.7844	4.2425	0.99601	6.3681	0.79174	4.2425	1.035
6.4404	0.76289	4.3135	1.0054	6.4404	0.77266	4.3135	1.0428
6.5127	0.74162	4.3844	1.0151	6.5127	0.75373	4.3844	1.0509
6.5724	0.75244	4.451	0.99704	6.5724	0.76509	4.451	1.0325
6.6322	0.76347	4.5175	0.97906	6.6322	0.77663	4.5175	1.014
6.6906	0.76181	4.6015	0.96257	6.6906	0.77699	4.6015	0.9965
6.7491	0.76073	4.6854	0.94612	6.7491	0.77769	4.6854	0.97899
6.8013	0.76131	4.7567	0.93881	6.8013	0.77934	4.7567	0.97048
6.8536	0.76394	4.828	0.93154	6.8536	0.78248	4.828	0.962
6.9047	0.75378	4.8932	0.91108	6.9047	0.77515	4.8932	0.94143
6.9558	0.74373	4.9584	0.89065	6.9558	0.76794	4.9584	0.92093
7.0077	0.754	5.0282	0.87764	7.0077	0.77939	5.0282	0.90717
7.0596	0.76435	5.0981	0.86465	7.0596	0.79088	5.0981	0.89344
7.1184	0.75103	5.1625	0.86305	7.1184	0.77768	5.1625	0.89112
7.1773	0.73808	5.2269	0.86156	7.1773	0.76488	5.2269	0.88892
7.252	0.7751	5.2952	0.84509	7.252	0.80367	5.2952	0.87155
7.3267	0.81222	5.3634	0.82865	7.3267	0.84256	5.3634	0.85424
7.4188	0.78095	5.4398	0.82129	7.4188	0.81444	5.4398	0.84636
7.511	0.74973	5.5161	0.81398	7.511	0.78637	5.5161	0.83851
7.5764	0.76539	5.5818	0.81572	7.5764	0.8055	5.5818	0.84038
7.6419	0.78129	5.6475	0.81761	7.6419	0.82479	5.6475	0.84232
7.7098	0.76962	5.7008	0.80571	7.7098	0.81388	5.7008	0.82965
7.7776	0.7581	5.7541	0.79391	7.7776	0.80314	5.7541	0.81712
7.8595	0.74238	5.8115	0.77702	7.8595	0.78769	5.8115	0.8005
7.9414	0.72673	5.8688	0.76015	7.9414	0.77232	5.8688	0.78391
8.0093	0.74284	5.9232	0.75225	8.0093	0.79059	5.9232	0.77679
8.0771	0.7591	5.9775	0.74443	8.0771	0.80895	5.9775	0.76972
8.1297	0.77891	6.0318	0.75456	8.1297	0.83301	6.0318	0.77841
8.1823	0.79895	6.0861	0.765	8.1823	0.85733	6.0861	0.78738
8.2373	0.77788	6.139	0.73757	8.2373	0.8348	6.139	0.76081
8.2923	0.75713	6.1918	0.71032	8.2923	0.81258	6.1918	0.73451
8.3465	0.74716	6.255	0.71918	8.3465	0.80394	6.255	0.74332

8.4007	0.73733	6.3181	0.72831	8.4007	0.79544	6.3181	0.75231
8.4528	0.75146	6.3824	0.7049	8.4528	0.81156	6.3824	0.72933
8.5048	0.76559	6.4466	0.6817	8.5048	0.8277	6.4466	0.7066
8.5554	0.75515	6.5011	0.68345	8.5554	0.81786	6.5011	0.70821
8.606	0.74474	6.5556	0.68548	8.606	0.80805	6.5556	0.71009
8.6637	0.74528	6.609	0.67913	8.6637	0.81203	6.609	0.70355
8.7214	0.74599	6.6625	0.67287	8.7214	0.81616	6.6625	0.69714
8.7974	0.74354	6.7156	0.66443	8.7974	0.81253	6.7156	0.68813
8.8735	0.74116	6.7687	0.65607	8.8735	0.80898	6.7687	0.67917
8.9584	0.76769	6.8224	0.65948	8.9584	0.83934	6.8224	0.68282
9.0433	0.79446	6.8761	0.66312	9.0433	0.86981	6.8761	0.68667
9.111	0.76986	6.9399	0.65397	9.111	0.84828	6.9399	0.67705
9.1787	0.74561	7.0038	0.64491	9.1787	0.82711	7.0038	0.6675
9.2473	0.74409	7.0724	0.64005	9.2473	0.82557	7.0724	0.66163
9.3159	0.74267	7.1411	0.63544	9.3159	0.82409	7.1411	0.65587
9.3945	0.75629	7.2155	0.62853	9.3945	0.83956	7.2155	0.65046
9.4732	0.77008	7.29	0.62228	9.4732	0.85521	7.29	0.64577
9.5308	0.76063	7.3577	0.62601	9.5308	0.84658	7.3577	0.65057
9.5885	0.75134	7.4253	0.63025	9.5885	0.83805	7.4253	0.65594
9.6449	0.74777	7.4962	0.61786	9.6449	0.83966	7.4962	0.64241
9.7013	0.74689	7.5671	0.60567	9.7013	0.84347	7.5671	0.62915
9.7731	0.76504	7.6422	0.61131	9.7731	0.85952	7.6422	0.63209
9.845	0.78391	7.7173	0.61747	9.845	0.87633	7.7173	0.63536
9.9181	0.77169	7.7866	0.61561	9.9181	0.86452	7.7866	0.63539
9.9912	0.7599	7.8559	0.61444	9.9912	0.85316	7.8559	0.63612
10.044	0.76584	7.9198	0.6211	10.044	0.85986	7.9198	0.64469
10.097	0.77179	7.9836	0.62823	10.097	0.86656	7.9836	0.65372
10.162	0.74859	8.0541	0.61855	10.162	0.8457	8.0541	0.6423
10.227	0.72547	8.1246	0.60913	10.227	0.8249	8.1246	0.63123
10.312	0.72728	8.2028	0.60032	10.312	0.82562	8.2028	0.62109
10.397	0.7293	8.2811	0.59171	10.397	0.82646	8.2811	0.61113
10.464	0.72958	8.3473	0.59399	10.464	0.82874	8.3473	0.61332
10.531	0.73007	8.4136	0.59655	10.531	0.83124	8.4136	0.61575
10.596	0.72318	8.4735	0.60866	10.596	0.82599	8.4735	0.62705
10.661	0.71747	8.5333	0.62098	10.661	0.82175	8.5333	0.63854
10.747	0.72104	8.5863	0.63608	10.747	0.82714	8.5863	0.65409
10.832	0.72471	8.6392	0.65147	10.832	0.83261	8.6392	0.66991
10.907	0.73209	8.7044	0.6486	10.907	0.84096	8.7044	0.66392
10.981	0.74016	8.7697	0.646	10.981	0.84993	8.7697	0.65816
11.04	0.72239	8.8378	0.64753	11.04	0.82956	8.8378	0.6589
11.099	0.70471	8.9061	0.64916	11.099	0.80926	8.9061	0.65976
11.17	0.72014	8.9727	0.65606	11.17	0.82743	8.9727	0.6704
11.242	0.73561	9.0393	0.66423	11.242	0.84567	9.0393	0.68198
11.304	0.71909	9.1007	0.65963	11.304	0.82679	9.1007	0.67506
11.367	0.70272	9.1621	0.65513	11.367	0.80798	9.1621	0.66827
11.421	0.7055	9.2274	0.66406	11.421	0.81231	9.2274	0.67451
11.476	0.70834	9.2927	0.6734	11.476	0.8167	9.2927	0.68114
11.53	0.72035	9.3519	0.67691	11.53	0.83096	9.3519	0.68569
11.584	0.73251	9.4112	0.68071	11.584	0.84544	9.4112	0.69048
11.637	0.71759	9.4674	0.67297	11.637	0.82829	9.4674	0.68293
11.69	0.70269	9.5236	0.66551	11.69	0.81116	9.5236	0.6757
11.743	0.69782	9.5758	0.6863	11.743	0.80547	9.5758	0.69393
11.797	0.69327	9.6281	0.70745	11.797	0.8001	9.6281	0.71255
11.852	0.69099	9.6803	0.70542	11.852	0.7995	9.6803	0.71082
11.907	0.68918	9.7325	0.7035	11.907	0.7993	9.7325	0.7092
11.973	0.69089	9.7893	0.69215	11.973	0.79997	9.7893	0.69762

12.038	0.6931	9.846	0.68109	12.038	0.80115	9.846	0.68641
12.096	0.69505	9.8987	0.69068	12.096	0.80485	9.8987	0.6956
12.154	0.69707	9.9514	0.70035	12.154	0.80862	9.9514	0.70485
12.205	0.69079	10.005	0.69352	12.205	0.80431	10.005	0.69764
12.257	0.68505	10.058	0.68683	12.257	0.80044	10.058	0.6906
12.311	0.6806	10.111	0.69959	12.311	0.79312	10.111	0.7021
12.365	0.67623	10.164	0.71252	12.365	0.78583	10.164	0.71376
12.423	0.67454	10.22	0.70336	12.423	0.78512	10.22	0.705
12.481	0.67286	10.276	0.69437	12.481	0.78446	10.276	0.69648
12.537	0.67242	10.338	0.69743	12.537	0.77902	10.338	0.69973
12.594	0.67215	10.4	0.70053	12.594	0.77375	10.4	0.70302
12.648	0.67374	10.469	0.70377	12.648	0.77586	10.469	0.70629
12.702	0.67538	10.538	0.70713	12.702	0.778	10.538	0.70969
12.774	0.67097	10.617	0.74228	12.774	0.77213	10.617	0.74176
12.846	0.66659	10.695	0.77893	12.846	0.76628	10.695	0.77536
12.906	0.66335	10.766	0.74827	12.906	0.76112	10.766	0.74685
12.967	0.66062	10.837	0.71931	12.967	0.75634	10.837	0.72013
13.021	0.65076	10.901	0.74078	13.021	0.74823	10.901	0.74149
13.075	0.64207	10.966	0.76243	13.075	0.74114	10.966	0.76302
13.143	0.6473	11.04	0.75867	13.143	0.74516	11.04	0.75973
13.211	0.65261	11.115	0.75502	13.211	0.74922	11.115	0.75656
13.267	0.6541	11.172	0.77005	13.267	0.74694	11.172	0.77061
13.322	0.65584	11.229	0.78514	13.322	0.74488	11.229	0.78474
13.375	0.64646	11.286	0.76902	13.375	0.7349	11.286	0.76908
13.428	0.63746	11.343	0.7533	13.428	0.7253	11.343	0.75391
13.494	0.63779	11.4	0.76246	13.494	0.72462	11.4	0.76272
13.56	0.63829	11.456	0.7718	13.56	0.72411	11.456	0.77173
13.615	0.63793	11.517	0.76476	13.615	0.72418	11.517	0.76514
13.669	0.63787	11.578	0.75785	13.669	0.72445	11.578	0.7587
13.722	0.63056	11.636	0.77117	13.722	0.71341	11.636	0.77196
13.776	0.62332	11.694	0.78456	13.776	0.7024	11.694	0.78526
13.842	0.62413	11.745	0.79643	13.842	0.70156	11.745	0.79648
13.909	0.62498	11.796	0.80834	13.909	0.70073	11.796	0.80776
13.964	0.62756	11.851	0.79202	13.964	0.70567	11.851	0.79184
14.02	0.63018	11.905	0.776	14.02	0.71068	11.905	0.77625
14.078	0.6266	11.961	0.7912	14.078	0.70438	11.961	0.79015
14.135	0.62317	12.018	0.80658	14.135	0.69823	12.018	0.80428
14.203	0.62007	12.083	0.80529	14.203	0.69097	12.083	0.80297
14.27	0.61699	12.149	0.80412	14.27	0.68373	12.149	0.80177
14.325	0.61405	12.219	0.80966	14.325	0.67758	12.219	0.80633
14.379	0.61115	12.289	0.81542	14.379	0.67146	12.289	0.81106
14.441	0.61472	12.366	0.7948	14.441	0.67443	12.366	0.79289
14.502	0.61832	12.443	0.77457	14.502	0.67746	12.443	0.77507
14.569	0.60271	12.507	0.77593	14.569	0.65846	12.507	0.77683
14.635	0.58748	12.572	0.77733	14.635	0.63982	12.572	0.7786
14.688	0.59499	12.645	0.7987	14.688	0.64494	12.645	0.79908
14.742	0.60255	12.718	0.82025	14.742	0.65013	12.718	0.81976
14.812	0.59742	12.787	0.8122	14.812	0.64626	12.787	0.81208
14.881	0.59302	12.857	0.80426	14.881	0.64308	12.857	0.80452
14.943	0.59366	12.922	0.81134	14.943	0.6368	12.922	0.81127
15.005	0.59549	12.987	0.81864	15.005	0.63175	12.987	0.81821
15.059	0.58691	13.051	0.821	15.059	0.62226	13.051	0.82169
15.113	0.57875	13.115	0.82427	15.113	0.61321	13.115	0.82591
15.166	0.57117	13.169	0.81674	15.166	0.60039	13.169	0.81967
15.218	0.56392	13.223	0.80964	15.218	0.58778	13.223	0.81378
15.269	0.55352	13.277	0.81611	15.269	0.57424	13.277	0.82178

15.319	0.54355	13.331	0.82258	15.319	0.56106	13.331	0.82979
15.372	0.55388	13.385	0.82334	15.372	0.57241	13.385	0.82827
15.425	0.56456	13.439	0.82415	15.425	0.58401	13.439	0.82682
15.482	0.56751	13.496	0.82916	15.482	0.58428	13.496	0.83337
15.538	0.57062	13.553	0.83423	15.538	0.58471	13.553	0.83998
15.594	0.57341	13.619	0.82952	15.594	0.58776	13.619	0.83555
15.649	0.57634	13.685	0.82492	15.649	0.59091	13.685	0.83118
15.716	0.5556	13.754	0.82996	15.716	0.56153	13.754	0.83675
15.783	0.53532	13.823	0.83506	15.783	0.53247	13.823	0.84237
15.842	0.54617	13.881	0.83124	15.842	0.54394	13.881	0.83899
15.901	0.55707	13.938	0.82752	15.901	0.55541	13.938	0.83569
15.962	0.55301	14.008	0.82672	15.962	0.54924	14.008	0.8371
16.022	0.54912	14.079	0.82677	16.022	0.54331	14.079	0.83935
16.101	0.54827	14.139	0.81324	16.101	0.53527	14.139	0.825
16.179	0.54756	14.2	0.79996	16.179	0.5273	14.2	0.81088
16.243	0.53879	14.256	0.81032	16.243	0.51269	14.256	0.82087
16.306	0.53061	14.312	0.82087	16.306	0.49872	14.312	0.8311
16.365	0.52785	14.383	0.81805	16.365	0.49104	14.383	0.82859
16.425	0.52522	14.453	0.81532	16.425	0.48343	14.453	0.82612
16.483	0.52324	14.509	0.81503	16.483	0.47925	14.509	0.82694
16.541	0.52149	14.565	0.81488	16.541	0.47538	14.565	0.82788
16.623	0.5265	14.618	0.81293	16.623	0.47572	14.618	0.82637
16.705	0.53192	14.671	0.81099	16.705	0.47639	14.671	0.82486
16.772	0.53052	14.728	0.83123	16.772	0.47481	14.728	0.84508
16.838	0.52916	14.784	0.85173	16.838	0.47326	14.784	0.86562
16.902	0.52065	14.838	0.83626	16.902	0.45888	14.838	0.85122
16.966	0.5124	14.891	0.8209	16.966	0.44472	14.891	0.83694
17.025	0.5101	14.942	0.81752	17.025	0.43722	14.942	0.83359
17.083	0.50787	14.993	0.81419	17.083	0.42979	14.993	0.83027
17.144	0.52001	15.045	0.82123	17.144	0.44086	15.045	0.83855
17.204	0.53219	15.097	0.82833	17.204	0.45196	15.097	0.84691
17.261	0.51958	15.158	0.82361	17.261	0.43315	15.158	0.84167
17.317	0.50736	15.218	0.81899	17.317	0.41484	15.218	0.83653
17.394	0.51053	15.276	0.81876	17.394	0.41691	15.276	0.83626
17.47	0.5148	15.334	0.81862	17.47	0.41995	15.334	0.83607
17.536	0.51197	15.392	0.81793	17.536	0.40827	15.392	0.83681
17.603	0.50969	15.45	0.81728	17.603	0.39725	15.45	0.83759
17.666	0.50502	15.52	0.80816	17.666	0.38863	15.52	0.82855
17.73	0.50049	15.589	0.79914	17.73	0.38019	15.589	0.81962
17.785	0.50367	15.652	0.79441	17.785	0.38114	15.652	0.81624
17.84	0.50693	15.715	0.78973	17.84	0.38221	15.715	0.81292
17.894	0.50456	15.78	0.7939	17.894	0.37693	15.78	0.81669
17.949	0.50239	15.845	0.79809	17.949	0.37198	15.845	0.82047
18.001	0.51449	15.911	0.7983	18.001	0.37905	15.911	0.82216
18.053	0.52685	15.977	0.79853	18.053	0.38667	15.977	0.82388
18.105	0.51215	16.038	0.79951	18.105	0.37136	16.038	0.82505
18.158	0.49805	16.099	0.80052	18.158	0.35704	16.099	0.82625
18.21	0.50341	16.164	0.80045	18.21	0.35923	16.164	0.82602
18.262	0.5089	16.23	0.80044	18.262	0.36168	16.23	0.82585
18.321	0.50066	16.304	0.79674	18.321	0.35225	16.304	0.82308
18.379	0.49332	16.379	0.79311	18.379	0.3442	16.379	0.82038
18.438	0.49932	16.446	0.78167	18.438	0.34398	16.446	0.8079
18.496	0.50642	16.513	0.77045	18.496	0.3454	16.513	0.79566
18.557	0.50187	16.568	0.77698	18.557	0.34186	16.568	0.8033
18.617	0.49898	16.623	0.78355	18.617	0.34058	16.623	0.81099
18.68	0.50441	16.689	0.77633	18.68	0.34261	16.689	0.80358

18.744	0.50989	16.754	0.76916	18.744	0.34479	16.754	0.79621
18.809	0.5142	16.819	0.7669	18.809	0.348	16.819	0.79393
18.874	0.51871	16.883	0.76465	18.874	0.35146	16.883	0.79166
18.935	0.51133	16.939	0.7671	18.935	0.34015	16.939	0.79464
18.995	0.5044	16.995	0.7696	18.995	0.32954	16.995	0.79766
19.053	0.51157	17.047	0.7723	19.053	0.33824	17.047	0.80086
19.11	0.51921	17.099	0.77503	19.11	0.34754	17.099	0.80411
19.162	0.50763	17.152	0.76958	19.162	0.33515	17.152	0.79923
19.214	0.49635	17.206	0.76415	19.214	0.32335	17.206	0.79438
19.266	0.49394	17.266	0.766	19.266	0.32094	17.266	0.79678
19.319	0.49164	17.325	0.76789	19.319	0.31879	17.325	0.79924
19.374	0.49827	17.387	0.75731	19.374	0.32515	17.387	0.78798
19.428	0.50526	17.448	0.74683	19.428	0.33196	17.448	0.77683
19.49	0.50834	17.503	0.74878	19.49	0.33229	17.503	0.7801
19.551	0.51151	17.558	0.75075	19.551	0.33288	17.558	0.78338
19.62	0.50842	17.633	0.75259	19.62	0.33134	17.633	0.78572
19.689	0.50545	17.707	0.75453	19.689	0.33001	17.707	0.78818
19.754	0.51389	17.787	0.74944	19.754	0.3389	17.787	0.78211
19.819	0.52252	17.866	0.74439	19.819	0.34804	17.866	0.77609
19.883	0.51532	17.933	0.74106	19.883	0.34199	17.933	0.77344
19.947	0.50836	18	0.73774	19.947	0.3366	18	0.7708
20.017	0.51402	18.063	0.73134	20.017	0.34261	18.063	0.76495
20.086	0.52005	18.126	0.72498	20.086	0.34898	18.126	0.75913
20.158	0.51127	18.194	0.71628	20.158	0.34646	18.194	0.74887
20.23	0.503	18.262	0.70764	20.23	0.34478	18.262	0.73866
20.317	0.50951	18.333	0.70419	20.317	0.35272	18.333	0.73595
20.403	0.5162	18.403	0.70076	20.403	0.36094	18.403	0.73328
20.485	0.50841	18.469	0.69906	20.485	0.35496	18.469	0.73144
20.566	0.50089	18.535	0.69738	20.566	0.34946	18.535	0.72961
20.645	0.49755	18.592	0.70724	20.645	0.35265	18.592	0.74047
20.725	0.49489	18.648	0.71731	20.725	0.35662	18.648	0.75161
20.815	0.50438	18.7	0.71006	20.815	0.36443	18.7	0.74526
20.905	0.51395	18.752	0.70283	20.905	0.37233	18.752	0.73895
20.989	0.50893	18.812	0.69197	20.989	0.36879	18.812	0.72787
21.074	0.50406	18.872	0.68129	21.074	0.3654	18.872	0.71694
21.146	0.49334	18.937	0.67849	21.146	0.35948	18.937	0.71324
21.218	0.48312	19.002	0.67578	21.218	0.35409	19.002	0.70964
21.283	0.4917	19.067	0.67823	21.283	0.36662	19.067	0.71373
21.348	0.50048	19.131	0.68076	21.348	0.37967	19.131	0.71793
21.403	0.50429	19.19	0.6757	21.403	0.38219	19.19	0.71167
21.459	0.50832	19.249	0.67067	21.459	0.38501	19.249	0.70544
21.511	0.50362	19.301	0.67437	21.511	0.38536	19.301	0.71016
21.564	0.4994	19.352	0.67818	21.564	0.38634	19.352	0.71505
21.616	0.49477	19.409	0.66987	21.616	0.38501	19.409	0.70646
21.669	0.49026	19.466	0.6616	21.669	0.38382	19.466	0.6979
21.725	0.48775	19.526	0.65835	21.725	0.38285	19.526	0.69583
21.781	0.48539	19.586	0.65513	21.781	0.38201	19.586	0.69382
21.86	0.48413	19.643	0.64772	21.86	0.38854	19.643	0.68514
21.939	0.48329	19.699	0.64042	21.939	0.39544	19.699	0.67654
22.02	0.47593	19.753	0.6377	22.02	0.39076	19.753	0.67525
22.1	0.46871	19.807	0.63516	22.1	0.38623	19.807	0.67415
22.175	0.47323	19.86	0.63254	22.175	0.39398	19.86	0.67074
22.251	0.47797	19.913	0.62993	22.251	0.40207	19.913	0.66733
22.31	0.48102	19.968	0.62877	22.31	0.40244	19.968	0.66693
22.369	0.48466	20.023	0.62763	22.369	0.40358	20.023	0.66656
22.426	0.47948	20.087	0.6234	22.426	0.40395	20.087	0.66232

22.482	0.47463	20.151	0.61923	22.482	0.40475	20.151	0.65813
22.534	0.47817	20.228	0.61464	22.534	0.41095	20.228	0.65131
22.585	0.48208	20.305	0.61017	22.585	0.41765	20.305	0.6446
22.639	0.48764	20.384	0.60353	22.639	0.42488	20.384	0.63948
22.693	0.49346	20.463	0.59708	22.693	0.43232	20.463	0.63465
22.758	0.4822	20.533	0.59544	22.758	0.42442	20.533	0.63494
22.823	0.47129	20.602	0.59387	22.823	0.41713	20.602	0.63535
22.897	0.47973	20.66	0.58811	22.897	0.42852	20.66	0.62818
22.97	0.48844	20.718	0.58236	22.97	0.44016	20.718	0.62101
23.055	0.4869	20.77	0.57758	23.055	0.43798	20.77	0.61757
23.139	0.48582	20.821	0.57291	23.139	0.43618	20.821	0.61424
23.233	0.49627	20.872	0.56551	23.233	0.45139	20.872	0.60686
23.326	0.50725	20.923	0.55816	23.326	0.46702	20.923	0.59953
23.41	0.51027	20.981	0.55494	23.41	0.47026	20.981	0.59579
23.494	0.51353	21.039	0.55174	23.494	0.4737	21.039	0.59209
23.573	0.51212	21.107	0.55022	23.573	0.47445	21.107	0.58876
23.653	0.5112	21.175	0.54882	23.653	0.47557	21.175	0.58554
23.735	0.51397	21.248	0.54388	23.735	0.47733	21.248	0.58268
23.817	0.51699	21.321	0.5391	23.817	0.47926	21.321	0.58012
23.897	0.5288	21.39	0.53213	23.897	0.49432	21.39	0.57321
23.977	0.54087	21.46	0.52521	23.977	0.50959	21.46	0.56639
24.052	0.55489	21.52	0.53178	24.052	0.51884	21.52	0.57454
24.127	0.57068	21.58	0.53868	24.127	0.53021	21.58	0.58314
24.191	0.57264	21.632	0.53105	24.191	0.53551	21.632	0.57501
24.255	0.57518	21.684	0.52352	24.255	0.54129	21.684	0.567
24.327	0.60118	21.735	0.52504	24.327	0.57023	21.735	0.57134
24.399	0.62769	21.786	0.52677	24.399	0.59969	21.786	0.57597
24.467	0.63553	21.844	0.51763	24.467	0.60776	21.844	0.56483
24.534	0.64344	21.901	0.50853	24.534	0.61593	21.901	0.55372
24.602	0.65174	21.973	0.50471	24.602	0.62141	21.973	0.5504
24.669	0.66038	22.044	0.50094	24.669	0.62739	22.044	0.54716
24.725	0.67405	22.117	0.49728	24.725	0.6418	22.117	0.54485
24.78	0.68785	22.189	0.49374	24.78	0.65635	22.189	0.54268
24.831	0.69707	22.255	0.48781	24.831	0.66683	22.255	0.53616
24.881	0.70643	22.321	0.48193	24.881	0.67743	22.321	0.52968
24.937	0.71038	22.378	0.47917	24.937	0.68296	22.378	0.52911
24.992	0.71553	22.435	0.47648	24.992	0.6898	22.435	0.52862
25.05	0.74724	22.486	0.47639	25.05	0.72418	22.486	0.52806
25.108	0.7794	22.538	0.47652	25.108	0.75904	22.538	0.52773
25.177	0.79392	22.589	0.47658	25.177	0.77037	22.589	0.53184
25.247	0.80883	22.64	0.47701	25.247	0.78216	22.64	0.53627
25.32	0.82863	22.697	0.47105	25.32	0.804	22.697	0.52774
25.393	0.84879	22.754	0.46519	25.393	0.82616	22.754	0.5193
25.46	0.86072	22.824	0.46522	25.46	0.82542	22.824	0.52114
25.527	0.87394	22.895	0.46545	25.527	0.82657	22.895	0.52327
25.585	0.89668	22.975	0.45994	25.585	0.85796	22.975	0.51766
25.642	0.92252	23.056	0.45455	25.642	0.89243	23.056	0.51219
25.699	0.95154	23.134	0.45019	25.699	0.91485	23.134	0.50797
25.756	0.98127	23.213	0.44594	25.756	0.93829	23.213	0.50386
25.808	1.0231	23.273	0.45065	25.808	0.97607	23.273	0.51177
25.86	1.0652	23.333	0.45561	25.86	1.0141	23.333	0.51995
25.915	1.0733	23.396	0.44765	25.915	1.0184	23.396	0.50912
25.97	1.0819	23.459	0.43976	25.97	1.0232	23.459	0.49835
26.021	1.106	23.543	0.44485	26.021	1.0398	23.543	0.50683
26.073	1.1304	23.628	0.45032	26.073	1.0569	23.628	0.51979
26.13	1.1636	23.722	0.44319	26.13	1.086	23.722	0.50816

26.188	1.1974	23.816	0.4362	26.188	1.1157	23.816	0.4967
26.246	1.21	23.897	0.43582	26.246	1.1224	23.897	0.50052
26.303	1.2232	23.978	0.43581	26.303	1.1301	23.978	0.50469
26.358	1.2621	24.046	0.4331	26.358	1.1615	24.046	0.50262
26.413	1.3012	24.114	0.43048	26.413	1.1932	24.114	0.5006
26.468	1.3206	24.197	0.42993	26.468	1.2045	24.197	0.5007
26.523	1.3406	24.28	0.42969	26.523	1.2166	24.28	0.50117
26.576	1.376	24.379	0.42556	26.576	1.2469	24.379	0.49642
26.628	1.4117	24.478	0.42157	26.628	1.2776	24.478	0.49178
26.681	1.4242	24.564	0.42219	26.681	1.2856	24.564	0.4922
26.734	1.4373	24.65	0.423	26.734	1.2948	24.65	0.4928
26.788	1.4721	24.726	0.42131	26.788	1.3221	24.726	0.49193
26.843	1.5084	24.801	0.41977	26.843	1.3512	24.801	0.49115
26.897	1.5345	24.888	0.42131	26.897	1.3774	24.888	0.49395
26.95	1.5612	24.975	0.42302	26.95	1.4042	24.975	0.49693
27.002	1.6084	25.077	0.42774	27.002	1.4501	25.077	0.50209
27.054	1.6564	25.179	0.43291	27.054	1.4969	25.179	0.50773
27.105	1.7016	25.262	0.43401	27.105	1.537	25.262	0.50998
27.156	1.7476	25.345	0.43527	27.156	1.5777	25.345	0.51237
27.208	1.7442	25.424	0.43206	27.208	1.5747	25.424	0.50747
27.26	1.7414	25.503	0.4289	27.26	1.5726	25.503	0.5026
27.313	1.7556	25.579	0.43438	27.313	1.5964	25.579	0.50862
27.366	1.7716	25.656	0.44006	27.366	1.622	25.656	0.51486
27.421	1.8104	25.715	0.43644	27.421	1.6668	25.715	0.51132
27.477	1.85	25.774	0.43286	27.477	1.7126	25.774	0.50784
27.529	1.8691	25.83	0.43604	27.529	1.7196	25.83	0.51179
27.581	1.8883	25.887	0.43927	27.581	1.7267	25.887	0.51576
27.632	1.9095	25.943	0.42961	27.632	1.7564	25.943	0.50291
27.683	1.9313	25.999	0.42014	27.683	1.7866	25.999	0.49026
27.735	1.9349	26.051	0.42462	27.735	1.7992	26.051	0.49491
27.787	1.9393	26.103	0.4293	27.787	1.8128	26.103	0.49982
27.84	1.9784	26.16	0.4303	27.84	1.8476	26.16	0.50011
27.893	2.0177	26.216	0.43148	27.893	1.8825	26.216	0.50054
27.951	2.0237	26.281	0.43679	27.951	1.8999	26.281	0.50637
28.008	2.0305	26.345	0.44218	28.008	1.9183	26.345	0.51229
28.06	2.0504	26.423	0.43522	28.06	1.9359	26.423	0.50331
28.111	2.0704	26.501	0.42844	28.111	1.9538	26.501	0.49459
28.161	2.1053	26.602	0.43504	28.161	1.9933	26.602	0.50183
28.211	2.1403	26.702	0.44208	28.211	2.033	26.702	0.50952
28.261	2.1506	26.813	0.43432	28.261	2.0357	26.813	0.49934
28.311	2.1619	26.923	0.42663	28.311	2.0394	26.923	0.4892
28.361	2.2118	27.018	0.43354	28.361	2.0931	27.018	0.49643
28.411	2.2625	27.114	0.44056	28.411	2.1478	27.114	0.50381
28.461	2.2563	27.204	0.43447	28.461	2.1274	27.204	0.49607
28.511	2.2537	27.295	0.42849	28.511	2.1123	27.295	0.48847
28.556	2.2169	27.397	0.41744	28.556	2.0764	27.397	0.47294
28.602	2.181	27.5	0.40714	28.602	2.0415	27.5	0.45828